Manipulating collective quantum states of ultracold atoms by probing

Andrew Christopher James Wade

PhD Dissertation

October 2015

Department of Physics and Astronomy
Faculty of Science and Technology
Aarhus University

AARHUS
UNIVERSITY
DEPARTMENT OF PHYSICS AND ASTRONOMY

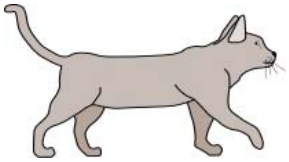

"Today I looked up at the sky, and I realised it was surprisingly big."

Jens Søren Sieg Svensmark

English summary

The field of cold gases has grown dramatically over the past few decades. The exquisite experimental control of their environment and properties has lead to landmark achievements, and has motivated the pursuit of quantum technologies with ultracold atoms. At the same time, the theory of measurements on quantum systems has grown into a well established field. Experimental demonstrations of nondestructive continuous measurements on individual quantum systems now occur in many laboratories. Such experiments with ultracold atoms have shown great progress, but the exploitation of the quantum nature of the measurement interaction and backaction is yet to be realised.

This dissertation is concerned with ultracold atoms and their control via fully quantum mechanical probes. Nonclassical, squeezed and entangled states of matter and single photon sources are important for fundamental studies and quantum technologies. By probing, the production of squeezed and entangled states of collective variables in a Bose-Einstein condensate is investigated. Thereafter, an atomic probe using the strong interactions between highly excited atomic states, manipulates the light-matter dynamics of an ultracold gas, storing a single photon. By manipulating the probe, the dynamics of the gas are also manipulated, causing the single photon to be deterministically emitted.

Dansk resumé

Forskningsfeltet, som beskæftiger sig med kolde gasser, er vokset betragteligt hen over de seneste årtier. Evnen til med stor finesse at kunne kontrollere deres omgivelser og egenskaber i laboratoriet har ført til epokegørende resultater og har motiveret udviklingen af kvanteteknologier, der involverer ultrakolde atomer.

Samtidig har teorien om målinger på kvantesystemer udviklet sig til et veletableret forskningsfelt. I mange laboratorier er man i dag i stand til at udføre eksperimentelle demonstrationer af ikke-destruktive kontinuerte målinger på individuelle kvantesystemer. På trods af store fremskridt inden for sådanne eksperimenter med ultrakolde atomer, har man endnu til gode at demonstrere i laboratoriet, at det er muligt at udnytte de kvantemekaniske aspekter af målinger, såsom vekselvirkninger og backaction.

Denne ph.d.-afhandling omhandler ultrakolde atomer og deres kontrol ved hjælp af fuldt ud kvantemekaniske prober. Forståelsen af ikke-klassiske, såkaldte "squeezed" og kvantemekanisk sammenfiltrede tilstande af stof samt enkelt-foton kilder er vigtig både fra et grundforsknings synspunkt og med henblik på nye kvanteteknologier.

Med hjælp af en probe bliver produktionen af "squeezed" og sammenfiltrede tilstande af kollektive variable i en Bose-Einstein-kondensat undersøgt. Efterfølgende bruges en atomar probe og de stærke vekselvirkninger mellem højt exciterede atomare tilstande til at manipulere lys-stof-dynamikken i en ultrakold gas. Denne proces resulterer i lagringen af en enkel foton. Ved derefter at manipulere proben, bliver gassens dynamiske processer også påvirket, hvilket forårsager en deterministisk emission af fotonen.

Preface

In this dissertation you will find a presentation of the work that I have carried out during my PhD education at the *Department of Physics and Astronomy* at *Aarhus University*, Denmark. The research was funded by *E.U. Marie Curie program ITN-Coherence 265031*. It was carried out in the period from May 2012 to October 2015 under the supervision of Professor Klaus Mølmer.

The manuscripts [1, 2] are part of a collaboration with Jacob Sherson, and are the subjects of Chapters 1 to 6. The manuscript [3] is part of a collaboration with Durga Dasari, and is the subject of Chapter 7.

In collaboration with Christian K. Andersen and Klaus Mølmer, we developed a PhD course, *Interpretation of Quantum Mechanics & Measurements*, resulting in the outreach publication [4]. The subject of this paper is not addressed in this thesis.

List of publications

[1] A. C. J. Wade, J. F. Sherson, and K. Mølmer, *Squeezing and Entanglement of Density Oscillations in a Bose-Einstein Condensate*, Phys. Rev. Lett. **115**, 060401 (2015)

[2] A. C. J. Wade, J. F. Sherson, and K. Mølmer, *Manipulation of collective quantum states in Bose-Einstein condensates by continuous imaging*, In preparation. (2015)

[3] A. C. J. Wade, D. D. Bhaktavatsala Rao, and K. Mølmer, *Efficient storage and retrieval of single photons from an ensemble of Rydberg interacting atoms*, In preparation. (2015)

[4] C. K. Andersen and A. C. J. Wade, *Bohr vs. Einstein: Fortolkning af kvantemekanikken*, Kvant **24**, 27 (2013)

Acknowledgements

I have been extremely blessed and honoured to have the privilege of undertaking my PhD studies within the yellow brick walls. I have gained great friends, work wives, god parents of my daughter, and a best man...

Many people who I appreciate, have strolled the 6th floor hallway during my time. Whenever I've needed someone to help me move, drink a beer with, play boardgames or ultimate frisbee with, or whatever, I've only needed to stroll the 6th floor hallway briefly. If I ever needed a good laugh to get me through the day, all I had to do was wander down to the indistinguishable Jens's. — Ultrafast —
I would like to especially show my appreciation towards the ever-changing bands of Lars Madsen and Klaus Mølmer. My introduction to the Danish "Julefrokost" was legendary, and I have enjoyed speculating on the next Christmas's "entertainment" as early as January.

I've had a great time exploring Denmark and Poland with Beccy and Jake Gulliksen, Maciek Śpiewanowski and Natalia Śpiewanowska, Friederike Stoehr and Malte Tichy. Too many good memories to point out, but damn, I will never forget that Polish wedding (not to mention our hotel that was evacuated due to a bomb threat). During the terminal end of my PhD studies, I've enjoyed sharing an office with Christian Kraglund Andersen – always ready with a sharp mind to discuss my confused state of physics. The problem was, our discussions continued for hours... Perhaps not always about physics. A special thanks goes to my two work wives Natasha Golubeva and Pinja Haikka, for applying me with cake, a hug, dark chocolate and wine, to get me through those hard times.

A thanks that I don't think I could ever possibly formulate in just a few words, he said word-writingly, goes to Ditte Både Sandkamm and Ole Søe Sørensen, who discovered The Long Lost Viking Of The South and the not-quite-so-long-lost girlfriend on that little-big island on the other side of the planet. They, along with Søren Bendlin Gammelmark (and by extension, also Rikke Bendlin Gammelmark) adopted me so quickly when I arrived in Denmark, and have always been supportive of my distinctive lack of pants. They have always been available for a cup of tea, a talk about power tools, algorithms making use of the peculiarities of binary code, figure advice, etc... Although nowadays, we just seem to copy each other at getting married and having babies.

I would also like to thank our great source of administrative power and wisdom, Grete Flarup, who I still can't believe puts up with me. Thanks also to my collaborators Jacob Sherson and Durga Dasari, and all my fellow Marie Curie Scholars. And of course my guide through the PhD journey, Klaus Mølmer, whose ability at generating fantastical tangents and motivation, has always astounded me.

A thank you to my family and friends outside of the yellow brick walls, for being so supportive during my PhD studies and escapades in Denmark.

To my beloved wife Line and our sweet little daughter Ella, whom I revel in rediscovering the world with.

Contents

A general introduction and outline

We are constantly creating devices to see what we otherwise cannot – glasses to bring the immediate world into focus, telescopes to see far into space, microscopes to see small things, X-ray machines to see inside of things, torches or night-vision goggles to see into the dark, and lasers to see straight, level lines. The world of ultracold and ultrasmall systems (e.g., a collection of atoms in a cold gas) is a world that our mind and senses can fail spectacularly at comprehending. Quantum mechanics is a tool to help us see and understand this quantum world, albeit an abstract tool that has caused people to question and ponder the notions of causality, locality, and reality [4]. We also create devices within this quantum world called "ancilla systems". These are quantum systems that can help other quantum systems to interact, transmit information, or be manipulated.

The theory of quantum mechanics can be summarised by only a few laws. These laws describe how the theory represents objects and their properties, how to measure these properties, and how an object and its properties change over time. On top of that, many physical systems are described by only a few building blocks within the theory. Although quantum mechanics and many physical systems can be boiled down to just a few core pieces, the possibilities and consequences are almost endless. Physicists are constantly being surprised and confused by new discoveries. Systems of many parts (atoms) can exhibit collective phenomena where all the smaller parts become interwoven, behaving as if the system is a single object. An example of this emergent phenomena is Bose-Einstein condensation, which is discussed in this thesis.

Another oddity of quantum mechanics is entanglement. This is when two parts become correlated (entangled) and are "inseparable" – meaning, to get the

full picture, they must be considered together and not as individual parts. There are mathematical inequalities that must be obeyed by the measurement results of everyday systems (e.g., the positions of balls on a pool table). This quantum entanglement breaks these inequalities, allowing possibilities beyond that of our everyday world. Conversely, there are also mathematical inequalities for quantum mechanics that limit how well you can know two "conjugate" properties at the same time. You are allowed to know how fast a thing moves, but you are not allowed to know where it is at the same time! Indeed, measurement in quantum mechanics plays an important and unique role. The dynamics of a quantum system are changed by measurements, whether performed by you or another person of whom you may have no knowledge about. This measurement backaction can be used to manipulate the dynamics of the system, either by choosing the type of measurement, how long and if you repeatedly measure the system, and by applying feedback depending on the measurement result.

In all of the earlier mentioned devices (e.g., the X-ray machine), light was either emitted from or it interacted with matter (the bones in your arm). Then, matter was used again to manipulate the light and turn the information (about your bones) into something we can understand (a picture on photographic paper). In this thesis, light-matter interactions, and some of the peculiarities of quantum mechanics are common themes. In particular, I focus on collective phenomena, entanglement, and the measurement backaction within quantum mechanics. I will use all of these concepts to manipulate ultracold collections of atoms, creating interesting collective quantum states with a mind towards the long-term goal of developing technologies that make use of quantum nature.

Chapters 1 to 6 investigate the probing of a Bose-Einstein condensate, where the atoms interact with a light field (the ancilla), imprinting information about themselves onto the light field. By measuring the light field, a measurement of the atomic system is made, and this measurement is used to create interesting collective states in the atomic system.

Chapter 7 also investigates a collection of atoms interacting with a light field. The difference in this case is another atomic system (the ancilla) also interacts with the atoms at the same time. This manipulates the evolution of the atoms, causing a single quantum of energy to be imprinted on the atoms. Afterwards, this quantum of energy is extracted as a useful quantum of light – a photon.

CHAPTER 1

SPATIALLY IMAGING BOSE-EINSTEIN CONDENSATES

In reducing the temperature of a Bose gas past some critical temperature T_{BEC}, macroscopic population accumulates in the lowest lying single particle mode leading to the particles losing their individual character and they behave as single matter-wave entity. This phenomenon, Bose-Einstein condensation (BEC), was first predicted by Einstein in 1925 [5] by applying Bose's work [6] of photon statistics to atoms. Seventy years later in 1995 saw the first conclusive demonstration of BEC by Cornell and Wiemen at JILA with a gas of Rubidium atoms [7], earning them the Nobel Prize in Physics in 2001 along with Ketterle "for the achievement of Bose-Einstein condensation in dilute gases of alkali atoms, and for early fundamental studies of the properties of the condensates." Since then, the field of cold gases has grown dramatically and the experimental control of atomic dynamics has demonstrated landmark achievements through laser and evaporative cooling [8], engineering of trapping potentials [9], and tuning of atomic interactions [10].

Nonclassical, squeezed and entangled states of light are important ingredients in quantum metrology and communication [11, 12]. Production of analogous states of matter has been a long quest in physics with implementations demonstrated in atomic ensembles, as well as in superconducting and nanomechanical devices. Relying on nonlinearities due to atomic interactions, ultracold atoms have been prepared in two-mode entangled states of split atomic clouds [13, 14] and internal state components [15–20] and in states that witness fundamental quantum properties through violation of inequalities obeyed by classical models [21–26].

The precision control of cold gases has motivated the pursuit of quantum technologies with ultracold atoms, such as, quantum computers [27], memories/repeaters, and simulators [28, 29], and, the realization of high precision metrology [14, 30, 31]. As this precision quantum control blossoms, new diagnostic and manipulative methods are required. Nondestructive methods using dispersive light-matter interactions and measurement backaction have demonstrated squeezed [32, 33] and entangled [34] states, quantum teleportation [35], and a quantum memory for light [36] in room temperature vapour experiments. In contrast, typical measurements of ultracold atomic systems, such as, imaging after time-of-flight measurements, are destructive and prohibit further interrogation or use of the system. Nondestructive experiments in ultracold atoms have shown great progress [37–44], and while numerous proposals exist [1, 45–48] to manipulate collective quantum states, the exploitation of the quantum nature of the measurement interaction and backaction is yet to be realised.

Individual quantum systems undergoing continuous monitoring via a dispersive light-matter interaction with a light field (probe) that is subsequently measured, obey stochastic master equations [49]. Their numerical solution for complex many-body systems is, however, problematic. For the continuous monitoring of a Bose-Einstein Condensate (BEC), stochastic mean field solutions have been developed [50, 51], while full quantum mechanical simulations have been possible for dynamics restricted to a few collective modes [52] and phase-space methods have been employed for larger multimodal treatments [47, 48].

Provided the atomic system is not significantly perturbed, a Gaussian state treatment of the atomic Bogoliubov excitation modes can be applied around the atomic mean field, allowing a fully quantum, multimodal treatment. We analyse the measurement backaction in detail, including the role of the finite spatial resolution and geometry of the detector, illustrating how they, and feedback, can be optimised. Additionally, we investigate stroboscopic probing in the selective preparation of squeezed and entangled states of the multimodal excitations of the BEC, as well as, the development of atomic spatial and momentum number correlations.

Chapter 2 presents the Bogoliubov description of the atomic system, while the treatments of the light field and the light-matter interaction are in Chapter 3. In Chapter 4, we derive the Gaussian description of the atomic dynamics under probing that is analysed in Chapter 5. Chapter 6 concludes and present an outlook.

CHAPTER 2

BOGOLIUBOV THEORY

There exists a colossal body of theoretical material on BECs, the book of Pethick and Smith [53] being an introductory reference. A significant portion of the body can be attributed to Bogoliubov theory [54, 55] which is utilized here. This theory enables us to identify the quantum fluctuations of the BEC with the elementary excitations of the BEC, the collective center-of-mass, breathing, and higher order modes. This description yields the atomic quantum state and the platform for the quantum response of the system to the measurement of the density.

Our starting point is the Hamiltonian in second quantisation

$$\hat{H} = \int d\mathbf{r} \hat{\psi}^\dagger(\mathbf{r}) \left[-\frac{\hbar^2}{2m}\nabla^2 + V(\mathbf{r}) + \frac{g_{3\mathrm{D}}}{2}\hat{\psi}^\dagger(\mathbf{r})\hat{\psi}^\dagger(\mathbf{r}) \right] \hat{\psi}(\mathbf{r}), \tag{2.1}$$

where $\hat{\psi}(\mathbf{r})$ is the bosonic field operator and the coupling strength is

$$g_{3\mathrm{D}} = \frac{4\pi\hbar^2 a_{\mathrm{sc}}}{m}, \tag{2.2}$$

with the s-wave scattering length a_{sc}. The 3D harmonic oscillator potential,

$$V(\mathbf{r}) = \frac{m}{2}\left(\omega_x^2 x^2 + \omega_y^2 y^2 + \omega_z^2 z^2\right), \tag{2.3}$$

is taken to be cylindrically symmetric, $\omega_y = \omega_z = \omega_0$.

2.1 1D Bose gas

We consider 1D Bose gases [56, 57], where the radial vibrational modes have been frozen out, reducing the problem to that of solving the axial configuration and dynamics.

2.1.1 Healing length

The freezing of the radial motion requires the radial trapping strength, ω_0, to be strong enough, such that, atoms can only occupy the radial harmonic ground state mode. Without interactions, the ground state of the system would find all the atoms in the single particle ground state of the 3D Harmonic oscillator. However, the interactions mix in higher energy states. The healing length l_{h} can indicate the extent of the population in the higher states, as it captures the length scale of defects that may exist within the system owing to the interactions. Roughly speaking, a defect of length l has a kinetic energy of $\hbar^2/2ml^2$, and an interaction energy of $g_{3\mathrm{D}}n/2$, associated with it. The healing length is where these two contributions are equal

$$l_{\mathrm{h}}^2 = \frac{\hbar^2}{g_{3\mathrm{D}}mn}. \tag{2.4}$$

In order for the single particle states in the radial direction to be unpopulated above the ground state, the length scale of the defects must be larger than the characteristic length scale of the quantum harmonic oscillator $l_0 = \sqrt{\hbar/m\omega_0}$,

$$l_{\mathrm{h}} \gg l_0. \tag{2.5}$$

In terms of the 1D density of the BEC, $n_{1\mathrm{D}} \sim nl_0^2$,

$$\frac{1}{4\pi} \gg n_{1\mathrm{D}}a_{\mathrm{sc}}. \tag{2.6}$$

2.1.2 Effective scattering length

To continue with the 1D description we must establish the 1D interaction strength $g_{1\mathrm{D}}$. If the length scale of the radial confinement is much larger than that of the

length scale of the interactions

$$l_0 \gg a_{\rm sc}, \tag{2.7}$$

then, the interaction between particles acquires 3D characteristics [58]. The result can be obtained by averaging over ground state harmonic oscillator profile in the radial directions

$$g_{\rm 1D} = \frac{g_{\rm 3D}}{2\pi l_0^2} = \frac{2\hbar^2}{m}\frac{a_{\rm sc}}{l_0^2}. \tag{2.8}$$

2.1.3 1D mean field regime

A system is said to be highly interacting when defects are sustained at length scales smaller than the interparticle spacing

$$l_{\rm h}^{\rm 1D} < \frac{1}{n_{\rm 1D}}, \tag{2.9}$$

where $l_{\rm h}^{\rm 1D} = \hbar/\sqrt{g_{\rm 1D} m n_{\rm 1D}}$. Thus, as the healing length scales as $\sim 1/\sqrt{n^{\rm 1D}}$, the 1D Bose system becomes more interacting with decreasing density. For very low densities, the 1D system enters the 1D Tonk-Girardeau regime, where the bosons acquire fermionic properties as the wave function strongly decreases at short interparticle distances. We wish to avoid this regime, remaining within the 1D mean field regime where Bogoliubov treatments are valid. Thus, we obtain our second condition

$$l_{\rm h}^{\rm 1D} \gg \frac{1}{n_{\rm 1D}}, \tag{2.10}$$

or equivalently,

$$n_{\rm 1D} a_{\rm sc} \gg 2\left(\frac{a_{\rm sc}}{l_0}\right)^2. \tag{2.11}$$

2.2 $U(1)$ symmetry breaking

Traditional Bogoliubov theory assumes that the macroscopic population of the lowest lying single particle mode allows one to replace the annihilation and creation operators of the mode with c-numbers,

$$\hat{a}_0 \to a_0, \qquad \hat{a}_0^\dagger \to a_0^*, \tag{2.12}$$

being akin to the parametric approximation of quantum optics. The resulting Hamiltonian is linearized in the other modes, owing to the expectation that only a small fraction of the population pertains to these modes. Indeed, great success has been achieved with this approximation in predicting the excitation spectrum and thermodynamic quantities [59]. However, the physical connotations of such a replacement are significant, as it negates the possibility of a fixed total number of atoms, implicitly assuming Poissonian number fluctuations and a definite phase.

The Bogoliubov replacement, Eq. (2.12), is an ansatz of broken symmetry. A BEC is often associated with the spontaneous symmetry breaking of the global $U(1)$ gauge symmetry responsible for total particle-number conservation

$$[\hat{H}, \hat{N}] = 0, \qquad \hat{N} = \sum_i \hat{a}_i^\dagger \hat{a}_i \,. \tag{2.13}$$

The evolution equations display symmetry under the transformations

$$\hat{U} = e^{-i\alpha\hat{N}}, \tag{2.14}$$

and there exists simultaneous eigenstates of the Hamiltonian and Number operator. This symmetry is broken for states with $\langle \hat{a}_0 \rangle \neq 0$. Spontaneous breaking of the $U(1)$ gauge symmetry occurs when the ground state of the system can be found in states that are not eigenstates of the number operator. This cannot occur when the ground state is nondegenerate.

For the case of free systems, a noninteracting finite extent system will always have a nondegenerate ground state, and for the interacting case, this is generally believed to be true (currently no proof). It has been shown that the symmetry breaking occurs in the thermodynamic limit, owing to the fact that a single particle

has negligible effect on the total energy. Additionally, it was seen that a BEC defined as

$$\lim_{\substack{N \to \infty \\ V \to \infty}} N^{-1} \langle \hat{a}_0^\dagger \hat{a}_0 \rangle = \text{const.}, \tag{2.15}$$

implies spontaneous symmetry breaking, and the Bogoliubov replacement [Eq. (2.12)] is justified [60, 61]. The relationship between BEC and spontaneous symmetry breaking in trapped systems is more intricate [62].

Experiments routinely demonstrate phase coherence associated with an indefinite number of particles, e.g., the observation of interference fringes [63], and measurement of the relative phase [41], between independent BECs. Why does a state of broken symmetry predict experiment so well when the symmetry is never broken in finite free systems, and one believes the notion of a definite number of particles? This issue led the cold gas community into a large debate between 1997 and the early 21st century. An answer is that the symmetry breaking is induced by the backaction of measuring the system. Javanainen and Yoo [64] demonstrated that two counterpropagating, phaseless BECs generate an interference pattern as they are progressively measured. In a simple sense, as the atoms are identical, the lack of knowledge of which BEC the atom triggering a detection event belongs to, installs a phase relationship [65, 66].

Associated with spontaneous breaking of a continuous symmetry are the Nambu-Goldstone modes. Goldstone's theorem [67] asserts that when a continuous symmetry is spontaneously broken, a massless mode exists. In the nonrelativistic case, the Nambu-Goldstone mode corresponds to a quasiparticle with no energy gap between itself and the ground state (gapless). Indeed, here one observes a Nambu-Goldstone mode associated with a quantum phase diffusion [68], illustrating a state of definite quantum phase is not an eigenstate and an approximation to the ground state of the system. Other examples of Nambu-Goldstone modes in BECs are the breaking of translational symmetry of dark [69] and bright [70] solitons, breaking of rotational symmetry of vortex positions [71–73], and in spinor BEC systems [74].

2.3 Bogoliubov approximation

Here, we consider the Bogoliubov approximation [75, 76], and obtain a bilinear Hamiltonian that will be diagonalized. Ultimately, we will assume the global gauge symmetry $U(1)$ is broken as a variational ansatz for the ground state of the Hamiltonian, i.e., the field operator coherent state

$$\hat{\psi}(x)|\psi(x)\rangle = \psi(x)|\psi(x)\rangle. \tag{2.16}$$

In anticipation of this, we write the annihilation field operator as

$$\hat{\psi}(x) = \psi(x) + \delta\hat{\psi}(x), \tag{2.17}$$

with $\langle\delta\hat{\psi}(x)\rangle = 0$, being a canonical transformation (Appendix A), $\delta\hat{\psi}(x) = \hat{S}\hat{\psi}(x)\hat{S}^{\dagger}$,

$$\hat{S} = \exp\left\{\int dx \left[\psi(x)\hat{\psi}^{\dagger}(x) - \psi^{*}(x)\hat{\psi}(x)\right]\right\}. \tag{2.18}$$

The excitations (quasiparticles) of the system are about the new Bogoliubov vacuum state, $|vac\rangle$, of $\delta\hat{\psi}(x)$, corresponding to the coherent state $|\psi(x)\rangle$ of $\hat{\psi}(x)$, and in general, are linear combinations of the single particle modes. We associate the shift $\psi(x)$ with the wavefunction of the lowest lying quasiparticle mode up to a proportionality constant $\sqrt{N_0}$ (taken to be real), $\hat{a}_0 = \sqrt{N_0} + \delta\hat{a}_0$. The Bogoliubov approximation is to assume macroscopic population in this mode

$$\langle\hat{a}_0^{\dagger}\hat{a}_0\rangle_0 \simeq N_0 \simeq N, \tag{2.19}$$

being valid for very low temperatures $T \simeq 0$, and to replace the creation and annihilation operator with

$$\hat{a}_0 \to \sqrt{N_0}, \qquad \hat{a}_0^{\dagger} \to \sqrt{N_0}. \tag{2.20}$$

As we are interested in the quantum nature of the mode, we do not make the Bogoliubov replacement. However, we do assume macroscopic population [c.f., Eq. (2.19)], to which, the Hamiltonian is truncated to second-order in the quantum fluctuations $\delta\hat{\psi}(x)$.

The approximated Hamiltonian no longer conserves total particle number, so we introduce the grand canonical Hamiltonian

$$\hat{H}_\mu = \hat{H} - \mu\hat{N} = H_0 + \hat{H}_1 + \hat{H}_2, \tag{2.21}$$

where the chemical potential μ is the Lagrange multiplier enforcing $N \simeq N_0$ particles on average. Thus, we have

$$H_0 = \int dx\, \psi^*(x) \left[H_{1\mathrm{D}} - \mu + \frac{g_{1\mathrm{D}}}{2} |\psi(x)|^2\right] \psi(x), \tag{2.22a}$$

$$\hat{H}_1 = \int dx\, \delta\hat{\psi}^\dagger(x) \left[H_{1\mathrm{D}} - \mu + g_{1\mathrm{D}} |\psi(x)|^2\right] \psi(x) + \mathrm{h.c.}, \tag{2.22b}$$

$$\hat{H}_2 = \int dx\, \delta\hat{\psi}^\dagger(x) \left[H_{1\mathrm{D}} - \mu + 2g_{1\mathrm{D}} |\psi(x)|^2\right] \delta\hat{\psi}(x) + \int dx\, \frac{g_{1\mathrm{D}}}{2} \left[\psi^*(x)^2 \delta\hat{\psi}(x)^2 + \mathrm{h.c.}\right], \tag{2.22c}$$

where $H_{1\mathrm{D}}$ is the 1D single atom Hamiltonian with the harmonic potential $V(x) = m\omega_x^2 x^2/2$,

$$H_{1\mathrm{D}} = -\frac{\hbar^2}{2m}\frac{\partial^2}{\partial x^2} + V(x). \tag{2.23}$$

Upon minimising the energy $E_0 = \langle \hat{H}_\mu \rangle \simeq H_0$ with respect to the BEC wavefunction, one obtains the Gross-Pitaevskii equation (GPE)

$$\left[H_{1\mathrm{D}} - \mu + g_{1\mathrm{D}} |\psi(x)|^2\right] \psi(x) = 0, \tag{2.24}$$

and as a result, $\hat{H}_1 = 0$.

The above methodology works well for most of the population in the lowest lying mode ($T \simeq 0$), but at higher temperatures ($T < T_{\mathrm{BEC}}$), a nonphysical gap in the quasiparticle spectrum appears. This is in violation with the Hugenholtz-Pines theorem [77], which asserts that a physically sound theory must be gapless. Nonselfconsistent introductions to the theory removed this gap, but lead to the breaking of conservation laws. The situation was summarised by Hohenberg and Martin [78] in the Hohenberg-Martin dilemma, where they showed that any theory

in the framework of the grand canonical ensemble (2.21), is either nonconserving or acquires a gap in the spectrum. This situation has been resolved by Yukalov [62], where it is stressed that we must introduce the same number of Lagrange multipliers as we have constraints in the system. One should introduce two chemical potentials for the BEC and excitations, as well as, a Lagrange multiplier for the conservation condition $\langle \delta\hat{\psi}(x)\rangle = 0$. The last Lagrange multiplier amounts to removing linear terms of the quantum fluctuation in the Hamiltonian.

2.4 Bogoliubov transformation

The approximated Hamiltonian, $\hat{H}_\mu = H_0 + \hat{H}_2$, is diagonalized with the Bogoliubov transformation [75, 76, 79]

$$\delta\hat{\psi}(x) = e^{i\Theta} \sum_j \left[f_j^-(x)\hat{x}_j + i f_j^+(x)\hat{p}_j \right], \tag{2.25}$$

where the wavefunctions $f_j^\pm(x)$ can be taken real, the quadratures obey $[\hat{x}_j, \hat{p}_k] = i\delta_{jk}$, and the BEC phase is Θ. I.e., $\psi(x) = e^{i\Theta}\sqrt{n_0(x)}$, and $n_0(x) = |\psi(x)|^2$ is the BEC density.

In Appendix A, we discuss in detail the method following the book of Blaizot and Ripka [79]. Here, we only cast the problem in terms of the matrix formalism developed there, and that of the more commonly seen picture of wavefunctions. We expand the field operator on a real complete basis φ,

$$\delta\hat{\psi}(x) = e^{i\Theta} \sum_j \varphi_j(x)\hat{a}_j. \tag{2.26}$$

We may write the Hamiltonian as

$$\hat{H}_\mu = H_0 + \sum_{ij} A_{ij}\hat{a}_i^\dagger\hat{a}_j + \frac{1}{2}\sum_{ij}\left(B_{ij}\hat{a}_i\hat{a}_j + B_{ij}\hat{a}_i^\dagger\hat{a}_j^\dagger \right), \tag{2.27}$$

where

$$A_{ij} = \int dx\, \varphi_i(x)\left[H_{1\mathrm{D}} - \mu + 2g_{1\mathrm{D}}n_0(x)\right]\varphi_j(x), \tag{2.28}$$

and

$$B_{ij} = g_{1\mathrm{D}} \int dx\, n_0(x)\varphi_i(x)\varphi_j(x), \tag{2.29}$$

are real. In the matrix formalism of Appendix A.3, we have

$$\hat{H}_\mu = H_0 + \frac{1}{2}\left(\boldsymbol{\alpha}^\dagger \mathbf{M}\boldsymbol{\alpha} - \mathrm{Tr}\mathbf{A}\right), \tag{2.30a}$$

$$\mathbf{M} = \begin{bmatrix} \mathbf{A} & \mathbf{B} \\ \mathbf{B} & \mathbf{A} \end{bmatrix}. \tag{2.30b}$$

To bring the Hamiltonian into diagonal form (a collection of noninteracting harmonic oscillators), we have to solve the eigenvalue problem Eq. (A.29)

$$\boldsymbol{\eta}\mathbf{M} \begin{bmatrix} \mathbf{U}_j \\ -\mathbf{V}_j \end{bmatrix} = \hbar\omega_j \begin{bmatrix} \mathbf{U}_j \\ -\mathbf{V}_j \end{bmatrix}, \tag{2.31}$$

equivalent to the Bogoliubov-de Gennes (BdG) equations [57]

$$\begin{bmatrix} 0 & \mathcal{L}_+ \\ \mathcal{L}_- & 0 \end{bmatrix} \begin{bmatrix} f_j^+(x) \\ f_j^-(x) \end{bmatrix} = \hbar\omega_j \begin{bmatrix} f_j^+(x) \\ f_j^-(x) \end{bmatrix}, \tag{2.32}$$

with $\mathcal{L}_\pm = H_{1\mathrm{D}} - \mu + (2 \pm 1)g_{1\mathrm{D}}n_0(x)$. The wavefunctions are given by

$$f_j^+(x) = \frac{1}{\sqrt{2}}\sum_i \left[\mathbf{U}_j + \mathbf{V}_j\right]_i \varphi_i(x), \qquad f_j^-(x) = \frac{1}{\sqrt{2}}\sum_i \left[\mathbf{U}_j - \mathbf{V}_j\right]_i \varphi_i(x), \tag{2.33}$$

with $\int dx f_j^+(x) f_k^-(x) = \int dx f_j^-(x) f_k^+(x)$, and, the normalization and orthogonality condition $\int dx f_j^+(x) f_k^-(x) = \delta_{jk}/2$.

The Hamiltonian is diagonalized resulting in

$$\hat{H} = \frac{\hbar\omega_0}{2}\hat{x}_0^2 + \sum_{j>0} \frac{\hbar\omega_j}{2}\left(\hat{x}_j^2 + \hat{p}_j^2\right), \tag{2.34}$$

neglecting energy constants. The quasiparticle annihilation operators are given by

$$\hat{b}_j = \int dx \left[u_j(x)\delta\hat{\psi}(x)e^{-i\Theta} + v_j(x)\delta\hat{\psi}^\dagger(x)e^{i\Theta}\right], \tag{2.35a}$$

$$\hat{b}_j^\dagger = \int dx \left[v_j(x)\delta\hat{\psi}(x)e^{-i\Theta} + u_j(x)\delta\hat{\psi}^\dagger(x)e^{i\Theta}\right], \tag{2.35b}$$

with $u_j(x) = [f_j^+(x) + f_j^-(x)]/\sqrt{2}$ and $v_j(x) = [f_j^+(x) - f_j^-(x)]/\sqrt{2}$.

2.4.1 Zero eigenvalue

The BdG equations (2.32) have a zero energy (gapless) solution proportional to the BEC

$$f_0^+(x) \propto \sqrt{n_0(x)}, \tag{2.36}$$

owing to the GPE (2.24). This is the Nambu-Goldstone mode associated with the $U(1)$ symmetry breaking (see Sec. 2.2), where the phase of the BEC is associated with $\hat{p}_0$. As the mode behaves like a free particle, the system exhibits phase diffusion [68]. The corresponding wavefunction $f_0^-(x)$ is missing owing to $\mathcal{L}_+$ being positive definite, i.e., $\mathcal{L}_+ f_0^-(x) = 0$ implies $f_0^-(x) = 0$. Consequently, we must introduce a generalized eigenvector to complete the canonical transformation that diagonalizes the Hamiltonian and provides the completeness relation. The details of this construction are in Appendix A.3.

The collective variables $\hat{x}_0$ and $\hat{p}_0$ represent the number and phase operators of the BEC mode, respectively, and can be associated with improving the ground state variational ansatz by allowing linear combinations of $U(1)$ broken symmetry states which reinstate the symmetry [79]. Here, we see that the ground state is

$$|\mathbf{0}\rangle, \qquad \hat{b}_j|\mathbf{0}\rangle = 0 \quad \forall\, j > 0, \qquad \hat{x}_0|\mathbf{0}\rangle = 0, \tag{2.37}$$

where the zero eigenstate of $\hat{x}_0$ implies no total number fluctuations and a completely illdefined phase.

Number conserving Bogoliubov theories can be formulated, being first put forth in 1959 by Girardeau and Arnowitt [80] seemingly unbeknownst to both Gardiner [81] and Castin and Dum [82] who put forward similar theories. Here, one does not consider a coherent state ansatz [Eq. (2.16)], but consider instead operators like

$$\hat{\Lambda}(x) = \frac{1}{\sqrt{\hat{N}}}\hat{a}_0^\dagger \delta\hat{\psi}(x), \tag{2.38}$$

which are then expanded in the quasiparticle modes as above. Ultimately, one finds the mode functions satisfy modified BdG equations [82] for which the solution space is orthogonal to the BEC wavefunction $|\psi(x)|$. This has the important consequence that we need no longer establish a generalized eigenvector Eq. (A.31) that is the origin of the free particle mode appearing in the Hamiltonian Eq. (2.34).

In other words, no symmetry was broken, and therefore, the Nambu-Goldstone mode does not appear. In the work presented here, if we wish to model a state of a definite number of particles, we may simply neglect the Nambu-Goldstone mode.

The linearization of the Hamiltonian breaks down if the quantum fluctuations become large. Owing to the large fluctuations of the zeroth mode in the ground state (2.37), the ground state will not be within the framework of our approximation. If the phase diffusion becomes significant the linearization will also breakdown, thus, we must restrict time evolution to times

$$t \sim t_{\mathrm{c}} = \frac{2\pi}{\omega_0}. \tag{2.39}$$

Later (stroboscopic probing in Chapter 5), we will require longer simulation times, in that case, we must use number-conserving Bogoliubov theory to avoid these requirements.

2.4.2 Fixing the free parameter: phase diffusion

As is discussed in Appendix A.3.2, we must introduce the generalized eigenfunction, to complete the canonical transformation, requiring

$$\mathcal{L}_+ f_0^-(x) = \hbar\omega_0 f_0^+(x). \tag{2.40}$$

Upon taking the partial derivative of the GPE with respect to N_0, one finds Eq. (2.40) with the identifications

$$f_0^-(x) = \sqrt{2N_0}\frac{\partial\sqrt{n_0(x)}}{\partial N_0}, \quad f_0^+(x) = \sqrt{\frac{n_0(x)}{2N_0}}. \tag{2.41}$$

and the phase diffusion parameter

$$\hbar\omega_0 = 2N_0\frac{\partial\mu}{\partial N_0}. \tag{2.42}$$

However, a free parameter α remains in the theory and must be fixed by appealing to the physics of the system. The free parameter amounts to a scale or squeezing transformation,

$$F_0^+(x) = \frac{1}{\alpha}f_0^+(x), \qquad F_0^-(x) = \alpha f_0^-(x), \qquad \omega_0' = \alpha^2\omega_0, \tag{2.43}$$

and the normalization, $\int dx F_0^+(x) F_0^-(x) = 1/2$, is preserved.

We now presume the equivalence of the vacuum state of the Nambu-Goldstone mode to the initial coherent state of the lowest lying single particle mode, Eq. (2.16). Later, it can be seen that

$$\mathrm{var}[\hat{N}_0] \simeq 2\alpha N_0 \mathrm{var}[\hat{x}_0]. \tag{2.44}$$

As the coherent state requires $\mathrm{var}[\hat{N}_0] = N_0$, for consistency, we must choose $\alpha = 1$. Conveniently, this well describes the physics. The phase diffusion of the atomic field follows the profile of the BEC, $f_0^+(x)$, and $f_0^-(x)$ describes the change to the BEC wavefunction by the addition and removal of condensed atoms, while Eq. (2.42) is the expected phase diffusion time scale [66, 68]. Owing to the interactions, the phase of the BEC becomes number dependent, $\exp[-i\mu(\hat{N}_0)t/\hbar]$. Thus, we expect phase collapse to occur on the timescale $t_\mathrm{c} \sim \hbar/\Delta\mu \sim 1$, where $\Delta\mu$ is the variation of the chemical potential over the particle distribution. Assuming the particle distribution to be Poissonian $\Delta N_0 = \sqrt{N_0}$, the variation is given by $\Delta\mu = \Delta N_0 \partial\mu/\partial N_0$. Thus, we have

$$t_\mathrm{c} \sim \frac{\hbar}{\sqrt{N_0}\partial\mu/\partial N_0} \sim \frac{1}{\omega_0}. \tag{2.45}$$

2.5 Nature of the quasiparticles and summary

The excitations of the BEC embody the quantum fluctuations of the density, $\hat{n}(x,t) = n_0(x) + \hat{n}_\mathrm{nc}(x,t)$, about the BEC mean field

$$n_0(x) = |\psi(x)|^2 . \tag{2.46}$$

The expansion of $\hat{n}_\mathrm{nc}(x,t)$ in terms of the excitation wavefunctions and quadratures is

$$\begin{aligned}\hat{n}_\mathrm{nc}(x,t) = 2\sqrt{n_0(x)} \sum_j f_j^-(x)\hat{x}_j - \sum_j f_j^-(x) f_j^+(x) \\ + \sum_{jk} \left[f_j^-(x) f_k^-(x) \hat{x}_j \hat{x}_k + f_j^+(x) f_k^+(x) \hat{p}_j \hat{p}_k \right] .\end{aligned} \tag{2.47}$$

The atomic density correlations are

$$\mathrm{covar}[\hat{n}(x_1), \hat{n}(x_2)] = n_0(x_1)\delta(x_1 - x_2) + \mathcal{N}(x_1, x_2), \tag{2.48}$$

and to second-order in quadratures,

$$\mathcal{N}(x_1, x_2) = -2\sqrt{n_0(x_1)n_0(x_2)} \sum_j f_j^-(x_1) \Bigg\{ f_j^+(x_2) - 2\sum_k f_k^-(x_2)\mathrm{covar}[\hat{x}_j, \hat{x}_k] \Bigg\}. \tag{2.49}$$

Poissonian fluctuations are represented by the delta-function term in Eq. (2.48), while deviations, and correlations between spatially separated regions, are signalled by nonzero values of $\mathcal{N}(x_1, x_2)$.

To relate to the quantum phase, we reinterpret the linearisation in terms of the quantum phase-density representation of the field operator [57]

$$\hat{\psi}(x) = e^{i\hat{\phi}}\sqrt{\hat{n}(x,t)}. \tag{2.50}$$

Linearizing about the BEC phase Θ and density $n_0(x)$, one can identify the relation

$$\hat{\phi}_{\mathrm{nc}}(x,t) = \frac{1}{\sqrt{n_0(x)}} \sum_j f_j^+(x)\hat{p}_j, \tag{2.51}$$

Thus, the phase correlations are

$$\mathrm{covar}[\hat{\phi}_{\mathrm{nc}}(x_1), \hat{\phi}_{\mathrm{nc}}(x_2)] = \frac{1}{4n_0(x_1)}\delta(x_1 - x_2) + \mathcal{P}(x_1, x_2), \tag{2.52}$$

with

$$\mathcal{P}(x_1, x_2) = \frac{1}{\sqrt{n_0(x_1)n_0(x_2)}} \sum_j f_j^+(x_1) \left\{ \sum_k f_k^+(x_2)\mathrm{covar}[\hat{p}_j, \hat{p}_k] - \frac{f_j^-(x_2)}{2} \right\}. \tag{2.53}$$

Poissonian fluctuations are represented by the delta-function term in Eq. (2.52) (associated with the uncertainty principle $\Delta\hat{n}\Delta\hat{\phi} \geq 1/2$), while deviations, and

correlations between spatially separated regions, are signalled by nonzero values of $\mathcal{P}(x_1, x_2)$.

Examples of $f_j^{\pm}(x)$ are shown in Fig. 2.1, while the frequency spectrum and number of atoms associated with a single excitation of the jth mode N_j are showcased in Fig. 2.2. For the noninteracting case $g_{1\mathrm{D}} = 0$ there is no

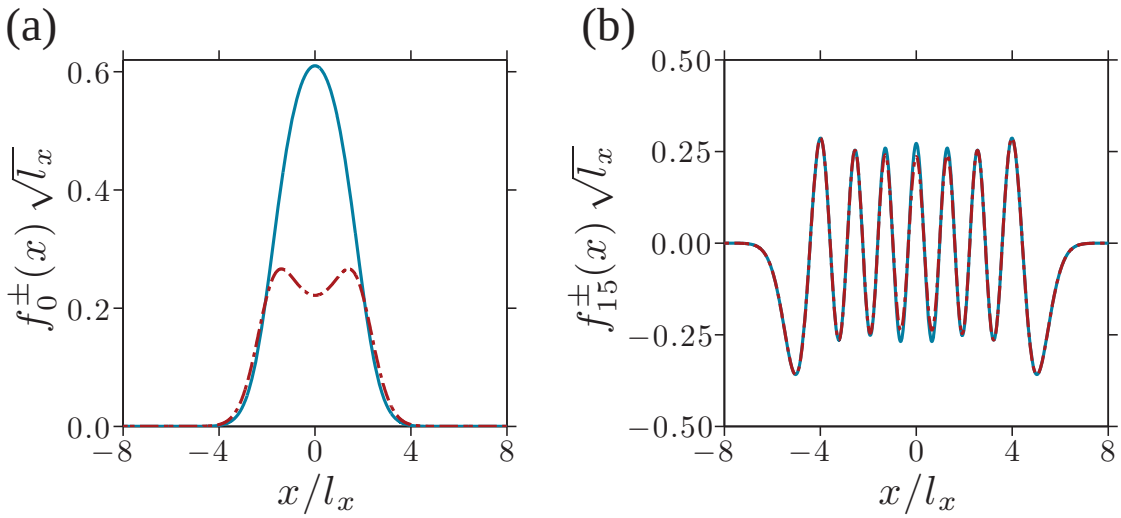

Figure 2.1: The mode functions $f_j^+(x)$ (blue) and $f_j^-(x)$ (red) associated with the zeroth mode (a) and 15th mode (b) for $\mu = 2\hbar\omega_x$. The collective mode (a) exhibits different density $[f_0^-(x)]$ and phase $[f_0^+(x)]$ fluctuations, while more particle-like high energy excitations (b) exhibits similar fluctuations $[f_{15}^-(x) \sim f_{15}^+(x)]$.

phase dispersion, $\omega_0 = 0$, and $\mu = \hbar\omega_x/2$. The system is simply described by the single particle harmonic oscillator, where the wavefunctions become equal, $f_j^+(x) = f_j^-(x)$, and the frequency spectrum is linear $\omega_j = j\omega_x$. Similarly, at high energies where the kinetic energy dominates the interaction energy, we have the single particle harmonic oscillator wavefunctions and the energies are given by

$$\hbar\omega_j = \hbar\omega_x \left(j + \frac{1}{2}\right) - \mu. \tag{2.54}$$

Conversely, in the interaction dominated regime, the so called Thomas-Fermi (TF)

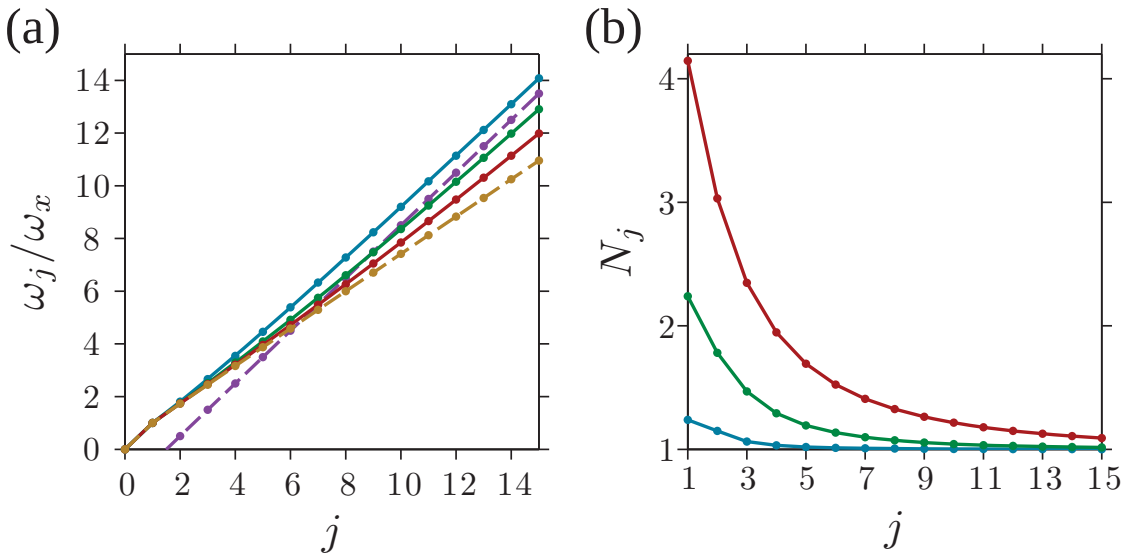

Figure 2.2: (a) The energy spectrum of the quasiparticles for the cases $\mu = 2\hbar\omega_x$ (blue), $5\hbar\omega_x$ (green), and $10\hbar\omega_x$ (red). The transition between the (low-energy) collective spectrum, Eq. (2.56) (gold), and the (high-energy) particle-like spectrum, Eq. (2.54) with $\mu = 2\hbar\omega_x$ (purple), is observed. The collective to particle-like cross-over is also illustrated in (b), showing the number of particles associated with a single excitation of the jth mode, $N_j = \int dx[f_j^+(x)^2 + f_j^-(x)^2]$, [53]. The lines are to guide the eye between discrete j values.

regime discussed in Appendix B, the wavefunctions are well described by

$$f_j^{\pm}(x) = \begin{cases} \left(\frac{2g_{1\mathrm{D}}}{\hbar\omega_j}\right)^{\pm\frac{1}{2}} \sqrt{\frac{2j+1}{4R_{\mathrm{TF}}}}\psi(x)^{\pm 1} P_j\left(x/R_{\mathrm{TF}}\right) & j > 0, \\ f_0^+(x) = \sqrt{\frac{n_0(x)}{2N_0}}, \qquad f_0^-(x) = \frac{1}{4R_{\mathrm{TF}}}\left[f_0^+(x)\right]^{-1} & j = 0, \end{cases} \tag{2.55}$$

with the Legendre polynomials P_j. The phase dispersion is $\hbar\omega_0 = 4\mu/3$ and the spectrum is irregular

$$\omega_j = \omega_x\sqrt{j(j+1)/2}. \tag{2.56}$$

CHAPTER 3

TREATMENT OF THE LIGHT AND INTERACTION

The continuous nondestructive monitoring of a system can be performed by interacting the system with an ancillary probe system which itself is subsequently measured [83]. Such monitoring is considered here, and a schematic of the system of interest is shown in Fig. 3.1. As the light interacts with the atomic system, the atomic mean field imprints a classical phase shift across the optical wavefront and through spatially resolved homodyne detection the mean atomic density profile [Eq. (2.46)] can be inferred. The quantum phase fluctuations in the light field, however, become entangled with multimodal quantum fluctuations of the atomic density [Eq. (2.47)] due to their interaction. This causes decoherence of the atomic quantum state, unless one detects the light field and keeps track of the measurement backaction on the atomic system. To maintain a pure, or, purify an initially impure atomic quantum state, the measurements should be sufficiently efficient, perfectly resolving the field fluctuations. Any information of the atomic fluctuations imprinted on the light field that remains unresolved will cause the atomic system to progressively decohere under the continuous interaction and probing.

In this chapter, we establish the interaction between the light field and atomic system (Sec. 3.1) and the treatment of the light field (Sec. 3.2). Through the interaction, it is identified how the atomic density information is imprinted on the light field, and consequently, the measurements required for full information

recovery. Although our example (Fig. 3.1) concerns only phase measurements, we establish the formalism to incorporate Faraday rotation experiments [84]. Later, their formal equivalence will be established (Chapter 4).

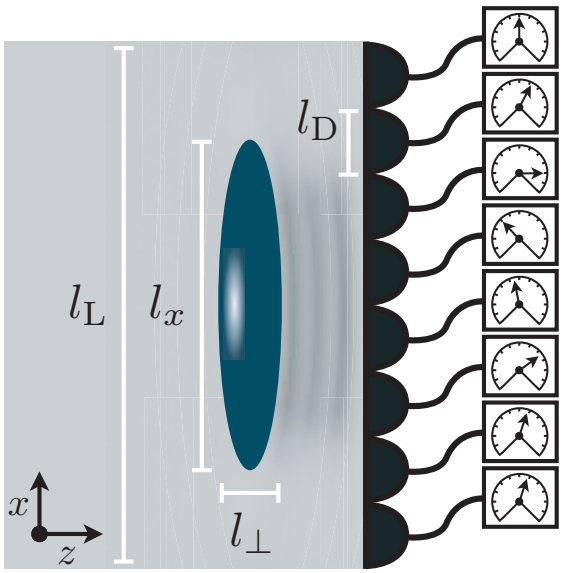

Figure 3.1: The far-detuned light field dispersively interacts with the atomic system, imprinting density-dependent phase shifts across the coherent planar light field propagating along the z-axis. The spatial detection of the atomic density along the BEC axis is achieved through the spatial detection of the imprinted phase shifts by an encapsulating ($l_{\mathrm{L}} > l_x$) array of homodyne detectors (pixels) of widths l_{D}. The simulated examples (unless stated otherwise) are performed for probing the D_2 line (σ_+ polarised light) of 1000 ^{87}Rb atoms in the $|F, m_F\rangle = |2, 2\rangle$ state with axial $\omega_x = 2\pi \times 150\mathrm{Hz}$ and radial $\omega_\perp = 100\omega_x$ trapping frequencies, and chemical potential $\mu = 2\hbar\omega_x$.

3.1 Light-matter interaction

The nondestructive continuous monitoring of the atomic density can be achieved via the dispersive interaction with far-detuned light that is subsequently measured [37–39], Fig. 3.1. For alkali atoms, and laser detuning Δ_{L} much larger than the hyperfine splittings of the far-detuned excited states, the interaction between the light field and a single atom is $\hat{H}_{\mathrm{I}} = \hat{\mathbf{E}}^{-}\boldsymbol{\alpha}\,\hat{\mathbf{E}}^{+}$ [84, 85] with the positive (negative) component of the electric field $\hat{\mathbf{E}}^{+(-)}$. The polarisability tensor operator is

$$\boldsymbol{\alpha} = -\frac{d_{JJ'}^2}{\hbar\Delta_{\mathrm{L}}}\left[\alpha_0 + \alpha_1\hat{F}_z\left(\mathbf{e}_1\otimes\mathbf{e}_1^* - \mathbf{e}_{-1}\otimes\mathbf{e}_{-1}^*\right)\right],$$

where $d_{JJ'} = |\langle J||d||J'\rangle|$ is the reduced dipole matrix element, α_0 and α_1 are constants depending on the specific atomic structure, $\hat{F}_z$ is the z-component of the ground state spin operator, and $\mathbf{e}_q$ are the complex spherical unit vectors. The term proportional to α_0 (scalar polarizability) corresponds to an ac Stark shift,

$$\hat{H}_{\mathrm{ac}} = -\alpha_0\frac{d_{J,J'}^2}{\hbar\Delta_{\mathrm{L}}}\int\hat{\mathbf{E}}^{-}(x)\cdot\hat{\mathbf{E}}^{+}(x)\hat{n}(x)dx, \tag{3.1}$$

while the α_1 term (vectorial polarizability) is an atomic spin-state dependent Faraday rotation,

$$\hat{H}_{\mathrm{Fr}} = -\alpha_1\frac{d_{J,J'}^2}{\hbar\Delta_{\mathrm{L}}}\int\left[\hat{E}_1^{-}(x)\hat{E}_1^{+}(x) - \hat{E}_{-1}^{-}(x)\hat{E}_{-1}^{+}(x)\right]\hat{F}_z(x)dx, \tag{3.2}$$

where $\hat{E}_{(-)1}^{\pm}$ are the spherical components of the positive and negative electric field.

Both the ac Stark shift [37, 38] and Faraday rotation [39, 43, 44] allow for the spatially resolved imaging of the atomic density. The Faraday rotation alone also allows for the probing [86–92] and quantum control [46] of spin correlations, and characterisation of Bose-Hubbard models [93]. However, both the ac Stark shift and Faraday rotation must be considered for the characterisation and quantum control of the density. In typical experiments, we have $\alpha_0 \sim \alpha_1$ [84, 85], therefore, measurement of only one will lead to decoherence associated with the atomic entanglement with the other.

In following, we will present the formalism for standard Faraday rotation experiments [84]. Later, Sec. 4.2.1, we will allow for measuring only the ac Stark shift or Faraday rotation. The formalism will also allow for the case where the atoms prepared in a particular hyperfine state $|F, m_F\rangle$ and the light is $\sigma_\pm$ polarised. In this case, the single-atom interaction is

$$\hat{H}_\mathrm{I} = -\frac{d_{JJ'}^2}{\hbar\Delta_\mathrm{L}} \left(\alpha_0 \pm \alpha_1 m_F\right) \hat{\mathbf{E}}^- \cdot \hat{\mathbf{E}}^+, \tag{3.3}$$

requiring only phase shift measurements for complete information recovery.

3.2 Treatment of the light field

To describe the light-matter interaction and measurement, we develop upon the methodologies of Ref. [94].

3.2.1 Modal decomposition

We model the planar coherent light field as discretized cuboidal mode functions $f_{jkl}(x, y, z)$ with Δx, Δy, and $c\tau$ being the widths in the x, y, and z directions, respectively, and c is the speed of light. The mode function is given as

$$f_{jkl}(x, y, z) = \frac{1}{\sqrt{\Delta x \Delta y c\tau}} \Pi\left(\frac{x - j\Delta x}{\Delta x}\right) \Pi\left(\frac{y - k\Delta x}{\Delta x}\right) \Pi\left(\frac{z - lc\tau}{c\tau}\right), \tag{3.4}$$

where $\Pi(x)$ is the top hat function

$$\Pi(x) = \begin{cases} 1 & \text{if } |x| < \frac{1}{2}, \\ 0 & \text{otherwise.} \end{cases} \tag{3.5}$$

That is, the light is segmented into chunks, where each chunk moves with the speed of light. Ultimately, these chunks will interact with the BEC, and after the interaction, the chunks are later detected via homodyne detection.

3.2.2 Stokes treatment

Set ups involving Faraday rotation use x-polarized coherent light [84]. The light field is decomposed into Stokes operators and effective quadrature operators are formulated (equivalent to a Holstein-Primakoff approximation) that describe the quantum polarization fluctuations that couple to the quantum fluctuations of the atomic spin state. The Stokes operators are

$$\hat{S}_0 = \hat{N}_{\rm ph} = \hat{a}_x^\dagger \hat{a}_x + \hat{a}_y^\dagger \hat{a}_y, \tag{3.6a}$$

$$\hat{S}_x = \frac{1}{2}\left(\hat{a}_x^\dagger \hat{a}_x - \hat{a}_y^\dagger \hat{a}_y\right), \tag{3.6b}$$

$$\hat{S}_y = \frac{1}{2}\left(\hat{a}_{+45}^\dagger \hat{a}_{+45} - \hat{a}_{-45}^\dagger \hat{a}_{-45}\right) = \frac{1}{2}\left(\hat{a}_x^\dagger \hat{a}_y + \hat{a}_y^\dagger \hat{a}_x\right), \tag{3.6c}$$

$$\hat{S}_z = \frac{1}{2}\left(\hat{a}_-^\dagger \hat{a}_- - \hat{a}_+^\dagger \hat{a}_+\right) = \frac{1}{2i}\left(\hat{a}_x^\dagger \hat{a}_y - \hat{a}_y^\dagger \hat{a}_x\right). \tag{3.6d}$$

The annihilation, $\hat{a}_i$, and creation, $\hat{a}_i^\dagger$, operators for light left $(+)$ and right $(-)$ circularly polarized, and linearly polarized in the $+45°$ $(+45)$ and $-45°$ (-45) directions, are described terms of linearly polarized light in the x-direction (x) and y-direction (y)

$$\hat{a}_+ = \frac{1}{\sqrt{2}}\left(\hat{a}_x + i\hat{a}_y\right), \qquad \hat{a}_- = \frac{1}{\sqrt{2}}\left(\hat{a}_x - i\hat{a}_y\right), \tag{3.7a}$$

$$\hat{a}_{+45} = \frac{1}{\sqrt{2}}\left(\hat{a}_x + \hat{a}_y\right), \qquad \hat{a}_{-45} = \frac{1}{\sqrt{2}}\left(\hat{a}_x - \hat{a}_y\right). \tag{3.7b}$$

The Stokes operators, $\hat{S}_x$, $\hat{S}_y$, and $\hat{S}_z$, have the cyclic angular momentum commutation relations,

$$[\hat{S}_y, \hat{S}_z] = i\hat{S}_x, \tag{3.8}$$

while $[\hat{S}_0, \hat{S}_i] = 0$.

The light in each segment is taken to be strong coherent field polarized in the x direction and $\hat{S}_x \approx S_x = N_{\rm ph}/2$. The polarization of each photon is an equal superposition of $+45°$ and $-45°$, or equivalently, an equal superposition of left and right circular. Thus, these components are equally populated on average with

a binomial distribution. Loosely speaking, the polarization state of the combined photon system can be taken to be

$$\begin{aligned}|\psi_{\mathrm{ph}}\rangle &= \frac{1}{\sqrt{2^{N_{\mathrm{ph}}}}}\left(|\mathrm{L}\rangle_1 + |\mathrm{R}\rangle_1\right) \otimes \ldots \otimes \left(|\mathrm{L}\rangle_{N_{\mathrm{ph}}} + |\mathrm{R}\rangle_{N_{\mathrm{ph}}}\right) \\ &= \frac{1}{\sqrt{2^{N_{\mathrm{ph}}}}} \sum_{k=0}^{N_{\mathrm{ph}}} \begin{pmatrix} N_{\mathrm{ph}} \\ k \end{pmatrix} |\mathrm{L}^k \mathrm{R}^{N_{\mathrm{ph}}-k}\rangle, \end{aligned} \tag{3.9}$$

where we have the understanding that $|\mathrm{L}^k\mathrm{R}^{N_{\mathrm{ph}}-k}\rangle$ represents any state with k photons with $|\mathrm{L}\rangle$ polarization, and $N_{\mathrm{ph}} - k$ photons with $|\mathrm{R}\rangle$ polarization (there being "N_{ph} choose k" such states). Thus, the probability of k photons with $|\mathrm{L}\rangle$ polarization, and $N_{\mathrm{ph}} - k$ photons with $|\mathrm{R}\rangle$ polarization is given by

$$\mathrm{B}\left(N_{\mathrm{ph}}, 1/2\right) = \frac{1}{2^{N_{\mathrm{ph}}}} \begin{pmatrix} N_{\mathrm{ph}} \\ k \end{pmatrix} \to \sqrt{\frac{2}{\pi N_{\mathrm{ph}}}} \exp\left[-\frac{2}{N_{\mathrm{ph}}}\left(k - \frac{N_{\mathrm{ph}}}{2}\right)^2\right]. \tag{3.10}$$

We have taken the limit of a large number of photons, yielding a Gaussian distribution centred at $N_{\mathrm{ph}}/2$ with variance $N_{\mathrm{ph}}/4$.

We can define the canonical position and momentum operators for the light field,

$$\hat{r}^- = -\frac{\hat{S}_z}{\sqrt{S_x}}, \qquad \hat{s}^- = \frac{\hat{S}_y}{\sqrt{S_x}}, \tag{3.11}$$

where $[\hat{r}^-, \hat{s}^-] = i$. Thus, we may write

$$\hat{a}_\pm^\dagger \hat{a}_\pm = \hat{S}_x \mp \hat{S}_z + \hat{a}_y^\dagger \hat{a}_y \approx \frac{N_{\mathrm{ph}}}{2} \pm \sqrt{\frac{N_{\mathrm{ph}}}{2}}\, \hat{r}^-, \tag{3.12}$$

and knowledge of the distribution (3.9) gives

$$\langle \hat{a}_\pm^\dagger \hat{a}_\pm \rangle = \frac{N_{\mathrm{ph}}}{2} \Rightarrow \langle \hat{r}^- \rangle = 0, \tag{3.13a}$$

$$\mathrm{var}[\hat{a}_\pm^\dagger \hat{a}_\pm] = \frac{N_{\mathrm{ph}}}{4} \Rightarrow \mathrm{var}[\hat{r}^-] = \frac{1}{2}. \tag{3.13b}$$

Similarly, from

$$\hat{a}^\dagger_{\pm 45}\hat{a}_{\pm 45} = \hat{S}_x \pm \hat{S}_y + \hat{a}^\dagger_y \hat{a}_y \approx \frac{N_{\rm ph}}{2} \pm \sqrt{\frac{N_{\rm ph}}{2}}\,\hat{s}^-,$$

we also have

$$\langle \hat{s}^- \rangle = 0, \qquad \mathrm{var}[\hat{s}^-] = \frac{1}{2}. \tag{3.14}$$

Since the quantum mechanical uncertainty of the canonical light operators is Heisenberg limited,

$$\mathrm{var}[\hat{r}^-]\mathrm{var}[\hat{s}^-] = \frac{1}{4}, \tag{3.15}$$

the initial state will be a Gaussian state.

We need also take into account the phase evolution of the light field through the ac Stark shift interaction. Thus, we also make the standard approximation of identifying quadratures to the Poissonian total number and phase fluctuations,

$$\hat{S}_0 = \hat{a}^\dagger_x \hat{a}_x + \hat{a}^\dagger_y \hat{a}_y \simeq N_{\rm ph} + \sqrt{2N_{\rm ph}}\hat{r}^+, \tag{3.16}$$

where $[\hat{r}^+, \hat{s}^+] = i$ with the initial vacuum state of $\hat{r}^+$ and $\hat{s}^+$.

3.3 Quadrature light-matter interaction

Photonic quadratures can be identified for each cuboidal mode, where we rename the index j as dl, indicating the lth light mode measured by the dth detector, c.f., Fig. 3.2,

$$\begin{aligned} \hat{N}^{dl}_{\rm ph} = \hat{a}^\dagger_+ \hat{a}_+ + \hat{a}^\dagger_- \hat{a}_- &\simeq \sqrt{2N_{\rm ph}}\hat{r}^+_{dl} + N_{\rm ph}, \\ \hat{a}^\dagger_+ \hat{a}_+ - \hat{a}^\dagger_- \hat{a}_- &\simeq \sqrt{2N_{\rm ph}}\hat{r}^-_{dl}, \end{aligned} \tag{3.17}$$

with $[\hat{r}^\pm_{dl}, \hat{s}^\pm_{d'l'}] = i\delta_{dd'}\delta_{ll'}$. The average photon number, $\langle \hat{N}^{dl}_{\rm ph} \rangle = N_{\rm ph}$, is the same in all modes owing to the planar wavefront assumption.

Armed with the discrete description (3.17), the dispersive interaction (3.3) with a set of light modes along the BEC axis interacting for time τ, $\hat{H}_{\rm I} = \hbar(\hat{h}_{\rm I} +$

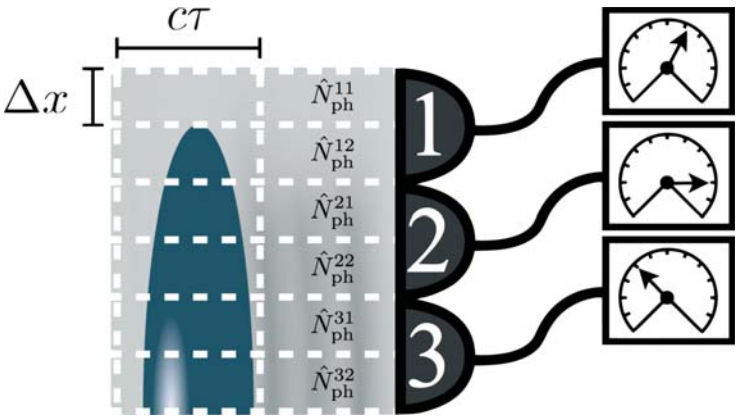

Figure 3.2: The planar coherent light field is discretized into cuboidal mode functions for the specific example of $N_{\rm L} = 2$. A set of light modes in the x direction after interacting with the atomic system are immediately detected, and the process repeats.

$\hat{h}_{\rm mf})(\Delta x/\tau)^{\frac{1}{2}}$, splits into a BEC mean field contribution,

$$\hat{h}_{\rm mf} = \kappa\sqrt{\frac{l_{\rm L}}{2N_0}}\sum_{dl} n_0(x_{dl})\,\frac{\alpha_0\hat{r}_{dl}^{+} + \alpha_1 m_F \hat{r}_{dl}^{-}}{\sqrt{\alpha_0^2 + \alpha_1^2 m_F^2}},$$

and a coupling of the quantum fluctuations,

$$\hat{h}_{\rm I} = \sqrt{2}\sum_{jdl}\kappa_j(x_{dl})\,\hat{x}_j\,\frac{\alpha_0\hat{r}_{dl}^{+} + \alpha_1 m_F \hat{r}_{dl}^{-}}{\sqrt{\alpha_0^2 + \alpha_1^2 m_F^2}}, \tag{3.18}$$

where

$$\kappa_j(x) = \kappa\sqrt{2l_{\rm L}}f_0^{+}(x)f_j^{-}(x).$$

We have neglected constant contributions and the relatively smaller $2^{\rm nd}$ order terms of the quadrature expansion of $\hat{n}_{\rm nc}(x,t)$, c.f., Eq. (2.47). The coupling constant $\kappa = -[(\alpha_0^2 + \alpha_1^2 m_F^2)d_0\eta]^{\frac{1}{2}}$ [84] governs the overall measurement strength. The light field with total photon flux Φ and cross-sectional area $A_{\rm L}$ has the on-resonance optical depth and cross-section, $d_0 = N_0\sigma_0/A_{\rm L}$ and $\sigma_0 = 3\lambda^2/2\pi$, respectively.

Although the light field is far-detuned, heating of the atomic system by an atomic absorption and spontaneous emission event occurs at the rate $\eta = \Phi\sigma_0\Gamma^2/4A_{\mathrm{L}}\Delta_{\mathrm{L}}^2$. This process is neglected in the current treatment, thus, restricted to times shorter than $1/\eta$. Decreasing η to allow longer interaction times requires increasing the optical depth to maintain κ.

As remarked, the BEC mean field induces a classical phase shift of the light ($\hat{h}_{\mathrm{mf}}$), ultimately having no affect on the quantum dynamics of the atomic system. The quantum fluctuations of the atomic density ($\hat{x}_j$) and light field number ($\hat{r}_{dl}^{+}$) and polarization ($\hat{r}_{dl}^{-}$) couple ($\hat{h}_{\mathrm{I}}$). Atomic density information is imprinted of the light field, and, by the detection of the photonic phase ($\hat{s}_d^{+}$) and $\pm 45^\circ$ polarization ($\hat{s}_d^{-}$) fluctuations in a pixel, yields information of (and causes back action on) a linear combination of many atomic modes.

We assume a temporal discretization such that only single light modes interact with the atomic system at any instance and are, hereafter, detected and the next light modes enter along the z direction. The propagation time of the mode through the BEC and the temporal resolution bandwidth of optical detection are both orders of magnitude faster than the msec-sec timescale of atomic evolution. Owing to finite spatial resolution, the dth detector pixel measures a sum of light quadratures

$$\hat{r}_d^{\pm} = \frac{1}{\sqrt{N_{\mathrm{L}}}}\sum_{l=1}^{N_{\mathrm{L}}} \hat{r}_{dl}^{\pm}, \qquad \hat{s}_d^{\pm} = \frac{1}{\sqrt{N_{\mathrm{L}}}}\sum_{l=1}^{N_{\mathrm{L}}} \hat{s}_{dl}^{\pm}, \tag{3.19}$$

where N_{L} is the number of light modes measured by each pixel. Here, we have implicitly assumed a dual-port detector where both the as Stark shift and Faraday rotation are (separately) measured by the detector pixel. An example of a dual-port detection scheme can be found in Ref. [43].

A physical description of the BEC dynamics should not depend on the arbitrary choice of the modal decomposition of the light field, here, the coarse graining mode parameters Δx, Δy, and τ [c.f., Eq. (3.17)]. Recalling the BEC dynamics are frozen in the y and z directions, only the discretization in the x (spatial) and z (temporal) directions is relevant. The dynamics will converge as the coarse graining is reduced, thus, in the following section we consider the continuous limits $\Delta x \to 0$ and $\tau \to 0$. In principle, the number and phase replacement (3.17) loses validity as the coherent state amplitudes vanishes in the limits. However, it

is the integrated effect of many light modes that is dynamically relevant, and the solution of the ensuing continuous evolution represents the system well.

The interaction time was considered to be so small that the temporal evolution of the mode function can be neglected. However, the dispersion of the light field propagating across the BEC is important, which we include in Sec. 4.2.6. We have also assumed that we may neglect the mode function evolution between the BEC and the detector. This is valid for short distances between the BEC and detector, or, a lens may be place in-between to refocus the mode functions giving a one-to-one correspondence. We will see later (Sec. 4.2.3) how this intermediate evolution can be directly incorporated into the theory.

CHAPTER 4

GAUSSIAN STATE FORMALISM

Only the first and second moments are required to fully characterize Gaussian states, allowing the full quantum description to simplify significantly. Additionally, Gaussian states are routinely produced and preserved by many experimental manipulations, thus, providing a strong motivation for their investigation. Indeed, in recent years, many tools for the analysis of the properties of Gaussian states have been established in the context of quantum information processing with continuous variables [95, 96].

Here, we utilise the machinery developed for Gaussian states to form our basis of the dynamical evolution of the BEC under measurement and subsequent analysis.

4.1 Gaussian states

For a system described with n bosonic modes with the annihilation operators $\hat{a}_j$ and the creation operators $\hat{a}_j^\dagger$, the canonical coordinates, $\hat{x}_j = (\hat{a}_j + \hat{a}_j^\dagger)/\sqrt{2}$ and $\hat{p}_j = i(\hat{a}_j^\dagger - \hat{a}_j)/\sqrt{2}$, are collected in $\hat{\mathbf{R}} = [\hat{x}_1, \hat{p}_1, \ldots, \hat{x}_n, \hat{p}_n]^T$. The commutation relations are given by

$$\left[\hat{R}_j, \hat{R}_k\right] = i\Omega_{jk}, \tag{4.1}$$

where Ω_{jk} are the elements of the symplectic matrix

$$\boldsymbol{\Omega} = \bigoplus_{k=1}^{n} \begin{bmatrix} 0 & 1 \\ -1 & 0 \end{bmatrix}. \tag{4.2}$$

Gaussian states are characterised by only the first, $[\mathbf{R}]_j = \langle \hat{\mathbf{R}}_j \rangle$, and second, $[\boldsymbol{\sigma}]_{jk} = \mathrm{cov}(\hat{\mathbf{R}}_j, \hat{\mathbf{R}}_k)$, moments of the canonical variables, $\hat{\mathbf{R}}$. The characteristic function $\chi[\hat{\rho}](\boldsymbol{\Lambda})$ of a Gaussian state, $\hat{\rho}$, is

$$\chi[\hat{\rho}](\boldsymbol{\Lambda}) = \exp\left(-\frac{1}{2}\boldsymbol{\Lambda}^T\boldsymbol{\Omega}\boldsymbol{\sigma}\boldsymbol{\Omega}^T\boldsymbol{\Lambda} - i\boldsymbol{\Lambda}^T\boldsymbol{\Omega}\mathbf{R}\right), \tag{4.3}$$

from which, the Weyl ordered averages can be obtained

$$\left\langle \left(\hat{x}_j^m \hat{p}_k^n\right)_W \right\rangle = (-i)^{m-n} \left.\frac{\partial^m \partial^n \chi[\hat{\rho}](\boldsymbol{\Lambda})}{\partial b_j^m \partial a_k^n}\right|_{\boldsymbol{\Lambda}=0}. \tag{4.4}$$

The Wigner distribution is obtained by the Fourier transform of the characteristic function,

$$W(\mathbf{X}) = \frac{1}{2^n \pi^{2n}} \int d^{2n}\boldsymbol{\Lambda} \exp\left(i\boldsymbol{\Lambda}^T\boldsymbol{\Omega}\mathbf{X}\right) \chi[\hat{\rho}](\boldsymbol{\Lambda}), \tag{4.5}$$

where $\boldsymbol{\Lambda} = [a_1, b_1, \ldots, a_n, b_n]$ and $\mathbf{X} = [x_1, p_1, \ldots, x_1, p_1]^T$. Thus, the Wigner function for the Gaussian state is given by

$$W(\mathbf{X}) = \frac{1}{\pi^n \sqrt{\det(\boldsymbol{\sigma})}} \exp\left[-\frac{1}{2}\left(\mathbf{X} - \mathbf{R}\right)^T \boldsymbol{\sigma}^{-1} \left(\mathbf{X} - \mathbf{R}\right)\right]. \tag{4.6}$$

It is useful to introduce the displacement operator of the system $\hat{D}(\boldsymbol{\lambda})$, from which, the characteristic function can be calculated $\chi[\hat{\rho}](\boldsymbol{\Lambda}) = \mathrm{Tr}[\hat{\rho}\hat{D}(\boldsymbol{\lambda})]$.

$$\hat{D}(\boldsymbol{\Lambda}) \equiv \hat{D}(\boldsymbol{\lambda}) = \bigotimes_{k=1}^{n} \hat{D}_k(\lambda_k) = \exp\left(i\mathbf{R}^T\boldsymbol{\Omega}\boldsymbol{\Lambda}\right), \tag{4.7}$$

where

$$\hat{D}_k(\lambda_k) = \exp(\lambda_k \hat{a}_k^\dagger - \lambda_k^* \hat{a}_k), \tag{4.8}$$

with $\lambda_k = (a_k + ib_k)/\sqrt{2}$. The resolution of the 2n-dimensional δ-function is

$$\mathrm{Tr}[\hat{D}(\boldsymbol{\lambda})] = \pi^n \delta^{2n}(\boldsymbol{\lambda}) = (2\pi)^n \, \delta^{2n}(\boldsymbol{\Lambda}). \tag{4.9}$$

4.1.1 Bilinear Hamiltonians

Bilinear Hamiltonians lead to linear symplectic transformations of the canonical variables, in particular, transformations of the form

$$\mathbf{R} \to \mathbf{F}\mathbf{R} + \mathbf{d}, \qquad \boldsymbol{\sigma} \to \mathbf{F}\boldsymbol{\sigma}\mathbf{F}^T. \tag{4.10}$$

Williamson's theorem, Appendix C, guarantees that any covariance matrix (symmetric and positive definite) can be diagonalized via a symplectic transformation,

$$\boldsymbol{\sigma} = \mathbf{S}^T\mathbf{W}\mathbf{S}, \tag{4.11}$$

where $\mathbf{S}$ is a symplectic transform, and $\mathbf{W}$ is in diagonal form with $\mathbf{W} = \bigoplus_{k=1}^{n} d_k \mathbf{I}_2$, where $\pm d_k$ are the eigenvalues of $i\boldsymbol{\Omega}\boldsymbol{\sigma}$. A thermal state is Gaussian with zero first moments and the covariance matrix is diagonal,

$$\boldsymbol{\sigma}_{\rm th} = \bigoplus_{k=1}^{n} \frac{1}{2}\left(1 + 2N_k\right)\mathbf{I}_2, \tag{4.12}$$

where $N_k = \left[\exp\left(\hbar\omega_k/k_{\rm B}T\right) - 1\right]^{-1}$ is the average number of thermal bosons in the kth mode with angular frequency ω_k and temperature, T. Thus, every Gaussian state can be generated from thermal states, and $N_k = d_k - 1/2$.

The symplectic transformations preserve the purity (determinant)

$$P = {\rm Tr}(\hat{\rho}^2) = \frac{1}{2^n\sqrt{\det(\boldsymbol{\sigma})}} = \frac{1}{\prod_{k=1}^{n} 2d_k}, \tag{4.13}$$

and the uncertainty principle,

$$\boldsymbol{\sigma} + \frac{i}{2}\boldsymbol{\Omega} \geq 0, \qquad \text{equivalently,} \qquad d_k \geq \frac{1}{2}. \tag{4.14}$$

Thus, a Gaussian state is only pure if and only if $N_k = 0$ ($d_k = \frac{1}{2}$, vacuum state), and, only a pure Gaussian state minimizes the uncertainty relation.

4.1.2 Transformation under homodyne measurement

We consider a total system of modes consisting of a system, s, and a probe system, p. Here, we seek to describe the affect on the system by measuring and subsequently tracing out the probe system. For ease of notation, we will allow first $2s$ canonical coordinates to be that of the atomic system and the final $2p$ to be that of the probe system.

If we measure the probe system and obtain the result μ, with the associated measurement operator $\hat{M}_\mu$, the system-probe density matrix $\hat{\rho}_{sp}$ transforms as

$$\hat{\rho}_{sp} \to \frac{\hat{\mathbb{I}}_{2s} \otimes \hat{M}_\mu \, \hat{\rho}_{sp} \, \hat{\mathbb{I}}_{2s} \otimes \hat{M}_\mu^\dagger}{p_\mu}, \tag{4.15}$$

where p_μ is the probability of the measurement outcome μ. The measured probe system is removed from the description by tracing it out, and we have the resulting density matrix for the system alone

$$\hat{\rho} = \frac{1}{p_\mu} \mathrm{Tr}_p \left[\hat{\mathbb{I}}_{2s} \otimes \hat{M}_\mu \, \hat{\rho}_{sp} \, \hat{\mathbb{I}}_{2s} \otimes \hat{M}_\mu^\dagger \right] = \frac{1}{p_\mu} \mathrm{Tr}_p \left[\hat{\rho}_{sp} \, \hat{\mathbb{I}}_{2s} \otimes \hat{\Pi}_\mu \right], \tag{4.16}$$

with $\hat{\Pi}_\mu = \hat{M}_\mu^\dagger \hat{M}_\mu$. An operator $\hat{\mathcal{O}}$ can be expanded on the displacement operators

$$\hat{\mathcal{O}} = \int \frac{d^{2n}\mathbf{\Lambda}}{(2\pi)^n} \chi[\hat{\mathcal{O}}](\mathbf{\Lambda}) \hat{D}(\mathbf{\Lambda})^\dagger. \tag{4.17}$$

Thus, we may write

$$\hat{\mathbb{I}}_{2s} \otimes \hat{\Pi}_\mu = \hat{\mathbb{I}}_{2s} \otimes \int \frac{d^{2p}\mathbf{\Lambda}_p}{(2\pi)^p} \chi[\hat{\Pi}_\mu](\mathbf{\Lambda}_p) \hat{D}(\mathbf{\Lambda}_p)^\dagger, \tag{4.18}$$

and

$$\hat{\rho}_{sp} = \int \frac{d^{2n}\mathbf{\Lambda}}{(2\pi)^n} \chi[\hat{\rho}_{sp}](\mathbf{\Lambda}) \hat{D}(\mathbf{\Lambda})^\dagger. \tag{4.19}$$

Using one additional identity

$$\mathrm{Tr}(\hat{\mathcal{O}}_1 \hat{\mathcal{O}}_2) = \int \frac{d^{2n}\mathbf{\Lambda}}{(2\pi)^n} \chi[\hat{\mathcal{O}}_1](\mathbf{\Lambda}) \chi[\hat{\mathcal{O}}_2](-\mathbf{\Lambda}), \tag{4.20}$$

we have for the resulting density matrix

$$\hat{\rho} = \frac{1}{p_\mu} \int \frac{d^{2s}\mathbf{\Lambda}_s}{(2\pi)^s} \left\{ \int \frac{d^{2p}\mathbf{\Lambda}_p}{(2\pi)^p} \chi[\hat{\rho}_{sp}](\mathbf{\Lambda}_s, \mathbf{\Lambda}_p) \chi[\hat{\Pi}_\mu](-\mathbf{\Lambda}_p) \right\} \hat{D}(\mathbf{\Lambda}_s)^\dagger. \quad (4.21)$$

The term in the curly brackets is the new characteristic function of the system

$$\chi[\hat{\rho}](\mathbf{\Lambda}_s) = \frac{1}{p_\mu} \int \frac{d^{2p}\mathbf{\Lambda}_p}{(2\pi)^p} \chi[\hat{\rho}_{sp}](\mathbf{\Lambda}_s, \mathbf{\Lambda}_p) \chi[\hat{\Pi}_\mu](-\mathbf{\Lambda}_p). \quad (4.22)$$

To proceed further, we must prescribe the form of the measurement operator. Using double homodyne detection, a Gaussian measurement can be performed with characteristic function

$$\chi[\hat{\Pi}_\mu](\mathbf{\Lambda}_p) = \frac{1}{\pi} \exp\left(-\frac{1}{2} \mathbf{\Lambda}_p^T \mathbf{\Omega} \boldsymbol{\sigma}_\mu \mathbf{\Omega}^T \mathbf{\Lambda}_p - i \mathbf{\Lambda}_p^T \mathbf{\Omega} \mathbf{R}_\mu \right), \quad (4.23)$$

where $\boldsymbol{\sigma}_\mu$ and $\mathbf{R}_\mu$ are the covariant matrix and first moments vector for the measurement outcome. To describe the measurement transformation, the modes are separated into system and probe (to be measured) modes

$$\boldsymbol{\sigma} = \begin{bmatrix} \mathbf{A} & \mathbf{C} \\ \mathbf{C}^T & \mathbf{B} \end{bmatrix}, \qquad \mathbf{R} = \begin{bmatrix} \mathbf{R}_s \\ \mathbf{R}_p \end{bmatrix}. \quad (4.24)$$

$\mathbf{A}$ ($\mathbf{B}$) is the covariance matrix for the system (probe) modes, and $\mathbf{C}$ is the covariance matrix between the two sets of modes, while $\mathbf{R}_s$ ($\mathbf{R}_p$) are the first moments of the system (probe) modes. The probability of the measurement outcome $\mathbf{R}_\mu$ is

$$p_\mu = \mathrm{Tr}[\hat{\rho}_{sp}\, \hat{\mathbb{I}}_{2s} \otimes \hat{\Pi}_\mu] = \frac{\exp\left[-\frac{1}{2} \mathbf{R}_\mu^T \left(\mathbf{B} + \boldsymbol{\sigma}_\mu \right)^{-1} \mathbf{R}_\mu \right]}{\pi \sqrt{\det(\mathbf{B} + \boldsymbol{\sigma}_\mu)}}. \quad (4.25)$$

Evaluating Eq. (4.22), one finds the system modes in a Gaussian state with the new covariance matrix

$$\mathbf{A}' = \mathbf{A} - \mathbf{C} \left(\mathbf{B} + \boldsymbol{\sigma}_\mu \right)^{-1} \mathbf{C}^T, \quad (4.26)$$

and new first moment vector

$$\mathbf{R}_s' = \mathbf{R}_s - \mathbf{C} \left(\mathbf{B} + \boldsymbol{\sigma}_\mu \right)^{-1} \mathbf{X}_\mu, \quad (4.27)$$

where $\mathbf{X}_\mu = \mathbf{R}_p - \mathbf{R}_\mu$.

We associate an ideal homodyne detection, projecting onto an eigenstate of the measured quadrature, with an infinitely squeezed Gaussian measurement. In this case [97],

$$\mathbf{A}' \to \mathbf{A} - \mathbf{C}\left(\boldsymbol{\pi}\mathbf{B}\boldsymbol{\pi}\right)^{MP}\mathbf{C}^T, \tag{4.28a}$$

$$\mathbf{R}_s' \to \mathbf{R}_s - \mathbf{C}\left(\boldsymbol{\pi}\mathbf{B}\boldsymbol{\pi}\right)^{MP}\mathbf{X}_\mu, \tag{4.28b}$$

where MP denotes the Moore-Penrose inverse. For p probes, and measuring the canonical position (momentum), we have $\boldsymbol{\pi} = \mathrm{diag}([\boldsymbol{\lambda}_1^T, \ldots, \boldsymbol{\lambda}_p^T])$ with $\boldsymbol{\lambda}_j = [1, 0]^T$ ($\boldsymbol{\lambda}_j = [0, 1]^T$). We need not specify the unmeasured first moment in $\mathbf{X}_\mu$, as the corresponding entry is multiplied by zero in Eqs. (4.28).

4.1.3 Quantum nondemolition variables

Quantum nondemolition measurements, or variables, initially arose in the context of gravity wave detection [98], where one wishes to perform beyond the standard quantum limit. A quantum nondemolition measurement is one where the uncertainty of the measured (QND) variable does not change during the subsequent natural evolution of the system (including during a continuous measurement), or, is invariant at specific times. Formally, this requires the measured observable $\hat{x}$ to fulfil $[\hat{x}(t_1), \hat{x}(t_2)] = 0$ in the Heisenberg picture. Here, the x quadrature of the free-mode associated with the BEC number and phase fluctuations (Sec. 2.4) is a continuous QND variable where the commutator is fulfilled for all times. The density oscillations being harmonic modes (Sec. 2.4) are stroboscopic QND variables, where the commutator is fulfilled periodically at half the frequency of the mode.

4.1.4 Continuous measurements: matrix Riccati differential equation

For the continuous monitoring of a quadrature, a natural choice, $\hat{G}$, of the Gaussian measurement operator (4.23) is one where the measurement variance of the quadrature decreases with the interrogation time, T, as $\propto 1/T$, reflecting the gradual increase of the knowledge of the quantum state. When it is not possible to directly enact such a measurement on the system, as considered here, it can be performed by constructing an interacting ancillary probe system. Entangling the two systems via their interaction, a subsequent projective measurement of the probe will yield information about the system and enact $\hat{G}$.

A continuous QND measurement requires the measured operator to commute with itself for all times, and in this case, the continuous measurement is equivalent to applying $\hat{G}$ for the total interrogation time with a single measurement result. In the non-QND case, the temporal limit $T \to 0$ is required to correctly account for the temporal evolution of the measured system. Under this temporal limit, the choice of $\hat{G}$ yields a continuum limit and one obtains a differential matrix Riccati equation for the covariance matrix [94, 99]

$$\dot{\mathbf{A}} = \mathbf{E} - \mathbf{D}\mathbf{A} - \mathbf{A}\mathbf{D}^T - \mathbf{A}\mathbf{M}\mathbf{M}^T\mathbf{A}, \tag{4.29}$$

being well known from classical optimal control [100]. Interestingly, a property of Gaussian states is that the covariance matrix evolution, Eq. (4.29), is independent of the specific outcomes of the measurement results. In contrast, the evolution of the first moments is driven by the (stochastic) measurement results,

$$d\mathbf{R} = -\mathbf{D}\mathbf{R}dt + \mathbf{A}\mathbf{M}\,d\mathbf{W}, \tag{4.30}$$

where the measurement result is now simulated with the Wiener increments $dW_j(t)$, and for the measured jth mode $[d\mathbf{W}]_j = dW_j(t)\boldsymbol{\lambda}_j$. The matrix $\mathbf{E}$ captures the environment backaction, while the coherent evolution of the system enters through $\mathbf{D}$. The measurement backaction is represented by $\mathbf{AM}$ and $\mathbf{AMM}^T\mathbf{A}$, depending on the measurement scheme $[\mathbf{M}]$ and the correlations between modes $[\mathbf{A}]$.

As the unmeasured evolution ($\mathbf{M} = \mathbf{0}$) corresponds to averaging over all measurement records [101], we have the intimate link $\mathbf{A}_{\mathrm{un}} = \mathbf{A} + \mathbf{A}_{\mathrm{ens}}$ between

the [un]measured covariance matrix $[\mathbf{A}_{\mathrm{un}}]$ $\mathbf{A}$ and the covariance matrix $\mathbf{A}_{\mathrm{ens}}$ of the stochastic trajectories $\mathbf{R}$. Consistent with this, taking the ensemble average of the solutions of Eq. (4.30) yields

$$\begin{aligned}\mathbf{A}_{\mathrm{ens}} &= \langle \mathbf{R}\mathbf{R}^T \rangle_{\mathrm{ens}} - \langle \mathbf{R} \rangle_{\mathrm{ens}} \langle \mathbf{R}^T \rangle_{\mathrm{ens}} \\ &= e^{-\mathbf{D}t} \int_0^t dt' e^{\mathbf{D}t'} \mathbf{A}(t') \mathbf{M}\mathbf{M}^T \mathbf{A}(t') e^{\mathbf{D}^T t'} e^{-\mathbf{D}^T t} \\ &= \mathbf{A}_{\mathrm{un}} - \mathbf{A}. \end{aligned} \tag{4.31}$$

If a steady-state exists for the covariance matrix, the steady-state equation, the so-called Algebraic Riccati equation, is

$$\mathbf{D}\mathbf{A} + \mathbf{A}\mathbf{D}^T + \mathbf{A}\mathbf{M}\mathbf{M}^T\mathbf{A} = \mathbf{E}, \tag{4.32}$$

and is solved by standard Schur decomposition methods [102].

4.2 Evolution of a BEC under continuous measurement

Having established the atomic system (Chapter 2), light field and light-matter interaction (Chapter 3), and Gaussian state methodologies (Sec. 4.1), we are now in position to describe the evolution of a BEC under continuous measurement. Here, the evolution equations for the second (Sec. 4.2.1) and first (Sec. 4.2.2) moments are obtained. We discus the roles of intermediate evolution between the BEC and detector (Sec. 4.2.3) and finite spatial resolution of the detector and unmeasured modes (Sec. 4.2.4). After taking the continuous spatial limit (Sec. 4.2.5), the dispersion of the light field as it propagates through the BEC is taken into account (Sec. 4.2.6).

4.2.1 Covariance matrix

To obtain the evolution equation for the covariance matrix, we consider the differential limit in time,

$$\dot{\mathbf{A}}(t) = \lim_{\tau\to 0} \frac{\mathbf{A}'(t+\tau) - \mathbf{A}(t)}{\tau}. \tag{4.33}$$

We assume all light modes are detected, while returning to finite resolution effects in Sec. 4.2.4. At the beginning of each time step, the system interacts with an uncorrelated set of light modes in their vacuum state

$$\boldsymbol{\sigma}(t) = \begin{bmatrix} \mathbf{A}(t) & \mathbf{0} \\ \mathbf{0} & \frac{\mathbf{I}_{2p}}{2} \end{bmatrix}. \tag{4.34}$$

After the interaction, we have to first-order in τ

$$\boldsymbol{\sigma}(t+\tau) = \begin{bmatrix} \mathbf{A}(t) + [\mathbf{E} - \mathbf{D}\mathbf{A}(t) - \mathbf{A}(t)\mathbf{D}^T]\tau & \sqrt{\frac{\tau}{2}}[\mathbf{A}(t)\mathbf{M} + \mathbf{N}] \\ \sqrt{\frac{\tau}{2}}[\mathbf{M}^T\mathbf{A}(t) + \mathbf{N}^T] & \frac{1}{2}\{\mathbf{I}_p + [\mathbf{M}^T\mathbf{A}(t)\mathbf{M}]\tau\} \end{bmatrix}, \tag{4.35}$$

where $\mathbf{E} = \mathbf{N}\mathbf{N}^T$. The rectangular matrices of 2×4 blocks accounting for the interaction between the atomic system and light, $\mathbf{M}$ and $\mathbf{N}$, are

$$[\mathbf{M}]_{j,dl} = -2\kappa_j(x_{dl})\sqrt{\Delta x} \begin{bmatrix} \mathbf{m}_{\mathrm{ac}} & \mathbf{m}_{\mathrm{Fr}} \end{bmatrix}, \tag{4.36}$$

$$[\mathbf{N}]_{j,dl} = -\kappa_j(x_{dl})\sqrt{\Delta x} \begin{bmatrix} \mathbf{m}_{\mathrm{ac}}^T & \mathbf{m}_{\mathrm{Fr}}^T \end{bmatrix}, \tag{4.37}$$

where

$$\mathbf{m}_{\text{ac}} = \begin{bmatrix} 0 & \frac{\alpha_0}{\sqrt{\alpha_0^2+\alpha_1^2 m_F^2}} \\ 0 & 0 \end{bmatrix}, \qquad \mathbf{m}_{\text{Fr}} = \begin{bmatrix} 0 & \frac{\alpha_1 m_F}{\sqrt{\alpha_0^2+\alpha_1^2 m_F^2}} \\ 0 & 0 \end{bmatrix}. \tag{4.38}$$

Thus,

$$[\mathbf{E}]_{jk} = [\mathbf{N}\mathbf{N}^T]_{jk} = \sum_{dl} \kappa_j(x_{dl})\kappa_k(x_{dl})\Delta x \begin{bmatrix} 0 & 0 \\ 0 & 1 \end{bmatrix}. \tag{4.39}$$

The block diagonal matrix $\mathbf{D}$ with 2×2 blocks

$$[\mathbf{D}]_j = \begin{bmatrix} 0 & -\omega_j \\ \omega_j & 0 \end{bmatrix}, \qquad [\mathbf{D}]_0 = \begin{bmatrix} 0 & 0 \\ \omega_0 & 0 \end{bmatrix}, \tag{4.40}$$

accounts for the harmonic rotation at frequency ω_j in all $\{\hat{x}_j, \hat{p}_j\}$ phase spaces with the exception of $[\mathbf{D}]_0$ accounting for the spreading of the BEC phase.

For the measurement update equation, Eq. (4.28a), where the light modes are measured and traced out, we need only consider $[\boldsymbol{\pi}\mathbf{B}\,(t+\tau)\,\boldsymbol{\pi}]^{MP}$ to zeroth order, as $\mathbf{C}\,(\tau) \sim \sqrt{\tau}$. To zeroth order,

$$[\boldsymbol{\pi}\mathbf{B}\,(t+\tau)\,\boldsymbol{\pi}]^{MP} \to \left(\frac{\boldsymbol{\pi}}{2}\right)^{MP} = 2\boldsymbol{\pi}, \tag{4.41}$$

being equivalent to neglecting the interaction evolution of the light for the covariance matrix. Using Eq. (4.41), $\mathbf{M}\boldsymbol{\pi} = \mathbf{M}$, and $\mathbf{N}\boldsymbol{\pi} = \mathbf{M}\mathbf{N}^T = \mathbf{0}$, we have the matrix Riccati differential equation, Eq. (4.29),

$$\dot{\mathbf{A}} = \mathbf{E} - \mathbf{D}\mathbf{A} - \mathbf{A}\mathbf{D}^T - \mathbf{A}\mathbf{M}\mathbf{M}^T\mathbf{A}. \tag{4.42}$$

Here, in the case where all the modes are measured, we have the relation

$$[\mathbf{M}\mathbf{M}^T]_{jk} = 4 \begin{bmatrix} 0 & 1 \\ 0 & 0 \end{bmatrix} [\mathbf{E}]_{jk} \begin{bmatrix} 0 & 0 \\ 1 & 0 \end{bmatrix}. \tag{4.43}$$

4.2.2 First moments

We now turn to the stochastic equation for the first moments. Before the interaction, first moments are

$$\mathbf{R}(t) = \begin{bmatrix} \mathbf{R}_s(t) \\ \mathbf{R}_p(t) = \mathbf{0} \end{bmatrix}. \tag{4.44}$$

After the interaction, we have to first order,

$$\mathbf{R}(t+\tau) = \begin{bmatrix} [\mathbf{I}_{2s} - \mathbf{D}\tau]\,\mathbf{R}_s(t) \\ \left[\mathbf{M}^T\mathbf{R}_s(t) + \mathbf{d}\right]\sqrt{\tau} \end{bmatrix}, \tag{4.45}$$

where

$$[\mathbf{d}]_{dl} = -\kappa\sqrt{\frac{\Delta x l_{\mathrm{L}}}{2N_0}}n_0(x_{dl}) \begin{bmatrix} 0 \\ 1 \end{bmatrix}. \tag{4.46}$$

Using the measurement update equation, Eq. (4.28b), we have

$$\mathbf{R}'_s(t+\tau) = [\mathbf{I}_{2s} - \mathbf{D}\tau]\,\mathbf{R}_s(t) - \mathbf{A}(t)\mathbf{M}\sqrt{2\tau}\mathbf{X}_\mu. \tag{4.47}$$

The probability distribution of $\mathbf{X}_\mu$ is $\propto \exp\{\mathbf{X}_\mu^T[\boldsymbol{\pi}\mathbf{B}(t+\tau)\boldsymbol{\pi}]^{MP}\mathbf{X}_\mu/2\}$, thus, $\sqrt{2\tau}\mathbf{X}_\mu$ will be distributed as $\propto \exp\{\mathbf{X}_\mu^T\boldsymbol{\pi}\mathbf{X}_\mu/2\tau + O(\tau^0)\}$. Hence, as τ decreases, the individual measurement results $\sqrt{2\tau}\mathbf{X}_\mu$ are independently distributed with the Gaussian distribution of standard deviation τ. In the infinitesimal limit, $\tau \to dt$, and $\mathbf{R}'_s(t+\tau) - \mathbf{R}_s(t) \to d\mathbf{R}$, we have the stochastic equation, Eq. (4.30),

$$d\mathbf{R} = -\mathbf{D}\mathbf{R}dt + \mathbf{A}\mathbf{M}\,d\mathbf{W}, \tag{4.48}$$

where the measurement results $\sqrt{2\tau}\mathbf{X}_\mu$ are now simulated with the Wiener increments $dW_j(t)$, and for the measured jth mode $[d\mathbf{W}]_j = dW_j(t)\boldsymbol{\lambda}_j$.

4.2.3 Intermediate transformations

Here, we consider the effect of linear canonical transformations (Sec. A) of the light field between the BEC and detector, e.g., free evolution or lenses. With the transform matrix $\mathbf{T}$, the effect on the update equations Eqs. (4.28) is

$$\mathbf{A}' = \mathbf{A} - \mathbf{C}\mathbf{T}^T\left(\boldsymbol{\pi}\mathbf{T}\mathbf{B}\mathbf{T}^T\boldsymbol{\pi}\right)^{MP}\mathbf{T}\mathbf{C}^T, \tag{4.49a}$$

$$\mathbf{R}'_s = \mathbf{R}_s - \mathbf{C}\mathbf{T}^T\left(\boldsymbol{\pi}\mathbf{T}\mathbf{B}\mathbf{T}^T\boldsymbol{\pi}\right)^{MP}\mathbf{X}'_\mu, \tag{4.49b}$$

where $\mathbf{X}'_\mu$ indicates the measurement results of the new quadratures. Again, the Moore-Penrose inverse is taken to zeroth order, i.e.,

$$\left(\boldsymbol{\pi}\mathbf{T}\mathbf{B}\mathbf{T}^T\boldsymbol{\pi}\right)^{MP} \to \left(\boldsymbol{\pi}\frac{\mathbf{T}\mathbf{T}^T}{2}\boldsymbol{\pi}\right)^{MP}. \tag{4.50}$$

Restricting the transformations to not mixing the measured and the unmeasured quadratures, then, $\boldsymbol{\pi}\mathbf{T} = \mathbf{T}\boldsymbol{\pi}$, $\boldsymbol{\pi}\mathbf{T}^{-1} = \mathbf{T}^{-1}\boldsymbol{\pi}$, and,

$$\left(\boldsymbol{\pi}\frac{\mathbf{T}\mathbf{T}^T}{2}\boldsymbol{\pi}\right)^{MP} = 2\boldsymbol{\pi}[\mathbf{T}\mathbf{T}^T]^{-1}\boldsymbol{\pi}. \tag{4.51}$$

Consequently, the update equation for the covariance matrix is invariant to the transformation

$$\mathbf{A}' = \mathbf{A} - \mathbf{C}(2\boldsymbol{\pi})\mathbf{C}^T, \tag{4.52}$$

however, the update equation for the first moments depends on $\mathbf{T}$

$$\mathbf{R}'_s = \mathbf{R}_s - \mathbf{C}\mathbf{T}^{-1}(2\boldsymbol{\pi})\mathbf{X}'_\mu. \tag{4.53}$$

This reflects that the individual pixels now receive different modes of light (information), however, the information of the atomic system is still fully recovered. This is not the case if the transformation mixes the measured and unmeasured quadratures, as it has the consequence of losing formation about the atomic system (on the unmeasured quadrature). Thus, $\mathbf{A}'$ depends on $\mathbf{T}$, and the purity of the atomic system is only partially restored by the measurement.

4.2.4 Finite spatial resolution and unmeasured modes

The above derivations of the atomic evolution assumes all of the light modes are detected. In reality, a detector will have a finite resolution length scale, and associated light modes, it can resolve. We model this here by assuming each detector pixel only measures the homogenous mode of the light modes entering the pixel [Eq. (3.19)]. By applying the measurement update equations (4.28) only for this mode, the measurement backaction matrix $\mathbf{M}$ becomes

$$\mathbf{M} \to [\mathbf{M}]_{jd} = -\frac{2}{\sqrt{l_\mathrm{D}}}\sum_l \kappa_j(x_{dl})\Delta x \left[\begin{array}{cc} \mathbf{m}_\mathrm{ac} & \mathbf{m}_\mathrm{Fr} \end{array}\right], \tag{4.54}$$

where $N_{\mathrm{L}} = l_{\mathrm{D}}/\Delta x$, and we have

$$[\mathbf{M}\mathbf{M}^T]_{jk} = \frac{4}{l_{\mathrm{D}}} \sum_{dll'} \kappa_j(x_{dl})\kappa_k(x_{dl'})\Delta x^2 \begin{bmatrix} 1 & 0 \\ 0 & 0 \end{bmatrix}. \tag{4.55}$$

Similarly, by not measuring the ac Stark shift, or, Faraday rotation, the associated modes are not included in the update equations (4.28), amounting to setting $\mathbf{m}_{\mathrm{ac}} = \mathbf{0}$, or, $\mathbf{m}_{\mathrm{Fr}} = \mathbf{0}$, respectively. I.e.,

$$\begin{bmatrix} \mathbf{m}_{\mathrm{ac}} & \mathbf{m}_{\mathrm{Fr}} \end{bmatrix} \to \begin{bmatrix} 0 & 1 \\ 0 & 0 \end{bmatrix}, \tag{4.56}$$

and $\kappa \to -\alpha_0(d_0\eta)^{\frac{1}{2}}$, and, $\kappa \to -\alpha_1 m_F(d_0\eta)^{\frac{1}{2}}$, respectively. In all these cases, the information of that atomic system imprinted on the unmeasured modes leads to only partial purity restoration by measurement.

4.2.5 The continuous spatial limit

As discussed prior (Sec. 3.3), we take the continuous limit $\Delta x \to 0$ to avoid the dynamics depending on the discretization parameter (Δx) of our modal decomposition ansatz of the light field (Sec. 3.2.1). Taking the continuous spatial limit $\Delta x \to 0$, we have for the environment backaction matrix

$$[\mathbf{E}]_{jk} = \begin{bmatrix} 0 & 0 \\ 0 & \kappa_{jk}^2 \end{bmatrix}, \quad \text{with} \quad \kappa_{jk}^2 = \int dx \kappa_j(x)\kappa_k(x), \tag{4.57a}$$

and the measurement backaction matrices

$$[\mathbf{M}]_{jd} = \nu_{jd} \begin{bmatrix} \mathbf{m}_{\mathrm{ac}} & \mathbf{m}_{\mathrm{Fr}} \end{bmatrix}, \qquad [\mathbf{M}\mathbf{M}^T]_{jk} = \begin{bmatrix} K_{jk}^2 & 0 \\ 0 & 0 \end{bmatrix}, \tag{4.57b}$$

with

$$\nu_{jd} = -\frac{2}{\sqrt{l_{\mathrm{D}}}} \int_d dx \kappa_j(x), \qquad K_{jk}^2 = \sum_d \nu_{jd}\nu_{kd}. \tag{4.57c}$$

Only for pixel sizes (l_{D}) much smaller than the variations of $\kappa_j(x)$ and $\kappa_k(x')$ does $[\mathbf{M}\mathbf{M}^T]_{jk}$ become equivalent to the ideal full information retrieval case (4.43), i.e., $K_{jk}^2 = 4\kappa_{jk}^2$.

In case of Eq. (3.3), the atoms are prepared in a particular hyperfine state $|F, m_F\rangle$ and the light field is $\sigma_\pm$ polarised. This requires only phase shift measurements of the ac Stark shift for complete information recovery. The above formalism, Eqs. (4.57), holds with the replacements,

$$\left[\begin{array}{cc} \mathbf{m}_{\text{ac}} & \mathbf{m}_{\text{Fr}} \end{array}\right] \to \left[\begin{array}{cc} 0 & 1 \\ 0 & 0 \end{array}\right], \quad \text{and} \quad \kappa \to -\left(\alpha_0 \pm \alpha_1 m_F\right)\left(d_0 \eta\right)^{\frac{1}{2}}. \tag{4.58}$$

4.2.6 Light dispersion: the measurement kernel

The treatments [50, 51] show that the natural dispersion of the light field while propagating through the BEC leads to a resolution limit l_{R}. This finite resolution, and dependence of $l_{\text{R}} = (l_\perp \lambda)^{\frac{1}{2}}$, can be understood in terms of the Raleigh length, demonstrating that l_{R} represents the smallest width of a light mode that has a limited diffraction across the BEC. Crudely, smaller light modes will diffract across the BEC and interact with a broad range of spatial regions. To account for the dispersion, and obtain agreement with [50, 51], we include the measurement kernel $\mathcal{K}_\alpha(x)$, and for $l_\perp > \lambda$,

$$\mathcal{K}_\alpha(x) = \frac{1}{2\pi}\int dk e^{-\frac{(\alpha l_{\text{R}} k)^4}{64\pi^2}} e^{ikx}. \tag{4.59}$$

The environment backaction couplings become

$$\kappa_{jk}^2 \to \bar{\kappa}_{jk}^2 = \int dx \int dx' \mathcal{K}_{\sqrt[4]{2}}(x - x')\kappa_j(x)\kappa_k(x'), \tag{4.60}$$

while the measurement backaction couplings become

$$\nu_{jd} \to \bar{\nu}_{jd} = -\frac{2}{\sqrt{l_{\text{D}}}}\int_d dx \int dx' \mathcal{K}_1(x - x')\kappa_j(x'). \tag{4.61}$$

The measurement kernel (diffraction) smears out spatial features smaller than l_{R}, decoupling [$\int dx \kappa_j(x) = 0$ for $j > 0$] high lying atomic modes with shorter spatial variations that as $\sim l_x/j$ (Fig. 4.1). The effect of which was observed in simulations of stochastic master equations investigating the probing and cooling via feedback of a BEC [47, 51, 103]. Smaller l_{R} caused an increased heating and a reduction in the effectiveness of low-order feedback schemes owing to the excitation of the otherwise decoupled higher-order modes.

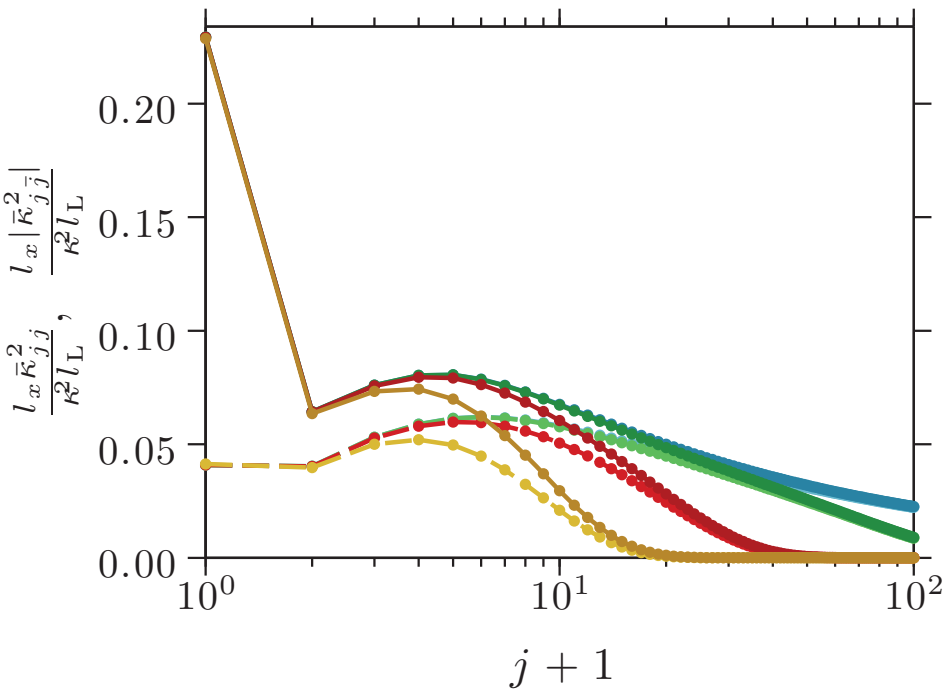

Figure 4.1: Shows the diagonal $\bar{\kappa}^2_{jj}$ (solid) and off-diagonal $\bar{\kappa}^2_{j\bar{j}}$ (dashed) couplings with $\bar{j} = j + 2$ for the ideal detector (blue) and for $l_{\mathrm{R}} = (0.2977, 0.6306, 1.0658)$ $[\lambda = (780.24\mathrm{nm}, 3.5\mu\mathrm{m}, 10\mu\mathrm{m})]$ corresponding to (green, red, yellow). The lines are to guide the eye between discrete j values.

CHAPTER 5

RESULTS AND ANALYSIS

Having specified the theoretical formalism, we now turn to the dynamics of the probed atomic system. The covariance matrix contains the correlations of the system (e.g., squeezing, purity, entanglement) and evolves independently (4.29) of the stochastic measurement results. We first analyse this evolution Sec. 5.1, and later in Sec. 5.2, we return to the stochastic evolution of the displacements (4.30) and the application of feedback. Finally in Sec. 5.3, we discuss the production of spatial and momentum number correlations by continuous probing with a spatially inhomogeneous probe and homogeneous stroboscopic probing.

5.1 Evolution of atomic correlations

In this section we consider the evolution of atomic correlations (4.29) in detail, characterising their relationship to physical parameters. First, we consider the evolution under continuous measurement (Sec. 5.1.1), and then, discuss the application of temporally modulated measurements. In particular, the production of selective squeezing (Sec. 5.1.2) and entanglement (Sec. 5.1.3) of modes via stroboscopic probing. The atomic interactions play an important role in the measurement scheme and are discussed in Sec. 5.1.4. For finite spatial detector resolution, the geometry of the detector establishes the subset of modes that are progressively decohered during the measurement, Sec. 5.1.5.

5.1.1 Evolution under the continuous measurement

The atomic system evolves dynamically following the frequency spectrum $\{\omega_j\}$, to which, the measurement strengths $\bar{\kappa}_{jj}^2$ must be comparable to temporally resolve the associated atomic density oscillations. This is reflected in Fig. 5.1 illustrating the variances $\mathrm{var}\,[\hat{x}_j]$ and $\mathrm{var}\,[\hat{p}_j]$ and covariances $\mathrm{covar}\,[\hat{x}_j, \hat{p}_j]$, assuming a perfectly resolving detector (4.43). Figure 5.1 demonstrates that density oscillation modes ($j > 0$) feature a transient minimum squeezing of the measured $\hat{x}_j$ quadrature before the anti-squeezed $\hat{p}_j$ rotates into $\hat{x}_j$. Thereafter, a steady-state is reached depending on the ratio of the measurement to rotation rates, $\tilde{\kappa}_{\omega_j} = \bar{\kappa}_{jj}^2/\omega_j$.

In describing the evolution of the covariance matrix of a particular mode j, $[\mathbf{A}]_{jj}$, reasonable agreement is found by assuming the modes are independently measured, i.e., $\bar{\kappa}_{jk}^2 \to 0$ for $j \neq k$. We will assume this for the remainder of this subsection. The unmeasured evolution of the zeroth mode is then

$$[\mathbf{A}_{\mathrm{un}}]_{00} = \frac{1}{2}\begin{bmatrix} 1 & -\omega_0 t \\ -\omega_0 t & 1 + 2\bar{\kappa}_{00}^2 t + \omega_0^2 t^2 \end{bmatrix}. \tag{5.1}$$

The natural evolution causes ballistic ($\propto t^2$) expansion of $\hat{p}_0$ and establishes the correlation between $\hat{x}_0$ and $\hat{p}_0$. The coupling to the probe system (light) to the $\hat{x}_0$ quadrature leads to an additional diffusive ($\propto t$) expansion of $\hat{p}_0$. Under the measurement, we have

$$[\mathbf{A}]_{00} = \frac{1}{2}\begin{bmatrix} \frac{1}{1+2\bar{\kappa}_{00}^2 t} & -\frac{\omega_0 t}{1+2\bar{\kappa}_{00}^2 t} \\ -\frac{\omega_0 t}{1+2\bar{\kappa}_{00}^2 t} & \frac{(1+2\bar{\kappa}_{00}^2 t)^2 + \omega_0^2 t^2}{1+2\bar{\kappa}_{00}^2 t} \end{bmatrix}, \tag{5.2}$$

and the backaction diffusion acts to preserve the uncertainty principle as the uncertainty of the measured $\hat{x}_0$ reduces. The total atom number observable $\hat{N}_0$ pertaining to the zeroth mode is a QND variable and undergoes the expected QND squeezing of $\hat{x}_0$ [104]. As the conjugate quadrature $\hat{p}_0$ depends on the progressively squeezed $\hat{x}_0$, the ballistic expansion of the BEC phase spreading ($\hat{p}_0$) is suppressed during probing, giving way to a solely diffusive expansion for $2\bar{\kappa}_{00}^2 t \gg 1$. Similarly, $\mathrm{covar}\,[\hat{x}_0, \hat{p}_0] \propto t \to \mathrm{const}$. However, the ballistic expansion associated with the natural evolution now features in the displacement

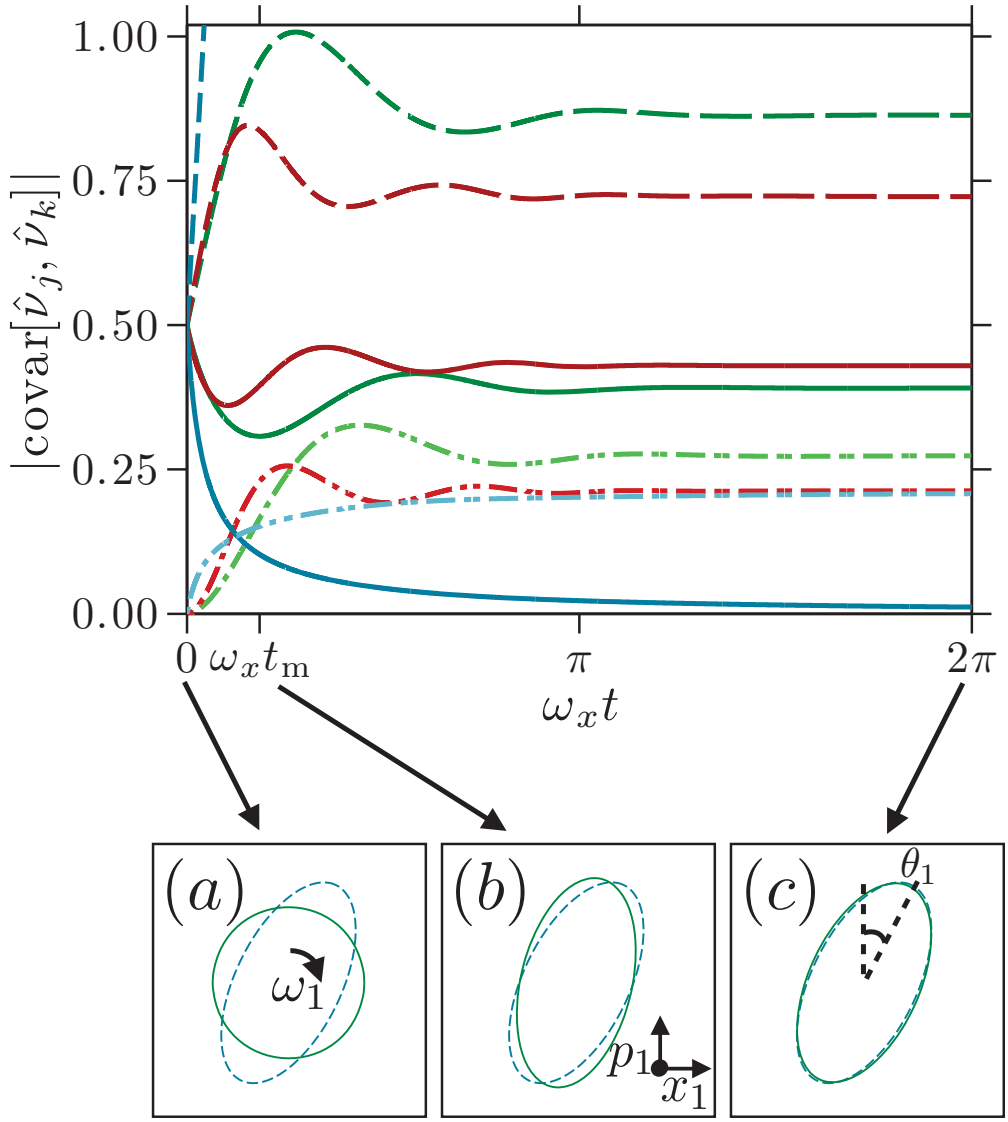

Figure 5.1: Illustrates the temporal dynamics of $\mathrm{var}\,[\hat{x}_j]$ (solid), $\mathrm{var}\,[\hat{p}_j]$ (dashed), and $\mathrm{covar}\,[\hat{x}_j, \hat{p}_j]$ (dashed-dotted), of the zeroth (blue), first (green), and second (red) modes, for $\bar{\kappa}_{11}^2 = \omega_x$. The uncertainty ellipse of the Gaussian Wigner function of the first mode (green) is illustrated at times $\omega_x t = (0, \omega_x t_\mathrm{m}, 2\pi)$ with the corresponding steady-state prediction Eq. (5.5) (dashed blue). Initially a circle (a), the distribution is squeezed along the x_1-axis. However, the antisqueezed p_1 quadrature rotates x_1, yielding a transient minimum squeezing of $\hat{x}_1$ (b). Ultimately, the dynamics average yielding a steady-state (c).

of $\hat{p}_0$,

$$[\mathbf{A}_{\text{ens}}]_{00} = \frac{\bar{\kappa}_{00}^2 t}{1 + 2\bar{\kappa}_{00}^2 t} \begin{bmatrix} 1 & -\omega_0 \\ -\omega_0 & \omega_0^2 t^2 \end{bmatrix}. \tag{5.3}$$

In the case of the density oscillations, the mode j has the unmeasured evolution

$$[\mathbf{A}_{\text{un}}]_{jj} = \frac{1}{8} \begin{bmatrix} 4(1 + \bar{\kappa}_{jj}^2 t) - \tilde{\kappa}_{\omega_j} \sin 2\omega_j t & \tilde{\kappa}_{\omega_j} \sin^2 \omega_j t \\ \tilde{\kappa}_{\omega_j} \sin^2 \omega_j t & 4(1 + \bar{\kappa}_{jj}^2 t) + \tilde{\kappa}_{\omega_j} \sin 2\omega_j t \end{bmatrix}. \tag{5.4}$$

The harmonic evolution of the mode spreads the backaction diffusion ($\bar{\kappa}_{jj}^2 t/2$) equally over the two quadratures, while interaction induced oscillations also feature. The corresponding steady-state covariance matrix under measurement is

$$\mathbf{A}_{jj}^{\text{ss}} = \frac{1}{4\tilde{\kappa}_{\omega_j}} \begin{bmatrix} [2(a_j - 1)]^{\frac{1}{2}} & a_j - 1 \\ a_j - 1 & [2(a_j - 1)a_j^2]^{\frac{1}{2}} \end{bmatrix}, \quad \text{with} \quad a_j = [1 + 4\tilde{\kappa}_{\omega_j}^2]^{\frac{1}{2}}. \tag{5.5}$$

The squeezing of $\hat{x}_j$ becomes significant for $\tilde{\kappa}_{\omega_j} \gg 1$, while for $1 \gg \tilde{\kappa}_{\omega_j}$, $\mathbf{A}_{jj}^{\text{ss}}$ is only slightly perturbed from initial vacuum fluctuations. Also owing to the competition between the harmonic rotation and the squeezing of $\hat{x}_j$ by the measurement backaction, maximal squeezing occurs along the quadrature $\hat{q}_j = \hat{x}_j \cos\theta_j - \hat{p}_j \sin\theta_j$ [Fig. 5.1(c)] where $\theta_j = 1/(4\tilde{\kappa}_{\omega_j})^{\frac{1}{2}}$ and $\theta_j = \pi/4 - \tilde{\kappa}_{\omega_j}/2$ in the two regimes, respectively. The steady-state can allow for variable state preparation, but any prior energy difference of the steady-state (5.5) and initial state will be funnelled into to the first moments that additionally grow with $\bar{\kappa}_{jj}^2 t$ ($\mathbf{A}_{\text{ens}} = \mathbf{A}_{\text{un}} - \mathbf{A}$). This residual energy can be damped through the feedback scheme introduced in Sec. 5.2.

In addition to the individual modal dynamics, intermodal correlations, and potential entanglement, develop via the off-diagonal couplings $\bar{\kappa}_{jk}^2$, before succumbing to a steady-state under continuous probing. Owing to the harmonic evolution of the density oscillations, we have seen here that the generation of squeezing and correlations is limited by a dynamical averaging. In the following subsections we will bypass these limitations by stroboscopically probing, investigating the generation of squeezing (5.1.2) and entanglement (5.1.3) of specific modes.

5.1.2 Stroboscopic squeezing

For a given density, the rate of squeezing can be increased by increasing the atomic depumping rate, η. Alternatively squeezing the $\hat{x}_j^0$ quadrature of the time dependent $\hat{x}_j(t) = \hat{x}_j^0 \cos\omega_j t + \hat{p}_j^0 \sin\omega_j t$ is possible by applying a temporally modulated field. The production of a squeezed oscillator by nondemolition stroboscopic probing was initially proposed in the context of gravity wave detection [98, 105, 106], and, has found application in mechanical oscillators [107, 108] and oscillator spin states of atomic ensembles [33, 109], in which, it was recently demonstrated [33]. Here, we implement stroboscopic probing with a sequence of constant intensity pulses determined by one or more frequencies ϖ_i. The timings t_l and durations Δt_l of the pulses are determined by ensuring, for each frequency, that $\varpi_i t$ is within $\Delta\varphi/2$ from a multiple of 2π. Probing at the single frequency $\varpi = 2\omega_j$ amounts to a train of n pulses centred on times $\omega_j t_l = [0, \pi, 2\pi, \ldots, (n-1)\pi]$ with identical durations, $\Delta t_l = \Delta t = \Delta\varphi/\varpi$. Such a field squeezes the $\pm\hat{x}_j^0$ quadrature, while avoiding its anti-squeezing at intermediate times. This enables squeezing well beyond the continuous probing case for the same strength κ. For small $\Delta\varphi$, effective QND probing of $\hat{x}_j^0$ is expected, and hence, $\mathrm{var}[\hat{x}_j^0]_{\mathrm{QND}} = 1/2(1+2\bar{\kappa}_{jj}^2 T)$ [104] with $T = n\Delta t$. This is observed (red line) in Fig. 5.2, where the first quarter of the trace squeezes the 3rd mode.

The atomic multimodal system is far from the single-mode squeezing picture. However, if no other mode nor coupled correlation has a rational frequency ratio to ω_j, the pulse train only addresses the jth mode. This modal selectivity is illustrated in Fig. 5.2, where the variances of modes 1 and 5 are essentially unaffected during probing of the 3rd mode. Here, the atomic interactions provide an irregular spectrum of mode frequencies (Sections 2.5 and 5.1.4) allowing separate addressing without crosstalk.

The simultaneous squeezing of two modes, j and k, is achieved with the two frequencies, $\varpi_1 = 2\omega_j$ and $\varpi_2 = 2\omega_k$, as featured in Fig. 5.2 for modes 1 and 5 after the time $\omega_x t = 25\pi$. The probing sequence is now out-of-phase with the 3rd mode, and hence, its prior squeezing is progressively lost returning to initial vacuum values. The final 5% of the sequence demonstrates reinitialization of all modes to vacuum fluctuations by switching to weak continuous probing. The preservation of vacuum fluctuations of the nontargeted modes, the loss of squeezing

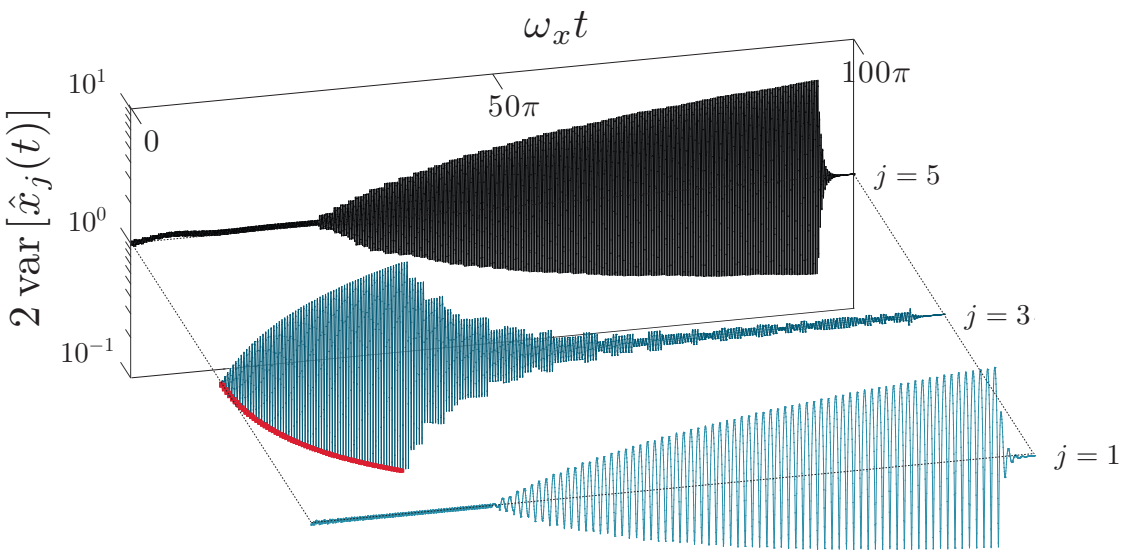

Figure 5.2: The atomic modes can be selectively addressed and squeezed, illustrated here, where first the 3rd mode, and subsequently, modes 1 and 5 are squeezed. The 3rd mode is squeezed until $\omega_x t = 25\pi$ by the stroboscopic probing with $\kappa^2 = 100\omega_x/2\pi$, $\varpi = 2\omega_3$ and $\Delta\varphi/2\pi = 0.05$. Thereafter, the dual squeezing is performed with $\varpi_1 = 2\omega_1$, $\varpi_2 = 2\omega_5$, and $\Delta\varphi/2\pi = 0.1$, until the final 5% of the sequence that is continuously probed with $\kappa^2 = 50\omega_x/2\pi$. The detector pixel width is taken to be $l_\mathrm{D} = l_x/10$.

of the 3rd mode, and the reinitialization of all modes to vacuum fluctuations, featured in Fig. 5.2, are demonstrations of the interplay between atomic dynamics, measurement strength, and stroboscopic probing, enacting a quantum eraser.

To further assess the performance of the operations, we study squeezing of the 3rd mode in Fig. 5.3 (similar results are found for other modes and for the joint squeezing or entangling of pairs of modes). The rate of squeezing is determined by $\Delta\phi$, as the accumulated probing time $T \propto \Delta\phi$ (inset). However, only for smaller $\Delta\phi$, the x-quadrature is probed in a QND fashion (red line), while the squeezing for larger $\Delta\phi$ is suboptimal as a result of the inadvertent probing of the p-component. The figure also addresses crosstalk between the $j = 1, 3, 5$ subsystem and its complement through the purity P of its reduced density matrix $\hat{\rho}_o$. The

Hellinger distance $D_{\mathcal{H}} = \mathrm{Tr}[\hat{\rho}_o^{\frac{1}{2}} - (\hat{\rho}_d)^{\frac{1}{2}}]^2/2$ [110] quantifies the selectivity within the subsystem. The desired state $\hat{\rho}_d$ assumes identical $\mathbf{R}$ to $\hat{\rho}_o$, but with all blocks $[\mathbf{A}]_{jk}$, except $j = k = 3$, replaced by their initial vacuum values. Excellent selectivity ($D_{\mathcal{H}} \simeq 0$) and little crosstalk ($P \simeq 1$) are observed for small $\Delta\phi$. For comparison (dotted lines), a noninteracting atomic system demonstrates similar squeezing, however, the corresponding linear spectrum $\omega_j = \omega_x j$ (Sections 2.5 and 5.1.4) results in significant crosstalk and poor mode selectivity.

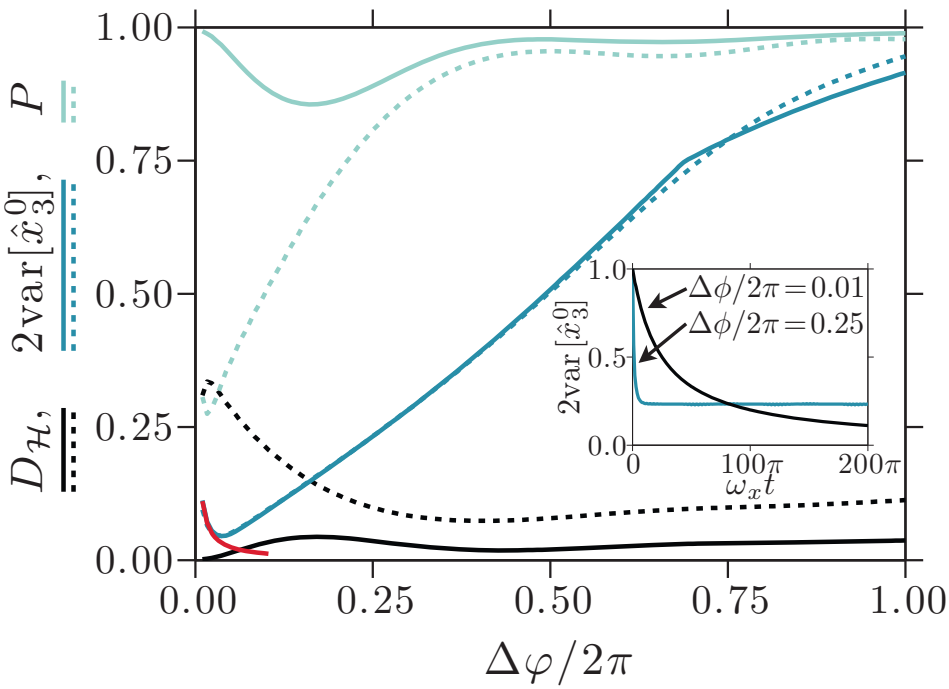

Figure 5.3: The squeezing of the 3rd mode after stroboscopically probing ($\kappa^2 = 100\omega_x/2\pi$ and $l_{\mathrm{D}} = l_x/10$) for 100 trap periods is shown, while the temporal evolution of the quadrature variance $\mathrm{var}[\hat{x}_3^0]$ is illustrated in the inset. Dotted lines indicate the results of the noninteracting atomic system for comparison. For small $\Delta\phi$ (pulse duration), $\mathrm{var}[\hat{x}_3^0]$ follows the QND result (red line, see text), while for larger $\Delta\phi$, the squeezing is faster but suboptimal. Excellent selectivity, Hellinger distance $D_{\mathcal{H}} \simeq 0$, and little crosstalk, Purity $P \simeq 1$, are observed for small $\Delta\phi$.

5.1.3 Stroboscopic entanglement

A probe transmitted through two atomic media reveals information about their collective rather than individual properties and may hence lead to their mutual entanglement [104]. Similarly, we may entangle two modes, j and k, of a single BEC by probing the density in a manner that does not discriminate contributions from the individual modes. The modes' respective spatial signatures, $\sim f_0^+(x)f_j^-(x)$ and $\sim f_0^+(x)f_k^-(x)$, must be indistinct ($\bar{\kappa}_{jk}^2 \neq 0$). Partial temporal distinguishability, owing to different oscillation frequencies ω_j and ω_k, is avoided by stroboscopically probing with a train of pulses at the single frequency $\varpi = \omega_j + \omega_k$. Analogous to the case of squeezing, entanglement is formed by squeezing collective variables of the modes, also allowing selective addressing of modes as illustrated in Fig. 5.4. The absolute value of the covariance matrix elements of the $j = 1, 3, 5$ subsystem is shown for (a) the steady-state of continuous probing and (b) stroboscopic probing for 100 trap periods. Although both cases reach the same level of entanglement of modes 1 and 3, the continuous probing requires a larger strength κ, addresses a swathe of modes, and causes significant squeezing.

The bipartite entanglement between modes j and k can be quantified by the logarithmic negativity $E_{jk} = \log_2 \left|\left|\hat{\rho}_{jk}^{\mathrm{Tp}}\right|\right|_{\mathrm{Tr}}$ [111] of the bipartite reduced density matrix $\hat{\rho}_{jk}$, where Tp denotes the partial transpose and $||\cdot||_{\mathrm{Tr}}$ the trace norm. Figure 5.5(a) shows the temporal buildup of entanglement between modes $j = 1$ and $k = 3$, and the comparison to an effective QND probing that converges for $\kappa^2 T \to \infty$ to the asymptotic limit $E_{\mathrm{QND}}^{jk} \to \log_4[\frac{1+\beta_{jk}}{1-\beta_{jk}}]$. The spatial distinguishability of the mode functions, Fig. 5.5(b), remains the limiting factor and is parameterised by $\beta_{jk} = |\bar{\kappa}_{jk}^2|/[\bar{\kappa}_{jj}^2\bar{\kappa}_{kk}^2]^{\frac{1}{2}}$. Deviations from E_{QND}^{13} and a small loss of purity, $P \sim 97\%$, are attributed to coupling to other modes with commensurate correlation frequencies [here, $\omega_1 + \omega_3 \simeq (\omega_1 + \omega_7)/2$]. The selectivity within the subsystem is excellent, $D_{\mathcal{H}} \simeq 0$, where $\hat{\rho}_d$ is identical to $\hat{\rho}_o$, except initial vacuum covariances of the 5th mode.

5.1.4 The role of atomic interactions

The atomic interactions change the properties, and in particular the frequency spectrum, of the density oscillations and, hence, the dynamical response of the

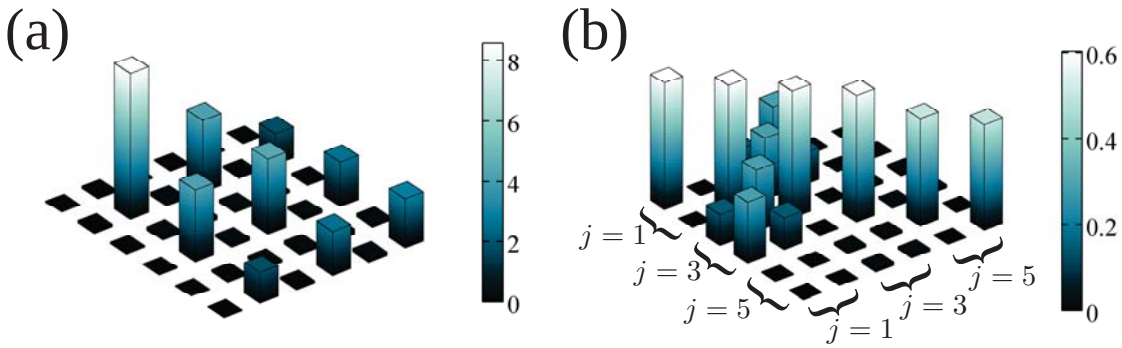

Figure 5.4: The absolute value of the covariance matrix elements for the first three odd modes. Continuous probing (i) squeezes and correlates a swathe of atomic modes, while stroboscopic probing (ii) can generate correlations between only selected modes. The same level of entanglement of modes 1 and 3 is achieved in (i) and (ii), while the strong squeezing and the addressing of 5th in (i) is absent in (ii). The measurement strength for the continuous probing is significantly higher ($\kappa^2 = 1000\omega_x/2\pi$) than the stroboscopic case ($\kappa^2 = 4\omega_x/2\pi$ and $\Delta\varphi/2\pi = 0.03$), and $l_{\mathrm{D}} = l_x/10$.

system to the probing. From the noninteracting to the interaction dominated TF regime, the excitations go from the single particle excitations with the harmonic spectrum $\omega_j = \omega_x j$, to the collective excitations with the irregular spectrum $\omega_j = \omega_x\sqrt{j(j+1)/2}$, Sec. 2.5.

In the noninteracting case, we may calculate

$$\kappa_{jk}^2 = \begin{cases} \frac{\kappa^2 l_{\mathrm{L}} i^{j-k}}{\pi\sqrt{2j!k!}l_x}\Gamma\left(\frac{j+k+1}{2}\right) & \text{if } j+k \text{ is even,} \\ 0 & \text{otherwise,} \end{cases} \tag{5.6}$$

with some integrals involving Hermite polynomials [112, 113]. For the TF regime, the analytic solutions for $f_j^{\pm}(x)$, Eqs. (2.55), yield ($\kappa_{j0}^2 = \kappa_{0j}^2$)

$$\kappa_{jk}^2 = \begin{cases} \frac{\kappa^2 l_{\mathrm{L}}}{2l_x}\sqrt{\frac{2\omega_x}{3\omega_0}} & \text{if } k = 0, \\ \frac{\kappa^2 l_{\mathrm{L}}\hbar\omega_j}{2N_0 g_{1\mathrm{D}}}\delta_{jk} & \text{otherwise} \end{cases} \tag{5.7}$$

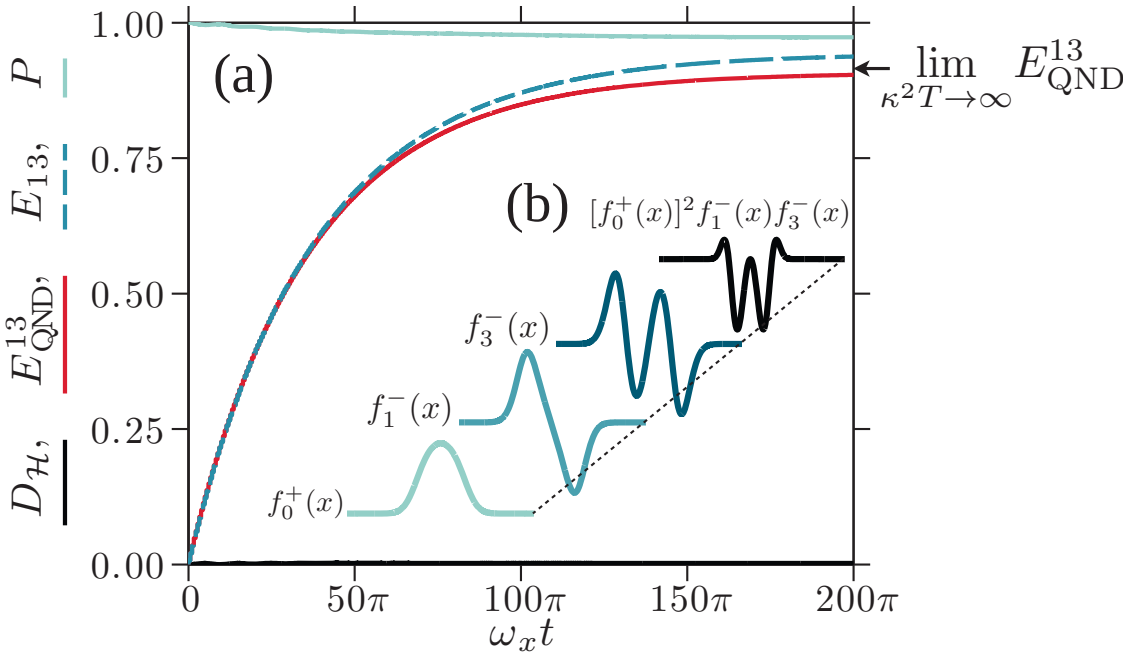

Figure 5.5: (a) Modes 1 and 3 are entangled by a pulse sequence of 100 trap periods with $\varpi_1 = \omega_1 + \omega_3$, $\Delta\varphi/2\pi = 0.03$, $\kappa^2 = 30\omega_x/2\pi$, and $l_{\mathrm{D}} = l_x/10$. The logarithmic negativity E_{13} slightly out-performs the corresponding QND result E^{13}_{QND}. The selectivity within the $j = 1, 3, 5$ subsystem is excellent ($D_{\mathcal{H}} \simeq 0$) and the subsystem's purity is $P \sim 97\%$. (b) The mode functions (not to scale) of the BEC $f_0^+(x)$, entangled modes $f_{1,3}^-(x)$, and the overlap $\sim [f_0^+(x)]^2 f_1^-(x) f_3^-(x)$.

illustrating that, in general, the measurement couplings $\bar{\kappa}^2_{jk}$ decrease with with increasing interactions. The cross-over between these regimes is featured in Fig. 5.6. The dominant density variation occurs as an interference between the BEC mean field and the Bogoliubov mode, Eq. (2.47), yielding and enhancement of the signal of the mode quadrature by $\sqrt{N_0}$. With increasing interactions, however, the overlap of these modes is reduced, as it is energetically unfavourable to overlap with BEC mean field. The signal gradually becomes comparable to the small second-order terms in the density [Eq. (2.47)] that where neglected in the light-matter interaction (Sec. 3.2). As the stroboscopic probing, only works in the absence of degeneracies

in the excitation spectra, we must, however, incorporate interactions. By choosing parameters, $Ng_{1\mathrm{D}}/\hbar\omega_x l_x = 4.953$, leading to $\mu = 2\hbar\omega_x$, we obtain a suitable compromise with a reasonable coupling and a sufficiently irregular spectrum for low energy excitations.

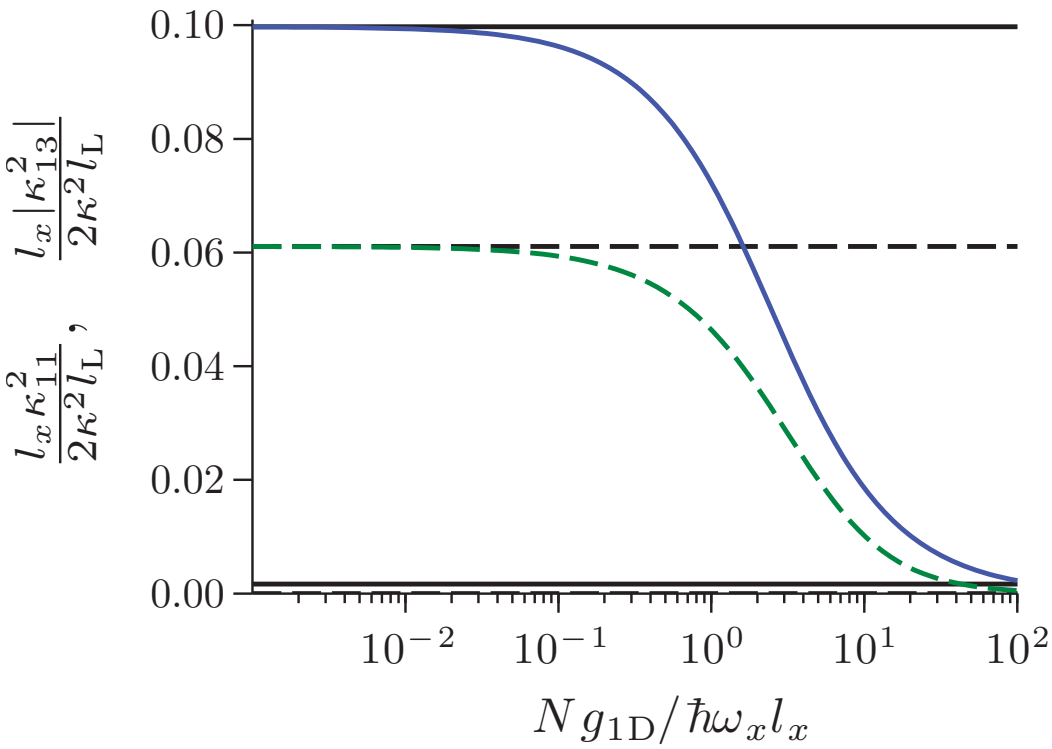

Figure 5.6: Illustrating interactions reduce κ_{jk}^2, where κ_{11}^2 (solid) and κ_{13}^2 (dashed) are featured. The analytical results for noninteracting Eq. (5.6) (upper lines) and TF regimes Eq. (5.7) (bottom lines, with $Ng_{1\mathrm{D}}/\hbar\omega_x l_x = 100$) are illustrated by the black lines.

5.1.5 The role of detector resolution

Section 5.1 presented results for perfect spatial detection of the light field, while Sections 5.1.2 and 5.1.3 assumed the finite resolution $l_{\mathrm{D}} = l_x/10$. Accounting for finite detector resolution amounts to tracing-out light field modes outside of the associated spatial bandwidth, consequently, the measurement cannot restore full coherence to the atomic system. This also accounts for features within individual pixels (or any other system) that in-principle measures the unresolved spatial structure of the light field. For continuous probing, the associated decoherence is demonstrated in Fig. 5.7, quantified by the purity, $P_m = \mathrm{Tr}(\hat{\rho}_m^2) = 1/2^m \det(\mathbf{A}_m)^{\frac{1}{2}}$, of the subsystem up to the mth mode [$\hat{\rho}_m = \mathrm{Tr}_{n>m}(\hat{\rho})$] with the covariance matrix $\mathbf{A}_m$. As m is increased, P_m becomes increasingly sensitive to l_{D} owing to the more rapid spatial variations (scale as l_x/j) of the included higher-order modes. We note that even in the case of the ideal detector, $P_m \leq 1$, as correlations with other modes are established by the probing.

The loss of information can also limit the amount of generable squeezing or entanglement of the atomic modes. Indeed, a completely unresolved density oscillation, j, pertains to a thermal state with thermal population $\bar{\kappa}_{jj}^2 t/2$ in the long-time limit. In Fig. 5.8, we consider the affect on the entanglement generation between modes 1 and 3 for the stroboscopic entanglement generation protocol of Fig. 5.5. The growth of the entanglement is most rapid, and attains the maximal value, for the ideal detector ($l_{\mathrm{D}} = 0$). However, similar entanglement is shown to be generated over a broad range of pixel widths l_{D}. Ideally, the pixel geometry retrieves all the information imprinted on the light field about modes 1 and 3. In general, there will be correlations (that must be retrieved) with the rest of the atomic system, however, owing to the selective nature of the stroboscopic probing, such correlations are negligible. Here, the effectiveness of the information retrieval is represented by $K_{jk}^2 = \sum_d \nu_{jd}\nu_{kd}$, where the ideal case (4.43) is $K_{jk}^2 = 4\bar{\kappa}_{jk}^2$. For a given detector resolution, the pixel geometry can be used itself, or, in unison with intervening optical elements, to optimise K_{jk}^2. Consider the large pixel regime, $l_{\mathrm{D}} \geq l_{\mathrm{x}}$. If the pixel $d = 0$ is centred with the BEC, even modes are primarily measured. This is owed to this pixel receiving the majority of the signal, however, the total field it detects is insensitive to the odd modes, i.e., $\bar{\nu}_{j0} \sim \int_{-l_{\mathrm{D}}/2}^{l_{\mathrm{D}}/2} f_0^+(x) f_j^-(x) dx \sim 0$ for odd j. Conversely, if a pixel

boundary is centred with the BEC, odd modes are primarily measured owing to the orthogonality with the zeroth mode [$\int_0^\infty f_0^+(x) f_j^-(x) dx = 0$ for even j]. The latter is the geometry considered here, and, although the odd modes 1 and 3 feature entanglement, the even modes are decohered for most of the pixel range in Fig. 5.8. The second maxima of the entanglement along $l_\mathrm{D} = 2l_x$ is an interplay between pixel geometry and modal structure, yielding a more optimal geometry.

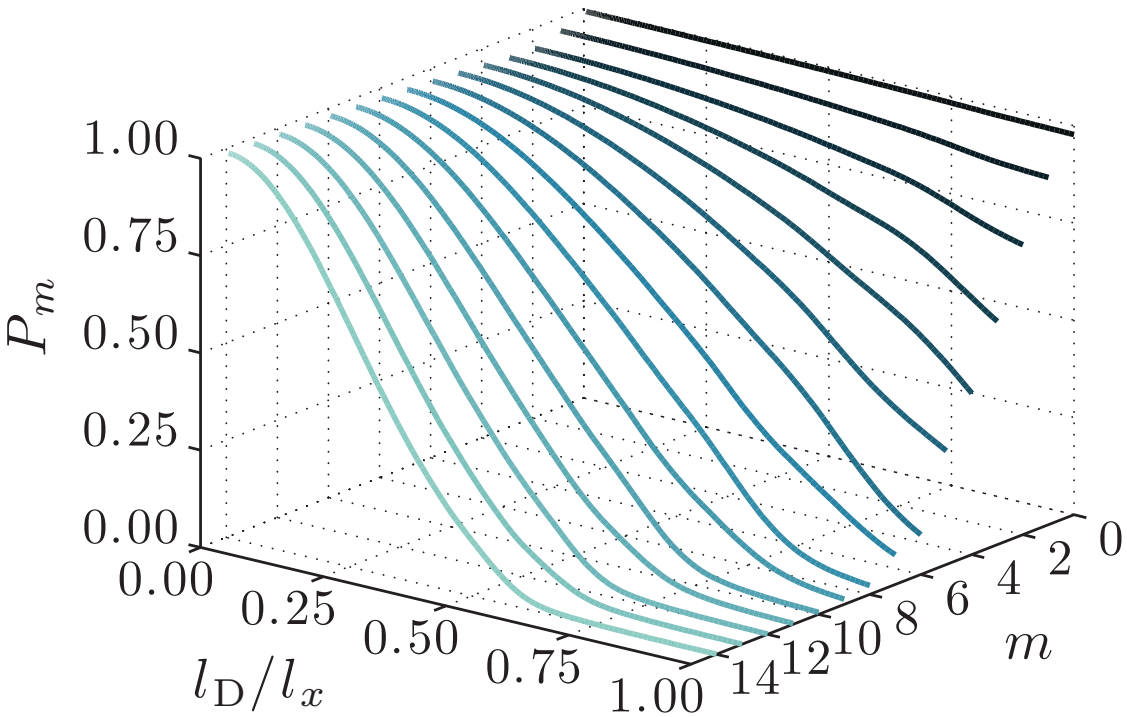

Figure 5.7: Illustrates the purity P_m of the subset of the first $m+1$ modes as a function of detector resolution l_D at time $\omega_x t = \pi$ for the simulation of Fig. 5.1 where the majority of the density oscillations have reached, or are close too, steady-state covariances.

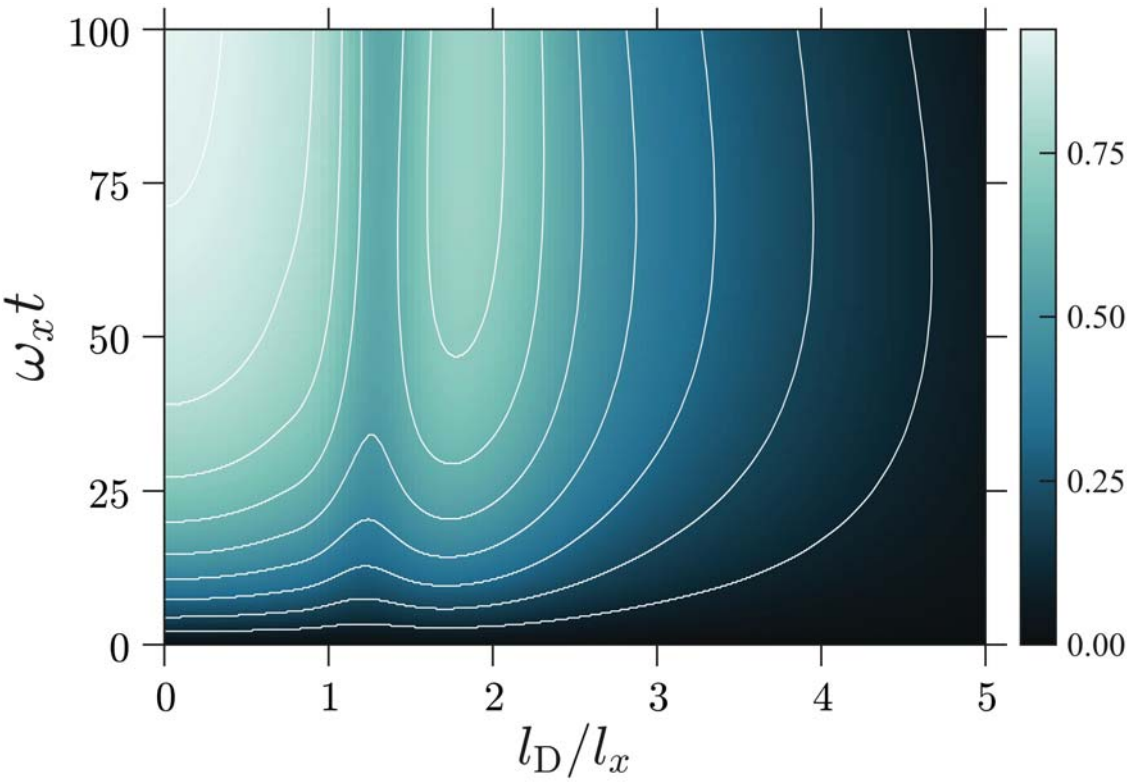

Figure 5.8: The bipartite entanglement, E_{13}, between modes 1 and 3, obtained by stroboscopic probing scheme of Fig. 5.5 is shown as function of pixel resolution and probing time. The degree of entanglement is represented by the colour brightness, and the white contours are to guide the eye.

5.2 Evolution of displacements and feedback

So far, we considered only the atomic covariance matrix, Eq. (4.29), while we know that the measurement backaction also leads to stochastic displacements of the Bogoliubov mode quadratures, cf., Eq. (4.30). When observed, these displacements are coherent and correspond to a modification of the Gross-Pitaevskii wavefunction about which the atomic system was linearized. We shall now address the stochastic evolution and discuss how one may employ feedback to maintain the ground state Gross-Pitaevskii wavefunction, Eq. (2.24).

The application of feedback to maintain a BEC ground state has been explored with phase-space methods [47], where it was found a steady-state close to the ground state is achievable provided sufficient control of the shape of the feedback potential. Here, the optimal feedback protocol of a mode is readily identifiable. Damping of the deterministic evolution of the jth mode is achieved through mode matching, and feedback of the measured $\langle \hat{p}_j(t) \rangle$, via a single atom position dependent Hamiltonian $H_{\mathrm{f}} = \hbar \sum_k h_k(x) \langle \hat{p}_k(t) \rangle$, where $h_k(x) = 2\epsilon\omega_j f_j^+(x)\delta_{jk}/\sqrt{n_0(x)}$, i.e., an adjustable potential. In the dynamics, this potential yields the replacement of the jth block of $\mathbf{D}$ in the evolution of the displacements Eq. (4.30) by

$$[\mathbf{D}]_j = \begin{bmatrix} 0 & -\omega_j \\ \omega_j & 2\epsilon\omega_j \end{bmatrix}. \tag{5.8}$$

The first and second density oscillation modes can be addressed by varying the trap position and strength, and the control of the higher-order modes [jth-order (Hermite) Legendre polynomials in the (non)interacting case] may be provided by adaptive lightshift potentials generated through a micro-mirror array [114], a spatial light modulator [115], or, an acousto-optic deflector [116].

An example of an undamped trajectory is illustrated in Fig. 5.9(a, purple) with constant measurement strength until $\omega_x t = \pi$, thereafter, ramped to zero as illustrated in Fig. 5.9(b, solid-gold). The random measurement results cause diffusive harmonic motion, progressively giving way to deterministic oscillatory motion while the measurement strength is ramped to zero. For the same measurement realization, the damped trajectory ($\epsilon = 1$) is shown Fig. 5.9(a, red), where the

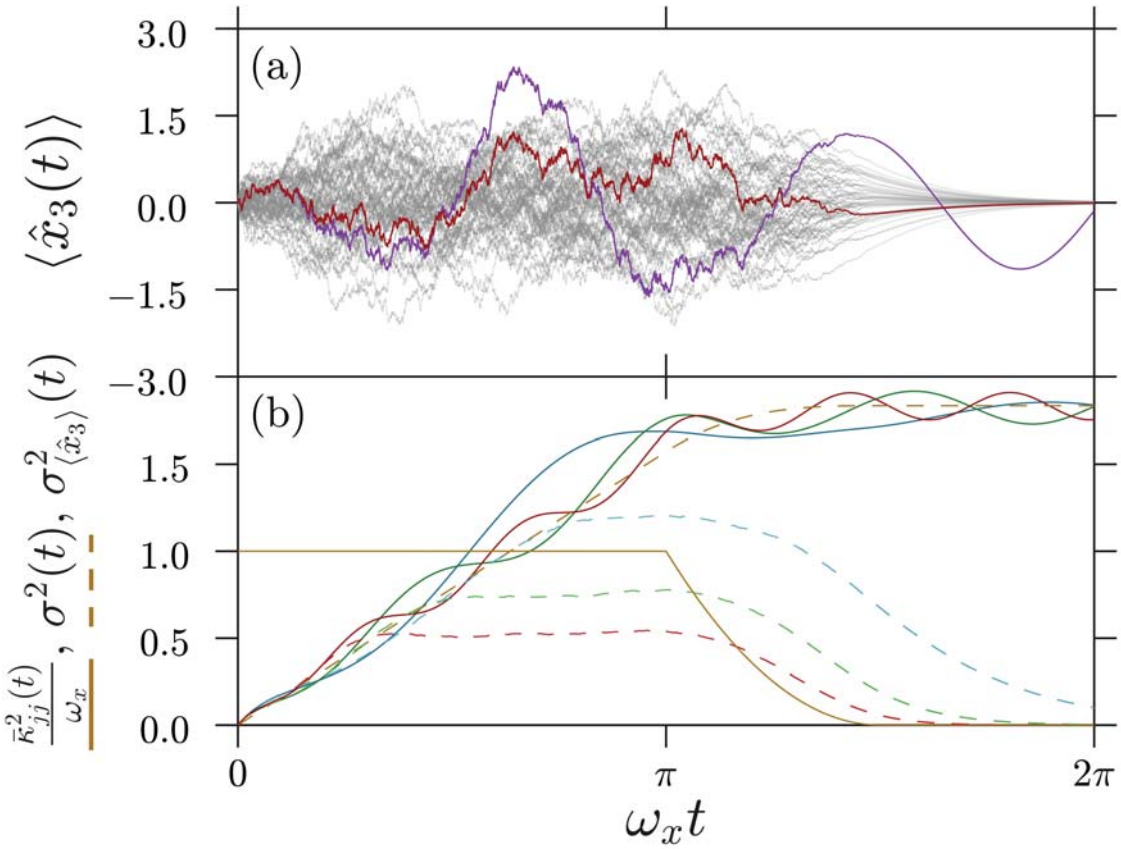

Figure 5.9: (a) The grey curves show individual trajectory results for $\langle \hat{x}_3(t) \rangle$. The purple (red) curve illustrates a single, undamped (damped) trajectory with the same particular measurement record. The measurement strength is ramped down after $\omega_x t = \pi$ as illustrated (solid-gold) by $\bar{\kappa}^2_{jj}(t)$ in (b) with $j = 3$. (b) also shows the variances, $\sigma^2_{\langle \hat{x}_j \rangle}(t)$, of 10^4 trajectories for the (un)damped cases of $j =$ 1-3 by the (solid)dashed blue, green, and red lines, respectively. The undamped $\sigma^2_{\langle \hat{x}_j \rangle}(t)$ oscillates around $\sigma^2(t) = \int_0^t dt' \bar{\kappa}^2_{jj}(t')/2$ (dashed-gold).

excursion of the diffusion is reduced and is critically damped as the measurement weakens.

The (un)damped variances of the trajectories are shown in Fig. 5.9(b) for $j = 1$-3 by the (solid)dashed-lines. Without damping, each case oscillates around $\sigma^2(t) = \int_0^t dt' \bar{\kappa}_{jj}^2(t')/2$ (dashed-gold), while with damping, a steady-state is approached during the continuous measurement phase, $0 \leq \omega_x t \leq \pi$. The differences between these steady-states are due to the damping occurring at different rates ω_j. Using Eq. (5.5), the steady-state $\mathbf{A}_{\text{ens}}^{\text{ss}}$ can be predicted, and upon minimising the ensemble average of the energy $\hbar\omega_j(\langle\hat{x}_j\rangle^2 + \langle\hat{p}_j\rangle^2)/2$, w.r.t. ϵ, the minimised energy is $2\bar{\kappa}_{jj}^2$ with $\epsilon = 1$, and,

$$\mathbf{A}_{\text{ens}}^{\text{ss}} = \tilde{\kappa}_{\omega_j} \begin{bmatrix} 3 & -1 \\ -1 & 1 \end{bmatrix},$$

for weak probing, $\tilde{\kappa}_{\omega_j} \ll 1$. In the case of strong probing, $\tilde{\kappa}_{\omega_j} \gg 1$, the minimised energy is $3\bar{\kappa}_{jj}^2$ with $\epsilon = (1 + 4\tilde{\kappa}_{\omega_j})^{\frac{1}{2}}/2$, and,

$$\mathbf{A}_{\text{ens}}^{\text{ss}} = \tilde{\kappa}_{\omega_j} \begin{bmatrix} 5 & -\tilde{\kappa}_{\omega_j}^{-\frac{1}{2}} \\ -\tilde{\kappa}_{\omega_j}^{-\frac{1}{2}} & 1 \end{bmatrix}. \tag{5.9}$$

For weak probing, the deterministic motion dominates, and hence, the regime of critical damping ($\epsilon = 1$) of the deterministic part of the evolution is more optimal. While, for strong probing, the overdamped ($\epsilon > 1$) regime is more efficient. The imbalance of the standard deviations of the quadratures is owed to the energy being damped from the p quadrature, c.f., Eq. (5.8). As $\tilde{\kappa}_{\omega_j}$ increases, the reduction of the relative importance of the correlations between the quadratures decreases [c.f., Eq. (5.9)], as the (larger) random displacements due to the measurement backaction work to dephase the individual trajectories.

As the measurement strength is reduced, the stochastic role of the measurement backaction weakens, Figs. 5.9. When the probing is completely absent, the excitation associated with the coherent displacements of the modes (first moments) can be critically damped ($\epsilon = 1$), without disruption of the covariance matrix (second moments). In the case of stroboscopic probing, as the majority of the evolution is unprobed, the ideal critical damping can be performed on the targeted mode bringing the first moments close to zero for the entire course of the state preparation Fig. 5.10.

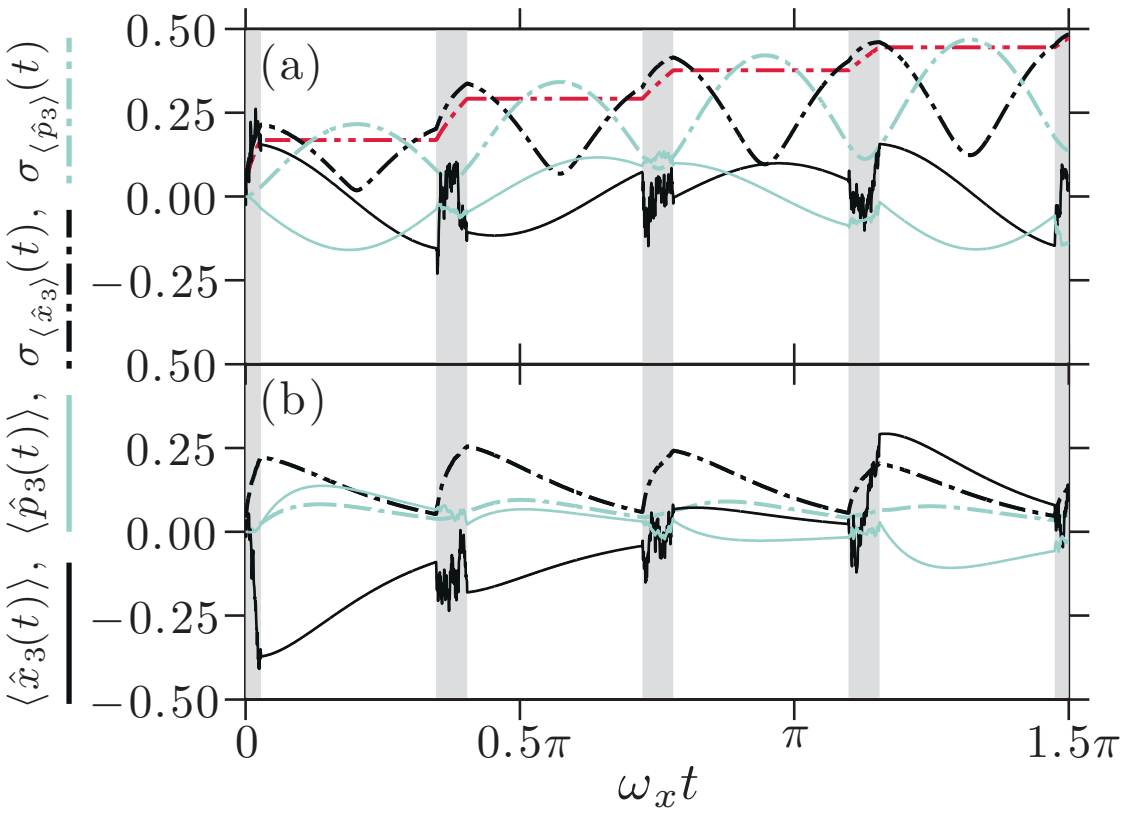

Figure 5.10: A stochastically evolving trajectory of $\langle\hat{x}_3(t)\rangle$ and $\langle\hat{p}_3(t)\rangle$, and the standard deviations of 1000 trajectories $\sigma_{\langle\hat{x}_3\rangle}(t)$ and $\sigma_{\langle\hat{p}_3\rangle}(t)$, corresponding to the simulation in Fig. 5.3 with $\Delta\phi/2\pi = 0.15$ (chosen to emphasize the measurement backaction). The grey regions indicate when the measurement occurs. (a) Without feedback, the trajectories diffuse and oscillate, and approximately $\sigma_{\langle\hat{x}_3\rangle}(t) = \sigma_{\langle\hat{p}_3\rangle}(t) = \sqrt{\bar{\kappa}_{33}^2 T/2}$ (red line). (b) With feedback, the desired damping of displacements is demonstrated.

For the considered examples [Fig. 5.1 for $\omega_x t \leq \pi$], the coherent displacements correspond to up to 10% population outside of the BEC mode. This can be reduced through different trapping geometries where the measurement kernel [Eq. (4.59)] reduces the number of addressed modes or through more elaborate feedback schemes. In the case of the damping presented here, the targeting of many modes (10s-100s) can lead to the feedback playing a small (stochastic) role in the dynamical evolution of the covariance matrix through the second-order terms in the density (2.47).

5.3 Spatial and momentum number correlations

Spatial inhomogeneous probing of ultracold atomic systems has been used to produce spatially structured density-density correlations [46], while the interplay between atomic and measurement dynamics has been seen to enrich this further [48, 117–119]. Similarly, the possibility of measurement induced momentum-momentum correlations is of interest [22, 120–122]. In the following, we consider (1) continuous local probing of the BEC with a spatially varying intensity profile and we (2) investigate the creation of correlations by a planar-wavefront through the stroboscopic probing introduced in Sec. 5.1.2.

Here, we quantify the atomic density correlations by the covariance, Eq. (2.48),

$$\mathrm{covar}[\hat{n}(x_1), \hat{n}(x_2)] = \psi(x_1)\psi(x_2)\delta(x_1 - x_2) + \mathcal{N}(x_1, x_2), \tag{5.10}$$

where $\mathcal{N}(x_1, x_2)$ is defined in terms of the atomic field quadratures, Eq. (2.49). Poissonian fluctuations are represented by the delta-function, while deviations, and correlations between spatially separated regions, are signalled by nonzero values of $\mathcal{N}(x_1, x_2)$. Here, the initial Bogoliubov vacuum state already features sub-Poissonian fluctuations [Fig. 5.11(b, dashed-blue)] owing to the atomic interactions [57].

5.3.1 Inhomogeneous continuous probing

A spatially inhomogeneous intensity profile $u(x)$ of the light modifies our treatment of the light field through Eq. (3.17) and yields the replacement $\kappa_j(x) \rightarrow$

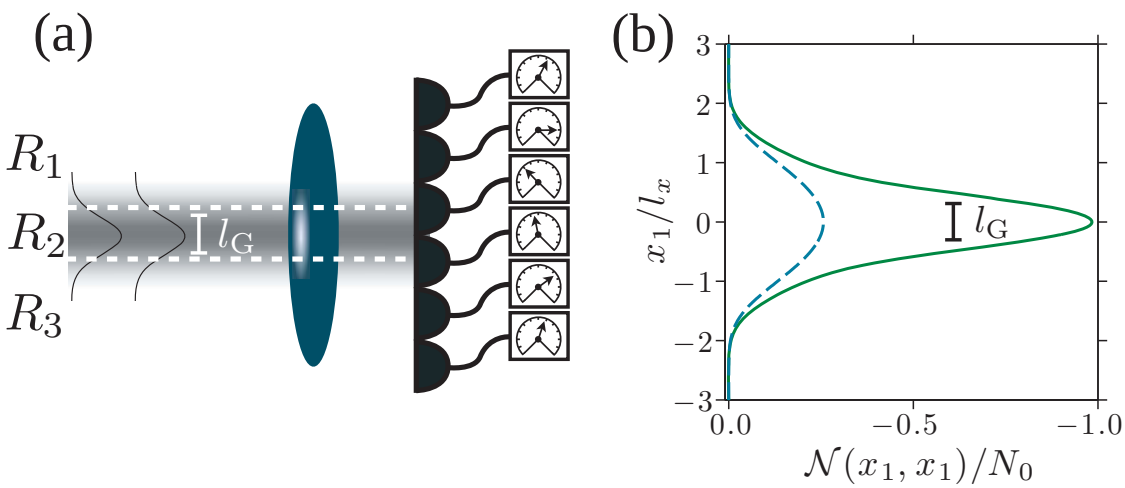

Figure 5.11: (a) The central region R_2 of width l_G is probed with a Gaussian beam of finite width l_G. (b) Due to interactions, the local density fluctuations along the BEC axis are sub-Poissonian in the unprobed state (dashed-blue), and they are further suppressed by the probing in the region R_2 (solid-green). The solid-green line corresponds to the simulation of Fig. 5.12 with $l_G = l_R$.

$\kappa_j(x)\sqrt{u(x)l_L}$. The mean field potential of the light caused by the probe field no longer yields an overall energy shift, but we assume for simplicity that the resultant potential can canceled by an adding a compensating potential.

A Gaussian probe beam with width l_G, Fig. 5.11(a), leads to a reduction of the density fluctuations in the probed region, Fig. 5.11(b). To discuss the interplay between the atomic dynamics, the measurement backaction, and, the value of l_G, we consider the three spatial regions indicated in Fig. 5.11(a). First, we consider the fluctuations of total atom number $\hat{N}_2$ in the central region R_2 of width l_G. In Fig. 5.12(a), the dashed, green curve recovers the mean field Poissonian fluctuations when R_2 is wide and contains the total atom number, while the atomic interactions lead to sub-Poissonian fluctuations in any finite part of the BEC. Within very small regions, the population statistics again tend towards the Poissonian. The solid, green curve shows results after probing, which suppresses the Poissonian number fluctuations of the whole BEC, and competes with the atomic exchange between the regions when the width of R_2 is decreased. Eventually, the detector and diffraction

resolution also becomes relevant. For small R_2, higher-order modes are required to describe the number fluctuations and the role of the squeezed lower-order modes decreases. Eventually, the results become sensitive to the discrete structure of the modes, as seen by the discrete steps in Fig. 5.12 for lower l_{G} values.

We now consider the spatially separated regions R_1 and R_3. If the system has a fixed total number of atoms ($\mathrm{var}[\hat{N}_0] = 0$), upon measuring R_2, squeezing $\hat{N}_2$, regions R_1 and R_3 can become anti-correlated (a squeezing of $\hat{N}_1 + \hat{N}_3$). In the Bogoliubov vacuum state, the Poissonian fluctuations of $\hat{N}_0$ cause R_1 and R_3 to share correlated fluctuations, Fig. 5.12(a, dashed-blue). Upon probing R_2, the coupling to the zeroth mode is held constant ($\omega_x \bar{\kappa}_{00}^2 = 3/2$), and consequently, squeezing $\hat{N}_0$ and $\hat{N}_2$ leading to R_1 and R_3 becoming anticorrelated as shown by the solid, blue curve. The anticorrelations are limited as $\hat{N}_1$ and $\hat{N}_3$ are individually squeezed, i.e., $\hat{N}_1 - \hat{N}_3$ is also squeezed. For small R_2, the anticorrelations are lost, as the squeezing of $\hat{N}_0 \sim \hat{N}_1 + \hat{N}_3$ is dynamically slowed by the strong coupling of the zeroth mode to many other modes.

For small R_2, the coupling of many modes induces a wave-packet in the fluctuations propagating towards the outer regions of the BEC (higher-order modes) and returning to the probed region with frequency $2\omega_x$ due to the linear spectrum of the higher-order modes. This causes the peak around $\omega_x t = \pi$ in the solid green and blue curves in Fig. 5.12(b). As R_2 increases, the feature is progressively lost with the decreased coupling to higher-order modes.

5.3.2 Planar stroboscopic probing

The spatially inhomogeneous probing in the previous section required the introduction of a tailored intensity profile of the probe and a corresponding compensating potential, while additionally competing with atomic dynamics. The created number correlations exist only for the steady-state under the continuous probing and couple many atomic modes when probing small subregions. Thus, upon suspension of the probing, the correlations will rapidly dephase. Avoiding these complications, uniform stroboscopic probing makes use of the natural evolution of the atomic system awarding mode selective squeezing that is persistent after preparation. We now examine the resulting correlations associated with the modal structure of the targeted mode in position space for the first three density modes shown in

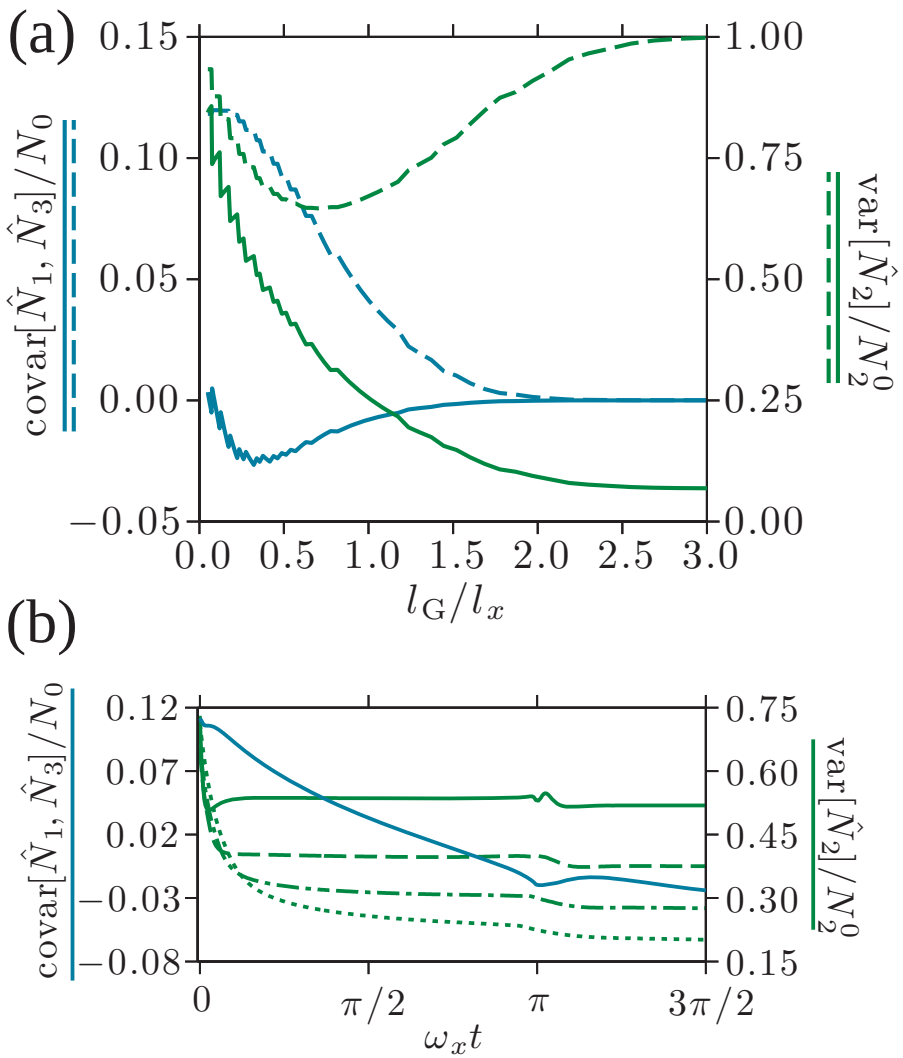

Figure 5.12: (a) Shows the (blue) covariance $\mathrm{covar}[\hat{N}_1, \hat{N}_3]$ (normalized to N_0) between the number of atoms in the unprobed regions R_1 and R_3 and the variance $\mathrm{var}[\hat{N}_2]$ (green) of the number of atoms in region R_2 normalized by the BEC population in R_2, $N_2^0 = \int_{R_2} dx n_0(x)$. The dashed curves show the results for the unprobed BEC. The solid curves show that after probing for a time $\omega_x t = 3\pi/2$ with constant $\omega_x \bar{\kappa}_{00}^2 = 3/2$ and $l_D = l_x/20$, $\mathrm{var}[\hat{N}_2]$ is reduced and the number fluctuations between regions R_1 and R_3 are reduced and can become anti-correlated. (b) The temporal evolution of the number fluctuations for $l_G = l_R$ (solid), $2l_R$ (dashed), $3l_R$ (dashed-dotted), and $4l_R$ (dotted). The sharp feature at $\omega_x t \sim \pi$ occurs because the measurement excites a wave-packet in the fluctuations with revival frequency $2\omega_x$.

Fig. 5.13(a-c). The upper(lower) panels show $\mathcal{N}(x_1, x_2)$ for times when maximal(minimal) squeezing occurs in the $\hat{x}$ quadrature of the targeted mode. In addition, to the long wavelength modal structure of the targeted low energy modes, higher frequency spatial structure can be seen. In particular, in the cases of the 1st and 3rd modes. It turns out that the 1st(3rd) mode frequencies are almost commensurate with the 20th(25th) mode ($\omega_{20}/\omega_1 = 19.0005$, $\omega_{25}/\omega_3 = 8.9971$) and the mode is squeezed, leading to the small scale spatial correlations.

Figures 5.13(d) show that structures appears in the momentum density correlations with deviations of $\mathrm{covar}[\hat{m}(k_1), \hat{m}(k_2)]$ from Poissonian statistics due to the squeezing of the first mode, where $\hat{m}(k) = \hat{\psi}^\dagger(k)\hat{\psi}(k)$ with $\hat{\psi}(k) = \int dx e^{ikx}\hat{\psi}(x)/\sqrt{2\pi}$.

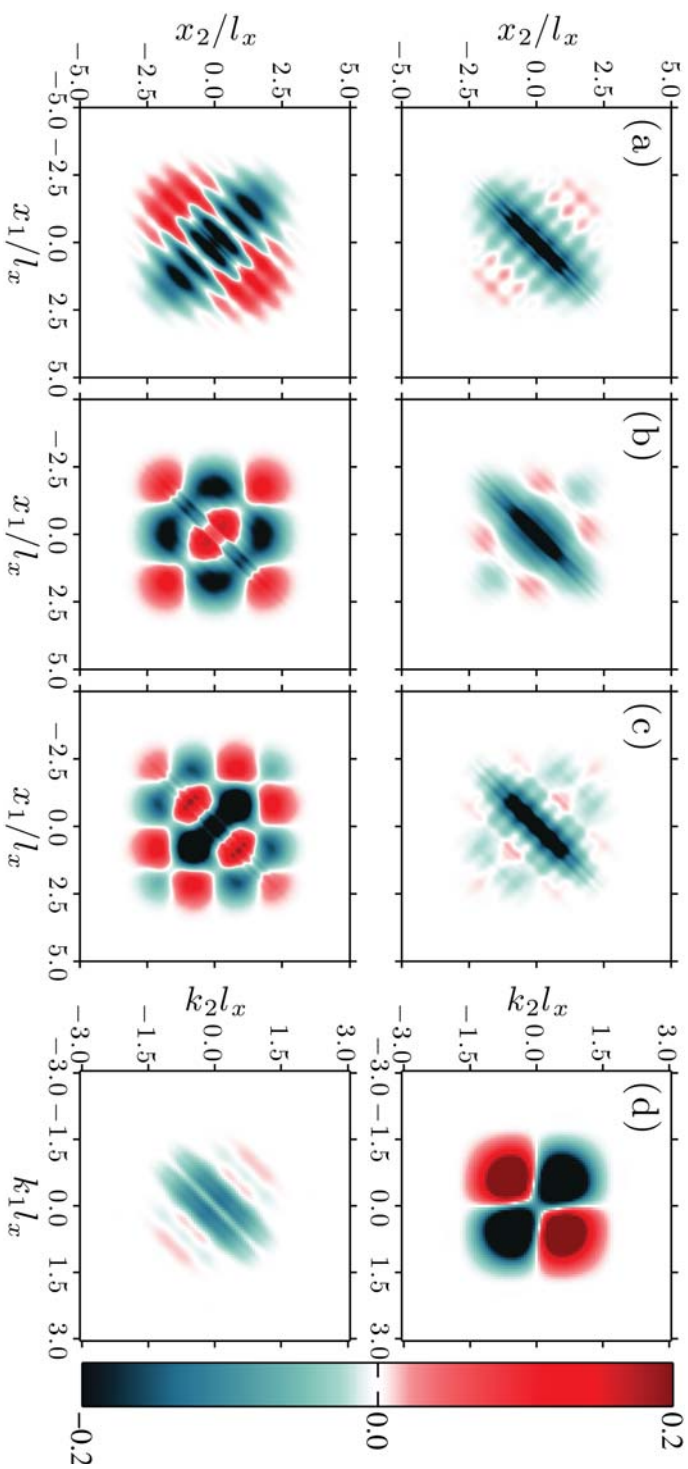

Figure 5.13: Dynamic correlations created by the stroboscopic scheme of Fig. 5.3, where the modes $j = 1$-3 (a-c) are squeezed. The upper panel shows $\mathcal{N}(x_1, x_2)$ when $\mathrm{var}[\hat{x}_j] = [0.0675, 0.0587, 0.0557]$ is minimal and for $j = [1, 2, 3]$, while the lower panel corresponds to the maxima $\mathrm{var}[\hat{x}_j] = [3.7089, 4.2692, 4.5057]$. (d) shows the deviations from Poissonian momentum-momentum correlations for $\mathrm{covar}[\hat{m}(k_1), \hat{m}(k_2)]/5$ in the case of squeezing $j = 1$.

CHAPTER 6

CONCLUSIONS AND OUTLOOK

We have demonstrated the quantum control of a matter-wave system via spatially resolved optical probing and feedback. Our Gaussian method of analysis permits the inclusion of the full quantum multimodal character of the problem. Within the limitations of our expansion of the atomic field about the Gross-Pitaevskii mean field, we are able to take into account the atomic motion, interactions, and measurement backaction in the full spatio-temporal evolution of the system. Using stroboscopic probing, we can address and correlate effective QND observables of selected density modes of a BEC, while preserving the initial vacuum fluctuations of nontargeted modes. Our method of spatially resolved imaging may hold similar prospects for squeezing and entanglement in other quantum many-body systems with harmonic excitation modes, such as, the center-of-mass Kohn mode [123], breathing modes of the Tonks-Girardeau gas [124], full quantum 2D systems [125], and the unitary 3D quantum gas [126]. In any of these cases the performance relies on independent excitation modes, and it is ultimately limited by the residual atomic depumping [127]. For small, 1D alkali condensates, we estimate that currently available experimental parameters [128–130] permit significant squeezing and entanglement of the selected modes.

The atomic interactions induce an irregular spectrum of density oscillations that is important for the selectivity of stroboscopic probing. However, the measurable signal is an interference between the atomic mean field and the Bogoliubov modes. Their spatial overlap becomes energetically unfavourable with increasing atomic interactions, consequently, the signal decreases. A compromise is made to allow for the irregular spectrum, while, retaining a significant signal. The other important

physical components in the probing of the BEC, (i) the light-matter interaction, (ii) the light field diffraction across the BEC, and (iii) the detection of the light field, each lead to distinct types of resolution. (i) leads to a dynamical resolution associated with the measurement's ability to temporally resolve the atomic dynamics. In the extreme case where the atomic dynamics are much faster than the light-matter interaction, the measurement is unable to resolve the motion and the associated density oscillation mode is unperturbed from, or evolves towards, (thermal)vacuum fluctuations for a (non)ideal detector. (ii) leads to a diffraction resolution where atomic modes are decoupled from the light field owing to the diffraction of the light field across the BEC during their interaction. Consequently, these modes are not addressed and remain unaffected by the measurement scheme. The spatial resolution of the detector (iii) leads to the decoherence of unresolved modes, where, if the mode is partially resolved, an impure steady-state is reached.

To overcome decoherence, we identified how to optimise the detector geometry and optical elements between the BEC and detector. In particular case of the stroboscopic generation of bipartite entanglement, the spatial distinguishability of the information about the modes imprinted on the light field limits generated entanglement. This distinguishability could be reduced by a spatially varying light intensity. Alternatively, one may consider the scattering into a Purcell coupled optical cavity while measuring the cavity output [48]. The advantage is that the coupling depends on the light and cavity mode functions opposed to the light field intensity as it does here, allowing for more tailoring possibilities.

A spatially varying light field intensity also creates nontrivial atomic spatial and momentum correlations which we investigated for a centred Gaussian probe that suppresses density fluctuation in the probed region and anticorrelates the unprobed outer regions. For the generation of interesting correlations, the spatial tailoring of the light field can be avoided by the selective manipulation of specific eigenmodes of the BEC through stroboscopic probing. The correlation structure is associated with the structure of the eigenmode functions, and, are persistent after their production, in contrast to the steady-state under probing correlations generated in the former case that rapidly dephase after probing.

The measurement backaction causes a stochastic diffusion of the displacements of the atomic modes. We have presented how to employ feedback via an adaptive potential to damp the displacements of specific modes. The ideal feedback parame-

ters are identified, in particular, it was found that the variances of the stochastic displacements grow linearly with the measurement strength for the case of continuous probing. Without probing, the displacements can, in principle, be fully damped. Ultimately, the level of control of the adaptive potential will limit which modes can be damped, including how well they may be damped.

The 1D treatment presented here can be readily extending to a 2D pancake BEC, where probing occurs through the smallest width of the BEC. In principle, it is possible to include the light mode function diffraction across the BEC in our treatment. This would allow the extension to 3D systems that are of interest as the coupling to the atomic modes will be nontrivial. This may offer possibilities in restricting the addressing to smaller subsets of modes in a similar fashion to the diffraction resolution identified here.

The results obtained here offer prospects for several interesting applications. Squeezing and entanglement are useful properties for precision sensing purposes, and the atomic system here may find applications for the sensing of field or inertial effects, if they couple to the atomic density. The ability to address particular modes of motion also paves the way for multimode quantum memory and repeater devices. The controlled generation of mode-squeezing makes this system a strong candidate for high fidelity storage of quantum light systems. In the ideal case, if several light fields can be stored in separate Bogoliubov modes sequentially without perturbing the previously stored states, this would further our setup in high capacity multimode quantum memory resources. In such a scenario one could also imagine utilising the entanglement generation scheme to generate controlled interaction between two stored light modes.

The study of the particle tunnelling and interference effects between two or more atomic ensembles has been of long standing interest for many-body and statistical physics, as it may reveal the character of ordered classical and quantum phases, coherent dynamics in 1D and 2D systems, and transport phenomena. We believe that continuous probing may not only yield detailed insight in many-body quantum dynamics, but it also contributes in a most nontrivial manner to the physical evolution of the system of interest. Analysis of the interplay between interactions and measurements may well begin with systems for which our Gaussian analysis applies.

CHAPTER 7

RYDBERG ENSEMBLES: EXCITATION DYNAMICS AND PHOTONIC DECAY

Here, we focus on cold gas systems that make use of Rydberg atoms. Such atoms are ordinary atoms, where an electron has been excited into a high-lying electronic state with principle quantum number $n \gg 1$. These atoms are of interest, as their properties become highly exaggerated. In particular, they can exhibit exceptionally strong attractive or repulsive dipole-dipole interactions (scale as n^4) and Van der Waals interactions (scale as n^{11}) between each other [131]. This can lead to the so-called Rydberg blockade effect; an effect which will be exploited heavily within this project.

When a classical light field (tuned to an atomic resonance) is incident on a collection of weakly interacting atoms, the atoms undergo Rabi oscillations between the resonant states giving way to dephasing and decay, and one may seek to employ the well-known Beer-Lambert law to describe the attenuation of the light beam. Rydberg blockade is an extreme case, where such traditional descriptions break down. Upon excitation of an atom to a Rydberg state, the strong Rydberg-Rydberg interactions energetically prohibit the excitation of an additional atom [131]. Thus, only a single excitation is allowed within the atomic system, and conversely, only a single photon is removed from the light field. This effect can extend over several μm; a volume that may contain many atoms. The possibility that any one of these atoms is excited must be taken into account,

hence, gives rise to many-body entangled states. Such highly correlated many-body situations are of focus here, as we seek interesting phenomena, and, the application of the manipulation of light. Already, single photon extraction from light beams is useful in the construction of exotic nonclassical light fields, but the many-body correlations of these Rydberg systems also give rise to counter intuitive results (e.g., [132]), giant nonlinear effects many orders of magnitude greater than previous records [133], and superradiance, where a single photon is emitted in a well defined direction [134].

The first component of work presented here will consist of the analytic part of our investigation of the efficient storage and retrieval of single photons. Owing to the delocalization of the excitation across the ensemble of N atoms, one observes a $\sqrt{N}$ speed up in the excitation dynamics. This collective enhancement is attractive, but in the case of, say, quantum gates, knowledge (potentially impractical to obtain) of N is required to achieve high fidelities. As the excitation dynamics are dependent on the distribution of N, deterministically imprinting a single Rydberg excitation in the system implies a process independent of N. Such a process would find application in performing deterministic quantum gates [135], loading of optical lattices [136], and inducing nonlinear effects in light fields [137–139].

Various approaches showed that by using time-dependent fields, such as, chirped pulses, STIRAP [135, 140], and random fluctuations of the excited level [137], one could make either the excitation process independent of N, or, approach a steady state where all the population is in the singly excited states. However, the adiabatic passage methods that preserve the coherence of the system are slow, while the steady-state methods destroy the coherence. Without coherences, the emission of the absorbed photon will be equally distributed over all the solid angles and rendered useless. Here, we investigate the deterministic excitation of a single excitation, while preserving the collective enhancement and coherences.

Coupling quantum systems to ancillary systems is widely used to measure and induce nonclassical effects in the original system by manipulating the ancilla alone, an example being the BEC probing we considered earlier. As the ancillary systems (probes) typically have lesser degrees of freedom in comparison to the full system, their control and readout is believed to be simpler. Ancillary systems have been widely used in characterising quantum processes, for quantum state engineering, dissipative quantum computation, measuring the non-Markovianity

of an open-quantum system, quantum error correction and quantum cooling. It was shown [141, 142] that the strong dipolar interaction between Rydberg atoms could enhance the imaging of individual (impurity) Rydberg atoms in dense gases. One can also understand this effect from the point of view that the impurity atom (ancilla/probe) is driving the large ensemble between the dark and bright states conditioned on it being excited to the Rydberg state or not. Our approach is inspired by the works of Refs. [141, 142], and Ref. [143], where it was demonstrated that the inherent inhomogeneity of the Rydberg interactions can be used to dephase multiply-excited states. Here, see Fig. 7.1, we use an ancilla to dephase the singly-excited states of an ensemble, leading to steady-state-like dynamics where the ensemble is singularly excited, while preserving the coherences. Thereafter, the ensemble emits a photon in a well-defined direction.

We present primarily our analytical contributions, as greatest insight can be found within. In addition to that we present some of the analytics (focusing on timescales) of another emerging project, where we investigate the excitation dynamics of multiple ensembles.

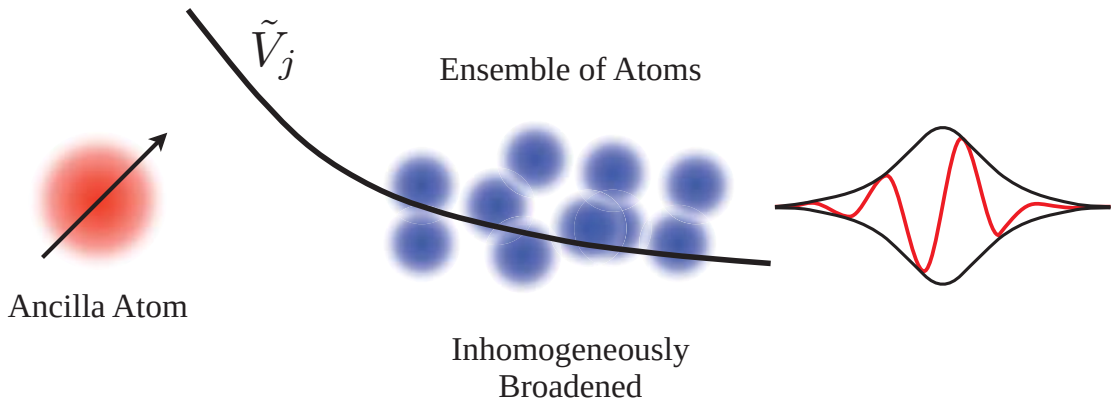

Figure 7.1: Cartoon of system: an ancilla atom inhomogeneously broadens a blockaded ensemble of atoms via the interaction potential $\tilde{V}_j$ on atom j, leading to the deterministic absorption of a single excitation that later decays as a photon in a well defined direction.

7.1 Hamiltonian

The setup is depicted in Fig. 7.1, while the level scheme is featured in Fig. 7.2. In general, we will treat both the system (S1) and ancilla system (S2) as ensembles of N_{Si} atoms. For the specific case of absorption and emission of a photon, the ancilla system will consist of a single excited atom (Sec. 7.2). The transitions occur with the effective Rabi frequencies Ω_{Si} and detuning Δ_{Si} between the collective ground states $|G_{\mathrm{Si}}\rangle$ and the excited Rydberg states with the jth (and kth) atom excited, $|r_j^{\mathrm{Si}}\rangle$ ($|r_j^{\mathrm{S1}}, r_k^{\mathrm{S2}}\rangle$) by a two-photon coupling with a far-detuned intermediate level. The Rydberg state of each system need not be the same, however, we do assume Rydberg blockade is fully active for the ground to Rydberg state transition in each system. That is, the intra-ensemble Rydberg interactions energetically prohibit more than one excitation in each ensemble, and we work within the strict single excitation regime with $(N_{\mathrm{S1}}+1)(N_{\mathrm{S2}}+1)$ basis states.

The Hamiltonian is

$$\hat{H} = \hat{H}_{\mathrm{S1}} + \hat{H}_{\mathrm{int}} + \hat{H}_{\mathrm{S2}}, \tag{7.1}$$

and the system hamiltonians $\hat{H}_{\mathrm{Si}}$ are given by

$$\hat{H}_{\mathrm{Si}} = \hbar\sqrt{N_{\mathrm{Si}}}\Omega_{\mathrm{Si}}\left[|G_{\mathrm{Si}}\rangle\langle \mathbf{0}_{\mathrm{Si}}| + \mathrm{h.c.}\right] - \hbar\Delta_{\mathrm{Si}}\sum_{j=1}^{N_{\mathrm{Si}}}|r_j^{\mathrm{Si}}\rangle\langle r_j^{\mathrm{Si}}|, \tag{7.2a}$$

where we have applied the rotating wave approximation (RWA) and work within the rotating frame. Owing to the single excitation restriction, we can write the laser coupling solely in terms of the (bright) fully symmetric excited state $|\mathbf{0}_{\mathrm{Si}}\rangle = \sum_{j=1}^{N_{\mathrm{Si}}}|r_j^{\mathrm{Si}}\rangle/\sqrt{N_{\mathrm{Si}}}$ and $|G_{\mathrm{Si}}\rangle$. The remaining excited states are not coupled by the laser field (dark-states). Consequently, the Hamiltonian (7.2a) describes an effective two-level system, $|G_{\mathrm{Si}}\rangle$ and $|\mathbf{0}_{\mathrm{Si}}\rangle$, where the ensemble of atoms behave as a single (super) atom with the enhanced Rabi frequency $\sqrt{N_{\mathrm{Si}}}$. The interaction hamiltonian $\hat{H}_{\mathrm{int}}$ is

$$\hat{H}_{\mathrm{int}} = \sum_{j=1}^{N_{\mathrm{S1}}}\sum_{k=1}^{N_{\mathrm{S2}}}\hbar\tilde{V}_{jk}|r_j^{\mathrm{S1}}, r_k^{\mathrm{S2}}\rangle\langle r_j^{\mathrm{S1}}, r_k^{\mathrm{S2}}|. \tag{7.2b}$$

The inter-ensemble interactions $\tilde{V}_{jk}$ can have the dipole-dipole ($\tilde{V}_{jk} \sim 1/|\mathbf{r}_{jk}|^3$) or Van der Waals ($\tilde{V}_{jk} \sim 1/|\mathbf{r}_{jk}|^6$) dependence on the distance between atoms $|\mathbf{r}_{jk}| = |\mathbf{r}_j^{\mathrm{S1}} - \mathbf{r}_k^{\mathrm{S2}}|$, where $\mathbf{r}_j^{\mathrm{S1}}(\mathbf{r}_k^{\mathrm{S2}})$ is the position of the jth(kth) atom in system 1(2). These interactions are responsible for the coupling between dark states, and, the bright state, leading to a leeching of the population from the bright state into the dark-state manifold. We will seek to abuse the leeching in the following sections to "trap" an excitation in the atomic system.

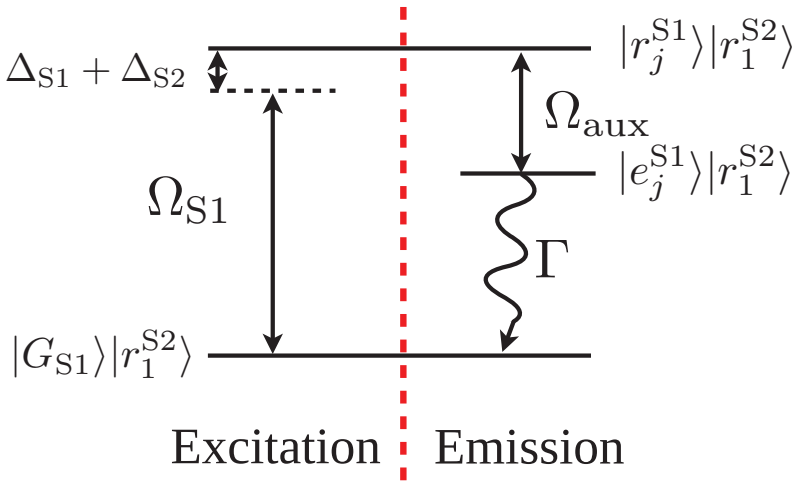

Figure 7.2: Energy level scheme for ancilla assisted deterministic absorption of a single excitation. Once excited, the excitation is then transferred to a decaying (at rate Γ) auxiliary state by a light field with Rabi frequency Ω_{aux}. The coherences are preserved, and the system emits a photon into a well defined direction.

7.2 Ancilla-assisted dynamics

We now specialise (c.f. Figs. 7.1 and 7.2) to the ancilla system containing a single initially excited atom without driving ($\Omega_{\mathrm{S2}} = 0$). In this case, effective Hamiltonian for system 1 is

$$\hat{H}_{\mathrm{S1}} = \hbar\sqrt{N_{\mathrm{S1}}}\Omega_{\mathrm{S1}}\left[|G_{\mathrm{S1}}\rangle\langle\mathbf{0}_{\mathrm{S1}}| + \mathrm{h.c.}\right] + \sum_{j=1}^{N_{\mathrm{S1}}} \hbar V_j |r_j^{\mathrm{S1}}\rangle\langle r_j^{\mathrm{S1}}|, \tag{7.3}$$

where $V_j = \langle r_1^{\mathrm{S2}}|\tilde{V}_{j1}|r_1^{\mathrm{S2}}\rangle - \Delta_{\mathrm{S1}} - \Delta_{\mathrm{S2}}$ are inhomogeneous energy shifts ultimately coupling the dark states. Such a system mimics spontaneous emission (c.f., Sec. 7.2.4), however, an initially unexcited state "decays" into an excited state. The energy quantum is lost into the manifold of singly excited states; unlike spontaneous emission there is a finite set of such states, thus, we expect revivals. We will investigate such dynamics (Secs. 7.2.1 and 7.2.3), and then, the spatial profile of the emitted photon (Secs. 7.2.4 and 7.2.5).

7.2.1 Markovian approximation

In writing the general quantum state as

$$|\psi\rangle = C_{\mathrm{g}}(t)|G_{\mathrm{S1}}\rangle + \sum_{j=1}^{N_{\mathrm{S1}}} C_j(t)|r_j^{\mathrm{S1}}\rangle, \tag{7.4}$$

the time-evolution of the ground state is readily decoupled

$$\dot{C}_{\mathrm{g}}(t) = -\Omega_{\mathrm{S1}}^2 \sum_{j=1}^{N_{\mathrm{S1}}} e^{-iV_j t} \int_0^t dt' e^{iV_j t'} C_{\mathrm{g}}(t'). \tag{7.5}$$

We employ the Markovian approximation $C_{\mathrm{g}}(t') \to C_{\mathrm{g}}(t)$, which is not strictly accurate as the exponential of the integrand Eq. (7.5) need not be rapidly varying in the following. However, significant insight can be gained from such an approximation and quantitative results are obtained in many relevant regimes. We have

$$C_{\mathrm{g}}(t) = \prod_{j=1}^{N_{\mathrm{S1}}} \exp\left[-\Omega_{\mathrm{S1}}^2 \frac{1 - iV_j t - e^{-iV_j t}}{V_j^2}\right], \tag{7.6}$$

giving the ground state population

$$P_{\mathrm{g}}(t) = |C_{\mathrm{g}}(t)|^2 = \prod_{j=1}^{N_{\mathrm{S1}}} \exp\left[-\frac{4\Omega_{\mathrm{S1}}^2}{V_j^2} \sin^2 \frac{V_j t}{2}\right]. \tag{7.7}$$

The short-time evolution is governed by

$$P_{\mathrm{g}}(t) = \exp\left[-N_{\mathrm{S1}}\Omega_{\mathrm{S1}}^2 t^2\right], \tag{7.8}$$

consistent with the super-atom Rabi oscillations at the effective Rabi frequency (c.f. Fig. 7.4),

$$\tau_1^{\mathrm{S1}} = \frac{1}{\sqrt{N_{\mathrm{S1}}}\Omega_{\mathrm{S1}}}. \tag{7.9}$$

This is expected, as the excitation initially feeds into the fully symmetric state (giving the enhancement), and is then redistributed into the dark-states.

7.2.2 Linear detuning

To obtain further analytical results, we now discus a special case that will serve as our best-case-scenario benchmark for following studies. That is, V_j is distributed linearly from $-V$ to V

$$V_j = \frac{2V}{N_{\mathrm{S1}} - 1}(j - 1) - V. \tag{7.10}$$

Here, we have implicitly assumed $N_{\mathrm{S1}} \in 2\mathbb{Z}$, as the Markovian approximation inadequately handles $V_j = 0$. Taking N_{S1} to be large, the ground state population

amplitude [Eq. (7.6)] is given by

$$C_{\mathrm{g}}(t) \simeq \exp\left[-\frac{2N_{\mathrm{S1}}^2\Omega_{\mathrm{S1}}^2}{V^2}\sum_{k=1}^{N_{\mathrm{S1}}/2}\left\{\frac{1}{(2k-1)^2}-\frac{\cos\left[\frac{V}{N_{\mathrm{S1}}}(2k-1)t\right]}{(2k-1)^2}\right\}\right]$$
$$= \exp\left[-\left\{\frac{A}{2}-\frac{4A}{\pi^2}\sum_{k=1}^{\infty}\frac{\cos\left[(2k-1)\omega t\right]}{(2k-1)^2}\right\}\right], \tag{7.11}$$

where the final line approximates the sum as an infinite sum. The term in the curly brackets is the Fourier series decomposition of the sharktooth function $f_{\mathrm{st}}(t)$, depicted in Fig. 7.3, with amplitude $A = \left[\pi N_{\mathrm{S1}}\Omega_{\mathrm{S1}}\right]^2/2V^2$, and period $T = 2\pi\frac{N_{\mathrm{S1}}}{V} = 2\pi/\omega$. Immediately yielded from this Markov-Shark approximation, the

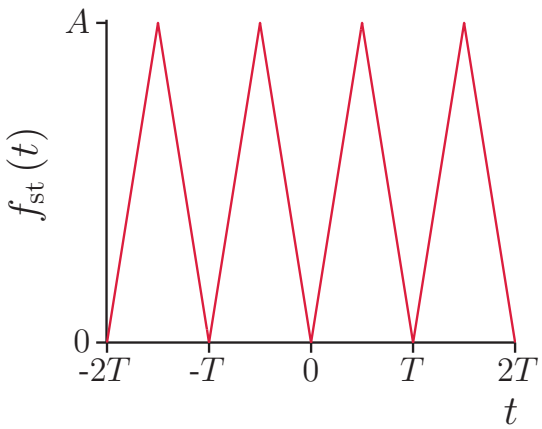

Figure 7.3: Sharktooth function of amplitude A and period T.

revival time is

$$\tau_{\mathrm{rev}}^{\mathrm{S1}} = 2\pi\frac{N_{\mathrm{S1}}}{V}. \tag{7.12}$$

As the summation realistically does not extend to infinity, we have the short-time dynamics governed by Eq. (7.8). In addition, we will also see in Sec. 7.2.3, the revival time is half that predicted here. After short-time dynamics, and before the

first half period, we have the exponential decay

$$C_{\mathrm{g}}(t) = \exp\left[-\frac{t}{2\tau_2^{\mathrm{S1}}}\right], \tag{7.13}$$

with

$$\tau_2^{\mathrm{S1}} = \frac{V}{\pi N_{\mathrm{S1}} \Omega_{\mathrm{S1}}^2}. \tag{7.14}$$

To summarise, the ground state dynamics are governed by three timescales τ_1^{S1}, τ_2^{S1}, $\tau_{\mathrm{rev}}^{\mathrm{S1}}$, given by Eqs. (7.9), (7.14), and (7.12), respectively. Initially, the system is dominated by the collective Rabi frequency $1/\tau_1^{\mathrm{S1}}$. Then, it transitions into exponential decay mimicking incoherent dynamics with the transfer rate $1/\tau_2^{\mathrm{S1}}$, also being the typical timescale for cases where rapidly oscillating modes have been eliminated, $(\mathrm{coupling\,frequency})^2/\mathrm{detuning}$. This transition is illustrated in Fig. 7.4. We expect the exponential decay not to exceed the super atom Rabi frequency, as it is the fastest timescale governing the excitation dynamics. Finally, we have the revival time, $\tau_{\mathrm{rev}}^{\mathrm{S1}}$, where the ground state is repopulated. Simple rephasing arguments also give the revival time scaling as $\sim N_{\mathrm{S1}}/V$.

After the ground state has entirely decayed into the excited states, the excited state populations become Lorentzian distributed around the atom with zero detuning,

$$P_j(t) = \frac{1}{2\pi} \frac{\gamma_{\mathrm{S1}}}{\left(j - \frac{N_{\mathrm{S1}}+1}{2}\right)^2 + \left(\frac{\gamma_{\mathrm{S1}}}{2}\right)^2}, \tag{7.15}$$

with width $\gamma_{\mathrm{S1}} = \tau_{\mathrm{rev}}^{\mathrm{S1}}/4\pi\tau_2^{\mathrm{S1}} = \pi N_{\mathrm{S1}}^2 \Omega_{\mathrm{S1}}^2/2V^2$. This is of course what one expects from parallels to spontaneous emission, but instead of the excitation being imparted on a spectrum of photons, the excitation is imparted onto atoms with the equivalent spectrum V_j.

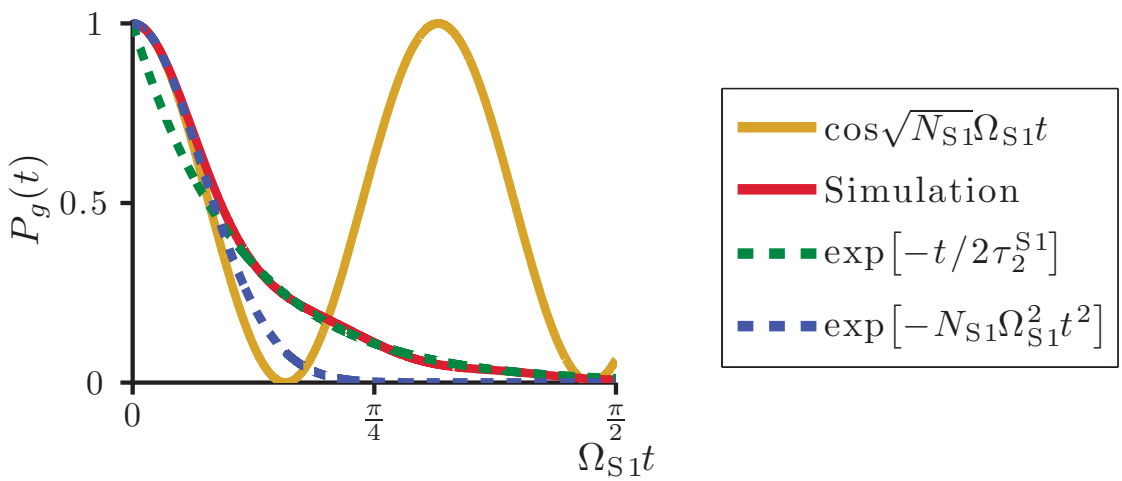

Figure 7.4: An illustrative example of the ground state decay with $N_{S1} = 10$ and $V/\Omega_{S1} = 10$. The gold curve illustrated the collectively enhanced Rabi oscillations without the inhomogeneous broadening.

7.2.3 Excited manifold dynamics

In characterising the ground state dynamics, we now turn to the excited manifold. An instructive basis to work within is that of plane waves:

$$|k\rangle = \frac{1}{\sqrt{N_{\mathrm{S1}}}} \sum_{j=-N_{\mathrm{S1}}/2+1}^{N_{\mathrm{S1}}/2} \exp\left[\frac{2\pi ijk}{N_{\mathrm{S1}}}\right] |r^{\mathrm{S1}}_{j+N_{\mathrm{S1}}/2}\rangle, \tag{7.16}$$

where $k \in [-N_{\mathrm{S1}}/2+1, N_{\mathrm{S1}}/2]$. After the ground state has decayed, we have plane-wave amplitudes

$$\begin{aligned} C_k^{\mathrm{pw}}(t) &= \frac{\Omega_{\mathrm{S1}}}{\sqrt{N_{\mathrm{S1}}}} \sum_{j=-N_{\mathrm{S1}}/2+1}^{N_{\mathrm{S1}}/2} \frac{\exp\left[-i\left(\frac{2\pi jk}{N_{\mathrm{S1}}} + tV_{j+N_{\mathrm{S1}}/2}\right)\right]}{V_{j+N_{\mathrm{S1}}/2} + \frac{i}{2\tau_2^{\mathrm{S1}}}} \\ &\simeq e^{\frac{2\pi it}{\tau_{\mathrm{rev}}^{\mathrm{S1}}}} \sqrt{\frac{\gamma_{\mathrm{S1}}}{2\pi N_{\mathrm{S1}}}} \sum_{j=-\infty}^{\infty} \frac{\exp\left[-2\pi i\left(\frac{k}{N_{\mathrm{S1}}} + \frac{2t}{\tau_{\mathrm{rev}}^{\mathrm{S1}}}\right) j\right]}{j + \frac{i\gamma_{\mathrm{S1}}-1}{2}} \\ &= \frac{\exp\left[-\pi(i+\gamma_{\mathrm{S1}}) \bmod \left(\frac{k}{N_{\mathrm{S1}}} + \frac{2t}{\tau_{\mathrm{rev}}^{\mathrm{S1}}}, 1\right) + \frac{2\pi it}{\tau_{\mathrm{rev}}^{\mathrm{S1}}}\right]}{i\sqrt{\frac{N_{\mathrm{S1}}}{2\pi\gamma_{\mathrm{S1}}}}}. \end{aligned} \tag{7.17}$$

In the second line, we have considered $N_{\mathrm{S1}} \gg 1$ and $\gamma_{\mathrm{S1}} \gg 1$, while the third line uses the Fourier series closed solution

$$\sum_{j=-\infty}^{\infty} \frac{\exp\left[-2\pi iaj\right]}{j+b} = -2\pi i \frac{\exp\left[2\pi ib \bmod(a,1)\right]}{1-e^{2\pi ib}}. \tag{7.18}$$

The populations are

$$P_k^{\mathrm{pw}}(t) = \frac{2\pi\gamma_{\mathrm{S1}}}{N_{\mathrm{S1}}} \exp\left[-2\pi\gamma_{\mathrm{S1}} \bmod \left(\frac{k}{N_{\mathrm{S1}}} + \frac{2t}{\tau_{\mathrm{rev}}^{\mathrm{S1}}}, 1\right)\right]. \tag{7.19}$$

Here, we see the exponential profile of temporal evolution of the ground state is imprinted on the excited states as $4\pi\gamma_{\mathrm{S1}}/\tau_{\mathrm{rev}}^{\mathrm{S1}} = 1/\tau_2^{\mathrm{S1}}$. This exponential wave packet is dispersionless and moves with speed V/π, as depicted in Fig. 7.5, where

we also see oscillatory effects neglected by the Markov-Shark approximation. Most prominent is the affect of the ground state to $|\mathbf{0}_{\mathrm{S1}}\rangle$ coupling, when the wave packet passes through $|\mathbf{0}_{\mathrm{S1}}\rangle$ at half the revival time. The Markov-Shark approximation describes the dynamics well for $0 \leq t \leq \tau_{\mathrm{rev}}^{\mathrm{S1}}/2$, thereafter, the coupling can transfer population to the ground state. The dispersionless evolution is owed to the linear distribution of detunings. This serves as our best-case-scenario, due to the dispersionless nature protecting against premature transitions to the ground state.

7.2.4 Emission scheme

Here, we adapt and develop upon the works Refs. [144, 145]. For the the excitation scheme discussed prior, the light field imprints a phase distribution over a spatially distributed ensemble. To to include this, the effective Hamiltonian Eq. (7.3) should read

$$\hat{H}_{\mathrm{S1}} = \hbar\Omega_{\mathrm{S1}} \left[\sum_{j=1}^{N_{\mathrm{S1}}} |G_{\mathrm{S1}}\rangle\langle r_j^{\mathrm{S1}}| e^{-i\mathbf{k}_1\cdot\mathbf{r}_j} + \mathrm{h.c.} \right] + \sum_{j=1}^{N_{\mathrm{S1}}} \hbar V_j |r_j^{\mathrm{S1}}\rangle\langle r_j^{\mathrm{S1}}|, \tag{7.20}$$

where $\mathbf{r}_j$ is the position of the jth atom. We see that all the previous sections are working within the phase shifted basis $|\mathscr{r}_j\rangle = e^{i\mathbf{k}_1\cdot\mathbf{r}_j}|r_j^{\mathrm{S1}}\rangle$.

We now introduce the transition from $|r^{\mathrm{S1}}\rangle$ to a decaying auxiliary state $|e^{\mathrm{S1}}\rangle$ at the Rabi frequency Ω_{aux} and zero detuning. Within the RWA and rotating frame, we have

$$\hat{H}_{\mathrm{aux}} = \hbar\Omega_{\mathrm{aux}} \left[\sum_{j=1}^{N_{\mathrm{S1}}} |\mathscr{r}_j\rangle\langle \mathscr{e}_j| + \mathrm{h.c.} \right], \tag{7.21}$$

where $|\mathscr{e}_j\rangle = e^{i\Delta\mathbf{k}\cdot\mathbf{r}_j}|e_j^{\mathrm{S1}}\rangle$, $\Delta\mathbf{k} = \mathbf{k}_1 - \mathbf{k}_2$, and $\mathbf{k}_2$ is the wavevector of the auxiliary light field. By applying a π pulse at time t_0, we enact

$$|\psi\rangle = \sum_{j=1}^{N_{\mathrm{S1}}} C_j(t_0)|\mathscr{r}_j\rangle \rightarrow \sum_{j=1}^{N_{\mathrm{S1}}} C_j(t_0)|\mathscr{e}_j\rangle. \tag{7.22}$$

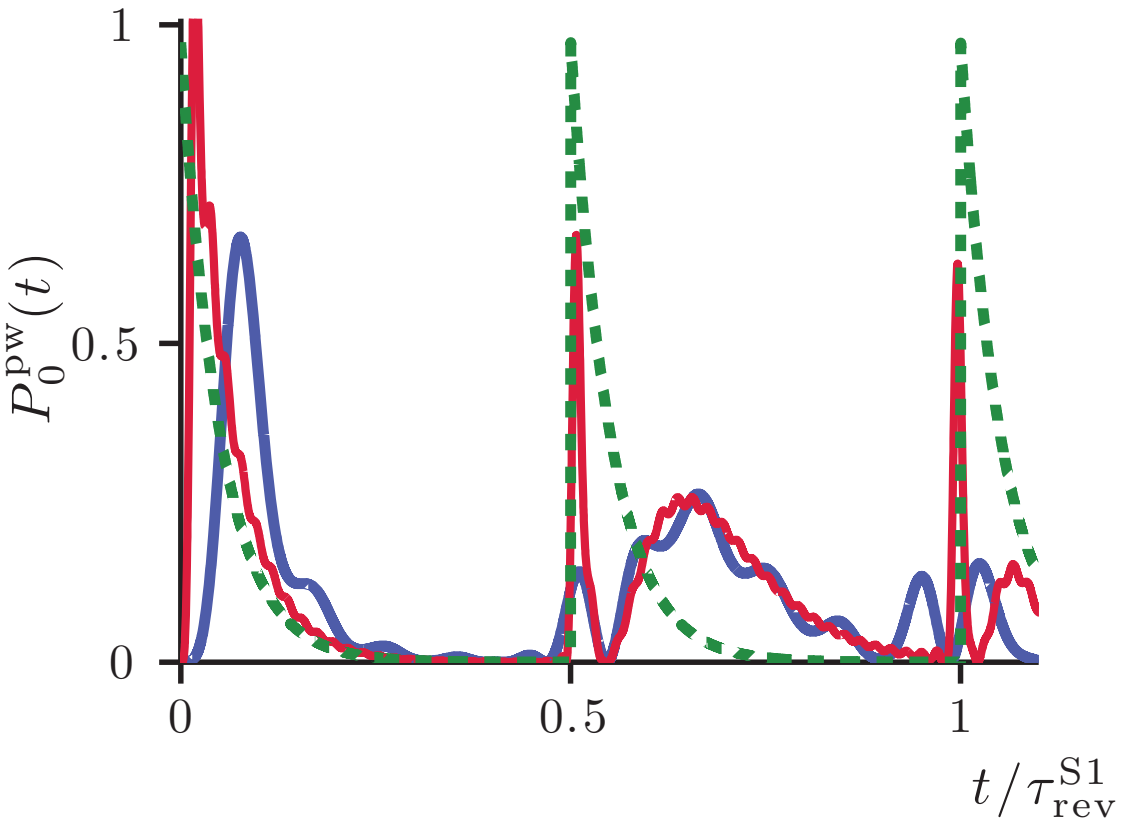

Figure 7.5: $P_0^{\mathrm{pw}}(t)$ for $V/\Omega_{\mathrm{S1}} = 10$, and, $N_a = 10$ (blue), $N_b = 50$ (red), and Eq. (7.19) (green). For comparison, the case of N_b has been scaled by $N_b/N_a = 5$ [cf. Eq. (7.19)]. The case of N_a demonstrates oscillations in the first peak, which are reduced by increasing the number of atoms, giving better agreement with the Markov-Shark approximation. The second peak exhibits strong oscillatory structure, which is attributed to the excitation passing through the symmetric state (neglected in the Markov-Shark approximation).

The state $|e^{\mathrm{S1}}\rangle$ decays into the electromagnetic vacuum, thus, we introduce the quantum field within the RWA and rotating frame

$$\hat{H}_{\mathrm{qtm}} = \hbar g_{\mathbf{k},\lambda} \left[\sum_{j=1}^{N_{\mathrm{S1}}} |e_j\rangle\langle G_{\mathrm{S1}}|\hat{a}_{\mathbf{k},\lambda} e^{i[\mathbf{k}-\Delta\mathbf{k}]\cdot\mathbf{r}_j - i(\omega_{\mathbf{k}}-\omega_0)t} + \mathrm{h.c.} \right], \tag{7.23}$$

where $\mathbf{k}$ and λ, are the wavevector and polarization of the emitted light, respectively. The annihilation operator for a photon with $\mathbf{k}$ and λ is $\hat{a}_{\mathbf{k},\lambda}$, while the quantum Rabi frequency is given by $\hbar g_{\mathbf{k},\lambda} = -\sqrt{\hbar\omega_{\mathbf{k}}/2\epsilon_0 L^3} d_{eg}^{\mathbf{k},\lambda}$, where $\omega_{\mathbf{k}}$ is the photon frequency, $d_{eg}^{\mathbf{k},\lambda}$ is the dipole matrix element for the transition for a photon with $\mathbf{k}$ and λ, and L^3 is the volume of the mode function to be taken to ∞ at the end of calculations.

Our wavefunction is now written as

$$|\psi\rangle = \sum_{\mathbf{k}} \sum_{\lambda=1}^{2} d_{\mathbf{k},\lambda}(t)|G_{\mathrm{S1}}\rangle|1_{\mathbf{k},\lambda}\rangle + \sum_{j=1}^{N_{\mathrm{S1}}} d_j(t)|e_j\rangle|\mathbf{0}_{\mathrm{ph}}\rangle, \tag{7.24}$$

where $|\mathbf{0}_{\mathrm{ph}}\rangle$ indicates the field vacuum state, $|1_{\mathbf{k},\lambda}\rangle$ the single photon state with $\mathbf{k}$ and λ, and $d_j(t_0) = C_j(t_0)$. Formally solving for $d_{\mathbf{k},\lambda}(t)$, we have

$$\dot{d}_j(t) = -\sum_{\mathbf{k}} \sum_{\lambda=1}^{2} \sum_{l=1}^{N_{\mathrm{S1}}} |g_{\mathbf{k},\lambda}|^2 \, e^{i(\mathbf{k}-\Delta\mathbf{k})\cdot\mathbf{r}_{jl}} \int_{t_0}^{t} dt' d_l(t') e^{i(\omega_{\mathbf{k}}-\omega_0)(t'-t)}, \tag{7.25}$$

where $\mathbf{r}_{jl} = \mathbf{r}_j - \mathbf{r}_l$. We take the large box limit, where $\sum_{\mathbf{k}} \to \frac{L^3}{(2\pi)^3}\int_{-\infty}^{\infty} d^3\mathbf{k}$, and sum over the polarisations $\sum_{\lambda=1}^{2} |g_{\mathbf{k},\lambda}|^2 = \omega_{\mathbf{k}} d_{eg}^2 [1-(\hat{\mathbf{d}}\cdot\hat{\mathbf{k}})^2]/2\hbar\epsilon_0 L^3$, where d_{eg} is the dipole matrix element, $\hat{\mathbf{d}}$ is the quantisation axis, and $\omega_{\mathbf{k}} = ck$. Performing the angular integrals, one obtains

$$\dot{d}_j(t) = -\frac{3\Gamma}{4\pi\omega_0^3} \sum_{l=1}^{N_{\mathrm{S1}}} e^{-i\Delta\mathbf{k}\cdot\mathbf{r}_{jl}} \times \int_0^{\infty}\int_{t_0}^{t} dt' d\omega_{\mathbf{k}} \omega_{\mathbf{k}}^3 \, \tau_1(\hat{\mathbf{d}}\cdot\hat{\mathbf{r}}_{jl}, \omega_{\mathbf{k}} r_{jl}/c) d_l(t') e^{i(\omega_{\mathbf{k}}-\omega_0)(t'-t)}, \tag{7.26}$$

where $\Gamma = \omega_0^3 d_{eg}^2/3\pi\epsilon_0\hbar c^3$ is the single atom decay rate, and

$$\tau_1(x,y) = (1-x^2)\frac{\sin y}{y} + (1-3x^2)\left(\frac{\cos y}{y^2} - \frac{\sin y}{y^3}\right), \tag{7.27}$$

where $\lim_{y\to 0}\tau_1(x,y) = 2/3$.

To proceed further, we make the Markovian approximation $d_l(t') \to d_l(t)$, and in the limit $t - t_0 \to \infty$,

$$\int_{t_0}^{t} dt' e^{i(\omega_{\mathbf{k}}-\omega_0)(t'-t)} = \pi\delta(\omega_{\mathbf{k}} - \omega_0) - i\mathrm{P}\frac{1}{\omega_{\mathbf{k}} - \omega_0}. \tag{7.28}$$

This leads to integrals like

$$\mathrm{P}\int_0^\infty d\omega_{\mathbf{k}} \frac{\omega_{\mathbf{k}}^3}{\omega_{\mathbf{k}} - \omega_0}, \tag{7.29}$$

which are formally divergent, arising due to the point particle approximation. These integrals lead to the single atom Lamb shift and the collective Lamb shifts. Following the Weisskopf-Wigner approximation, physically, one should only consider frequencies around the resonance frequency ω_0. Setting the powers of $\omega_{\mathbf{k}}$ to ω_0 in the numerator, setting the lower integration limit to $-\infty$, and absorbing the Lamb shift into the definition of the transition frequency, we have

$$\dot{d}_j(t) = -\frac{\Gamma}{2}d_j(t) - \frac{3\Gamma}{4}\sum_{l\neq j} F_{jl}(k_0, \mathbf{r}_{jk}, \Delta\mathbf{k}, \hat{\mathbf{d}})\, d_l(t), \tag{7.30}$$

where the second term describes the collective Lamb shifts,

$$F_{jl}(\omega_0, \mathbf{r}_{jk}, \Delta\mathbf{k}, \hat{\mathbf{d}}) = e^{-i\Delta\mathbf{k}\cdot\mathbf{r}_{jl}}\left[\tau_1(\hat{\mathbf{d}}\cdot\hat{\mathbf{r}}_{jl}, k_0 r_{jl}) - i\tau_2(\hat{\mathbf{d}}\cdot\hat{\mathbf{r}}_{jl}, k_0 r_{jl})\right], \tag{7.31}$$

where

$$\tau_2(x,y) = (1-x^2)\frac{\cos y}{y} - (1-3x^2)\left(\frac{\sin y}{y^2} + \frac{\cos y}{y^3}\right). \tag{7.32}$$

7.2.5 Emission profile

Here, we derive the angular profile of the emitted photon. We are concerned with the average number of photons with wavevector $\mathbf{k}$

$$N_{\mathrm{ph}}\left(\mathbf{k},t\right)=\sum_{\lambda=1}^{2}\langle\hat{a}_{\mathbf{k},\lambda}^{\dagger}\hat{a}_{\mathbf{k},\lambda}\rangle=\sum_{\lambda=1}^{2}\left|d_{\mathbf{k},\lambda}(t)\right|^{2}, \tag{7.33}$$

which is given by formally integrating $d_{\mathbf{k},\lambda}(t)$

$$\begin{aligned}N_{\mathrm{ph}}\left(\mathbf{k},t\right)=\sum_{\lambda=1}^{2}\left|g_{\mathbf{k},\lambda}\right|^{2}\sum_{j,l=1}^{N_{\mathrm{S1}}}e^{i(\mathbf{k}-\Delta\mathbf{k})\cdot(\mathbf{r}_{j}-\mathbf{r}_{l})}\\ \times\int_{t_0}^{t}\int_{t_0}^{t}dt'dt''d_{l}(t')d_{j}^{*}(t'')e^{i(\omega_{\mathbf{k}}-\omega_0)(t'-t'')}.\end{aligned} \tag{7.34}$$

Upon making the large box limit, we obtain the number of photons in the solid angle $d\Omega$

$$\begin{aligned}\frac{dN_{\mathrm{ph}}(\Omega,t)}{d\Omega}=\frac{3\Gamma[1-(\hat{\mathbf{d}}\cdot\hat{\mathbf{k}})^{2}]}{16\pi^{2}\omega_{0}^{3}}\sum_{j,l=1}^{N_{\mathrm{S1}}}\\ \times\int_{t_0}^{t}\int_{t_0}^{t}\int_{0}^{\infty}d\omega_{\mathbf{k}}dt'dt''d_{l}(t')d_{j}^{*}(t'')\omega_{\mathbf{k}}^{3}e^{i(\omega_{\mathbf{k}}/c\hat{\mathbf{k}}-\Delta\mathbf{k})\cdot\mathbf{r}_{jl}}e^{i(\omega_{\mathbf{k}}-\omega_0)(t'-t'')}.\end{aligned} \tag{7.35}$$

In the collectively radiating case, where the collective Lamb shifts in Eq. (7.30) are nonnegligible, we have

$$d_{l}(t)=\sum_{m=1}^{N_{\mathrm{S1}}}d_{m}^{e}(t_0)e^{-\lambda_{m}(t-t_0)}[\mathbf{v}_{m}]_{l},\quad t\geq t_0, \tag{7.36}$$

where the collective eigenvectors $\mathbf{v}_m$ are nonorthogonal with (decaying) complex eigenvalues λ_m, and $d_l^e(t_0)$ are the expansion coefficients of the eigenbasis. By choosing decaying eigenvalues, we are implicitly not considering the subradiant

regime where atomic spacings are smaller than the wavelength of the emitted light field. This requires a nonrotating-wave analysis [144, 145], and one can find nondecaying solutions.

Applying the Weisskopf-Wigner approximation, we have the solution

$$\frac{dN_{\rm ph}}{d\Omega} = \frac{3[1-(\hat{\mathbf{d}}\cdot\hat{\mathbf{k}})^2]}{8\pi}\sum_{j,l,m,n=1}^{N_{\rm S1}} \frac{\Gamma}{\lambda_m+\lambda_n^*} d_m^e(t_0)[d_n^e(t_0)]^*[\mathbf{v}_m]_l[\mathbf{v}_n]_j^* e^{i(k_0\hat{\mathbf{k}}-\Delta\mathbf{k})\cdot\mathbf{r}_{jl}}, \tag{7.37}$$

In the case of independently radiating atoms, being the solution of Eq. (7.25) for atomic separations much larger than the light wavelength,

$$d_j(t) = C_j(t_0)e^{-\frac{\Gamma}{2}(t-t_0)}, \quad t \geq t_0, \tag{7.38}$$

the differential cross section is

$$\frac{dN_{\rm ph}}{d\Omega} = \frac{3[1-(\hat{\mathbf{d}}\cdot\hat{\mathbf{k}})^2]}{8\pi}\sum_{j,l=1}^{N_{\rm S1}} C_l(t_0)C_j^*(t_0)e^{i(k_0\hat{\mathbf{k}}-\Delta\mathbf{k})\cdot\mathbf{r}_{jl}}. \tag{7.39}$$

In both cases, we see the single-atom dipole emission pattern,

$$\frac{3[1-(\hat{\mathbf{d}}\cdot\hat{\mathbf{k}})^2]}{8\pi}, \tag{7.40}$$

factors out from the collective contribution. The independently radiating case does not conserve the number of excitations (single photon) in general (improves with greater atomic separation), as it is not the general solution to Eq. (7.25). The full collective solutions of Eq. (7.30) conserve the number of excitations excellently.

1D emission profile: examples

To proceed further, we must select the geometry being the simplest case of a 1D chain (illustrated in Fig. 7.6), where we have $\mathbf{r}_j = \delta x(j - N_{\mathrm{S1}}/2)\hat{\mathbf{x}}$.

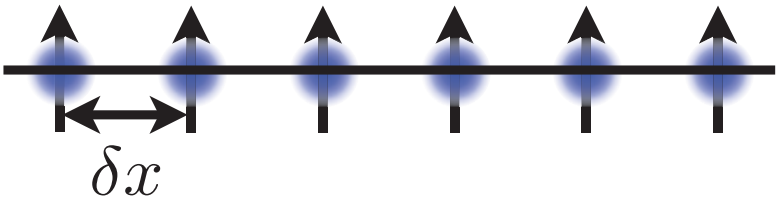

Figure 7.6: 1D chain of spacing δx, where we have assumed all dipoles are aligned (in some unspecified direction).

General plane-wave excitations

Assuming, we begin with a particular plane wave state $|k\rangle$ [cf. Eq. (7.16)], we have

$$C_{j+N_{\mathrm{S1}}/2}(t_0) = \frac{1}{\sqrt{N_{\mathrm{S1}}}} \exp\left[\frac{2\pi i j k}{N_{\mathrm{S1}}}\right]. \tag{7.41}$$

This yields

$$\frac{dN_{\mathrm{ph}}}{d\Omega} = \frac{3[1-(\hat{\mathbf{d}}\cdot\hat{\mathbf{k}})^2]}{8\pi N_{\mathrm{S1}}} \frac{\sin^2\left[N_{\mathrm{S1}}\delta x\hat{\mathbf{x}}\cdot(k_0\hat{\mathbf{k}}-\Delta\mathbf{k}')/2\right]}{\sin^2\left[\delta x\hat{\mathbf{x}}\cdot(k_0\hat{\mathbf{k}}-\Delta\mathbf{k}')/2\right]}, \tag{7.42}$$

where $\Delta\mathbf{k}' = \Delta\mathbf{k} + 2\pi k/N_{\mathrm{S1}}\delta x\hat{\mathbf{x}}$. We see, intuitively, that the plane-wave excitation of the atoms acts to give a boost to the effective wavevector. The angular distribution (7.42) pertains to either a peak or a series of peaks positioned at $\delta x\hat{\mathbf{x}}\cdot(k_0\hat{\mathbf{k}}-\Delta\mathbf{k}') = 2\pi n$, and is attenuated by the single dipole emission profile $[1-(\hat{\mathbf{d}}\cdot\hat{\mathbf{k}})^2]$. As, $N_{\mathrm{S1}} \to \infty$, Eq. (7.42) becomes

$$\frac{dN_{\mathrm{ph}}}{d\Omega} \propto [1-(\hat{\mathbf{d}}\cdot\hat{\mathbf{k}})^2]\delta\left[\delta x\hat{\mathbf{x}}\cdot(k_0\hat{\mathbf{k}}-\Delta\mathbf{k}') - 2\pi n\right], \tag{7.43}$$

where $\delta(x)$ is the Dirac-delta function, and $n \in \mathbb{Z}$. This is a simple example of Bragg scattering, and can be obtained by simple geometric arguments.

Markov-Shark approximation

Now, we consider the Markov-Shark approximation in Sec. 7.2.2, and proceed with the amplitudes in the atomic basis,

$$C_j\left(t\right) = \frac{\Omega_{\mathrm{S1}}}{V_j + \frac{i}{2\tau_2^{\mathrm{S1}}}}[\exp(-iV_j t) - C_{\mathrm{g}}\left(t\right)]. \tag{7.44}$$

As before, the ground state is taken to have completely decayed. Here, we have

$$\frac{dN_{\mathrm{ph}}}{d\Omega} = \frac{3[1-(\hat{\mathbf{d}}\cdot\hat{\mathbf{k}})^2]}{8\pi}\sum_{j,l=1}^{N_{\mathrm{S1}}} T_j T_l^*, \tag{7.45}$$

where

$$T_j = \Omega_{\mathrm{S1}}\frac{e^{i\left[(k_0\hat{\mathbf{k}}-\Delta\mathbf{k})\cdot\mathbf{r}_j + t_0 V_j\right]}}{V_j - \frac{i}{2\tau_2^{\mathrm{S1}}}}. \tag{7.46}$$

We can evaluate this expression with the tools already utilized above.

$$\begin{aligned}\sum_{j=1}^{N_{\mathrm{S1}}} T_j &= \Omega_{\mathrm{S1}}\sum_{j=1}^{N_{\mathrm{S1}}}\frac{e^{i\left[(k_0\hat{\mathbf{k}}-\Delta\mathbf{k})\cdot\mathbf{r}_j + t_0 V_j\right]}}{V_j - \frac{i}{2\tau_2^{\mathrm{S1}}}} \\ &\simeq i\sqrt{2\pi\gamma_{\mathrm{S1}}}\exp\left[\pi\left(i-\gamma_{\mathrm{S1}}\right)\,\mathrm{mod}(x,1) + i\frac{Vt_0}{N_{\mathrm{S1}}}\right],\end{aligned} \tag{7.47}$$

where $x = \left[\delta x\hat{\mathbf{x}}\cdot(k_0\hat{\mathbf{k}}-\Delta\mathbf{k})/2\pi + \frac{Vt_0}{\pi N_{\mathrm{S1}}}\right]$. Thus, we have

$$\frac{dN_{\mathrm{ph}}}{d\Omega} = \frac{3\gamma_{\mathrm{S1}}[1-(\hat{\mathbf{d}}\cdot\hat{\mathbf{k}})^2]}{4}\exp\left[-2\pi\gamma_{\mathrm{S1}}\,\mathrm{mod}(x,1)\right]. \tag{7.48}$$

Again the angular distribution (7.48) is similar to that of (7.42), in that it pertains to a peak or a series of peaks attenuated by the single dipole emission pattern. However, the peaks are broadened by an exponential profile.

7.3 Ensemble - ensemble dynamics

In light of the conditioned dynamics we observed in Sec. 7.2, a glaring question to ask: what about the driving of multiple ensembles? Indeed, the driving of two ensembles we discuss here, leads to the deterministic excitation of both ensembles only in the presence of each other. Paralleling to [132, 146], the presence of another ensemble enables a two photon transition to the doubly-excited state, while alone excitation is prohibited by detuning. Owing to the inhomogeneity, this doubly-excited state remains excited squeezing the excitation statistics.

Ultimately, we wish to consider three ensembles where only two excitations may exist, such that, the double excitation will oscillate between the three. Additionally, the excitation avalanche dynamics where all ensembles are deterministically excited. Investigation into the characteristics of the emitted photons from such systems is curious, as the highly correlated characteristics of the system will be imprinted on the light field.

We present some analytical considerations for the timescales of the excitation dynamics of two ensembles, and find that they are readily understood in terms of the ancilla assisted dynamics discussed in Sec. 7.2.

7.3.1 Single atom

As Sec. 7.2, we first consider the case where system 2 contains only a single atom, however, we now include driving for this system $\Omega_{\mathrm{S1}} > 0$ and it is initial in the ground state. Taking the general quantum state to be

$$|\psi\rangle = c_{\mathrm{g}}(t)|G_{\mathrm{S1}}\rangle|G_{\mathrm{S2}}\rangle + c_{\mathrm{S2}}(t)|G_{\mathrm{S1}}\rangle|r_1^{\mathrm{S2}}\rangle + \sum_{j=1}^{N_{\mathrm{S1}}} c_j^{\mathrm{S1}}(t)|r_j^{\mathrm{S1}}\rangle|G_{\mathrm{S2}}\rangle + \sum_{j=1}^{N_{\mathrm{S1}}} d_j(t)|r_j^{\mathrm{S1}}\rangle|r_1^{\mathrm{S2}}\rangle, \quad (7.49)$$

and making the Markovian approximation Sec. 7.2.1, we have

$$d_j(t) = \left[\Omega_{\mathrm{S2}} c_j^{\mathrm{S1}}(t) + \Omega_{\mathrm{S1}} c_{\mathrm{S2}}(t)\right] \frac{e^{-iV_j t} - 1}{V_j}. \quad (7.50)$$

To a very good approximation (see Fig. 7.7), we need only consider the the symmetric state evolution, as the population is primarily shuffled between $|G_{\mathrm{S1}}\rangle|G_{\mathrm{S2}}\rangle$

and $|\mathbf{0}_{\mathrm{S1}}\rangle$ ($|\mathbf{0}_{\mathrm{S2}}\rangle$), while decaying into the doubly excited states. Denoting the probability amplitude for $|\mathbf{0}_{\mathrm{S1}}\rangle$ as $c_{\mathrm{S1}}(t)$, we have the approximate evolution equations of the effective three level system

$$i\dot{c}_g(t) = \sqrt{N_{\mathrm{S1}}}\Omega_{\mathrm{S1}}c_{\mathrm{S1}}(t) + \Omega_{\mathrm{S2}}c_{\mathrm{S1}}(t), \tag{7.51a}$$

$$\begin{aligned} i\dot{c}_{\mathrm{S1}}(t) = \sqrt{N_{\mathrm{S1}}}\Omega_{\mathrm{S1}}c_g(t) &+ \frac{\Omega_{\mathrm{S1}}\Omega_{\mathrm{S2}}}{\sqrt{N_{\mathrm{S1}}}}\sum_{j=1}^{N_{\mathrm{S1}}}\frac{e^{-iV_jt}-1}{V_j}c_{\mathrm{S2}}(t) \\ &+ \left[\frac{\Omega_{\mathrm{S2}}^2}{N_{\mathrm{S1}}}\sum_{j=1}^{N_{\mathrm{S1}}}\frac{e^{-iV_jt}-1}{V_j} - \Delta_{\mathrm{S1}}\right]c_{\mathrm{S1}}(t), \end{aligned} \tag{7.51b}$$

$$\begin{aligned} i\dot{c}_{\mathrm{S2}}(t) = \Omega_{\mathrm{S2}}c_g(t) &+ \frac{\Omega_{\mathrm{S1}}\Omega_{\mathrm{S2}}}{\sqrt{N_{\mathrm{S1}}}}\sum_{j=1}^{N_{\mathrm{S1}}}\frac{e^{-iV_jt}-1}{V_j}c_{\mathrm{S1}}(t) \\ &+ \left[\Omega_{\mathrm{S1}}^2\sum_{j=1}^{N_{\mathrm{S1}}}\frac{e^{-iV_jt}-1}{V_j} - \Delta_{\mathrm{S2}}\right]c_{\mathrm{S2}}(t). \end{aligned} \tag{7.51c}$$

Linear detuning

Considering again linear detunings, Sec. 7.2.2, and taking N_{S1} to be large, the equations of motion (7.51) are given by

$$i\dot{c}_g(t) = \sqrt{N_{\mathrm{S1}}}\Omega_{\mathrm{S1}}c_{\mathrm{S1}}(t) + \Omega_{\mathrm{S2}}c_{\mathrm{S2}}(t), \tag{7.52a}$$

$$i\dot{c}_{\mathrm{S1}}(t) = \sqrt{N_{\mathrm{S1}}}\Omega_{\mathrm{S1}}c_g(t) - \frac{i}{2\sqrt{\tau_2^{\mathrm{S1}}\tau_2^{\mathrm{S2}}}}c_{\mathrm{S2}}(t) - \left[\frac{i}{2\tau_2^{\mathrm{S2}}} + \Delta_{\mathrm{S1}}\right]c_{\mathrm{S1}}(t), \tag{7.52b}$$

$$i\dot{c}_{\mathrm{S2}}(t) = \Omega_{\mathrm{S2}}c_g(t) - \frac{i}{2\sqrt{\tau_2^{\mathrm{S1}}\tau_2^{\mathrm{S2}}}}c_{\mathrm{S1}}(t) - \left[\frac{i}{2\tau_2^{\mathrm{S1}}} + \Delta_{\mathrm{S2}}\right]c_{\mathrm{S2}}(t). \tag{7.52c}$$

Now, we have a system of equations very similar to that found in Fano Resonance physics, and, indeed, this system does exhibit resonance structure owing to the two

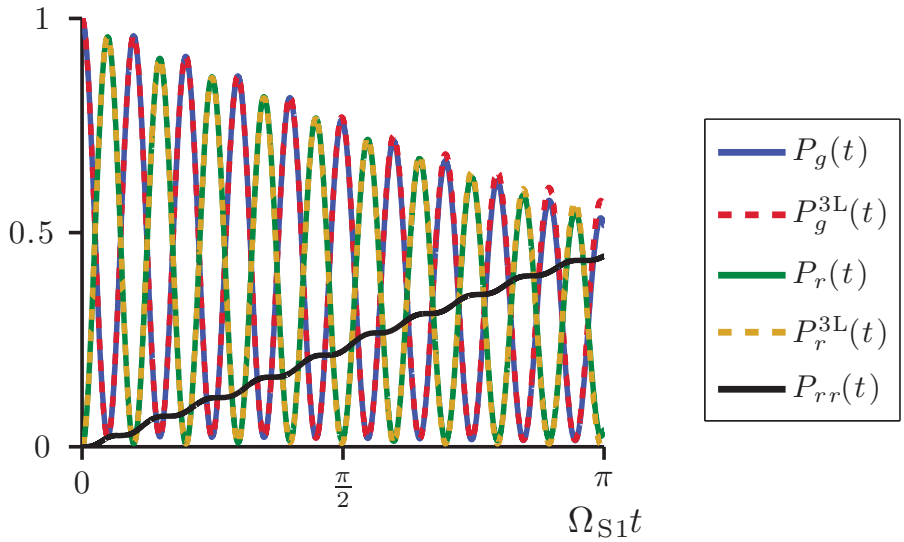

Figure 7.7: An example of the agreement between the full Markovian equations, and the effective three level system (3L) Eqs. (7.51). Subscripts indicate the ground (g), singly-excited (r), and doubly-excited (rr) populations. Simulations were performed with $N_{\mathrm{S1}} = 100$, and the randomly distributed positions for a gaussian distribution with a standard deviation σ. The ancilla is positioned 6σ away from cloud centre, $\Delta_{\mathrm{S1}}/\Omega_{\mathrm{S1}} = 6$, and $C_6/\Omega_{\mathrm{S1}}\sigma^6 = 7 \times 10^5$.

possible pathways in system can "decay" into the bath. The timescales are illustrated in Fig. 7.8, and are readily understood. The decay from $|G_{\mathrm{S1}}\rangle|r_1^{\mathrm{S2}}\rangle$ is owing to the many atom ensemble being excited, which features a N_{S1} enhancement, and the decay time is that derived in Sec. 7.2.2. The other pathway is attributed to the excitation of a single atom, thus decays without the enhancement. Finally, incoherent transfer of population $[1/(\tau_2^{\mathrm{S1}}\tau_2^{\mathrm{S2}})^{\frac{1}{2}}]$ is inherent to Fano physics.

We see that the fastest decay process is associated with the many atom system, thus for the fastest decay, we must keep this pathway open. That is, $\Delta_{\mathrm{S2}} \leq \Delta_{\mathrm{S1}}$ and $\Omega_{\mathrm{S2}} \geq \Omega_{\mathrm{S1}}$. The eigenvalue with the smallest real part (longest timescale) in magnitude will set the timescale for the decay dynamics. Owing to the system featuring resonance phenomenon, we must maximise this for the relevant cases $\Delta_{\mathrm{S1}} = \Delta_{\mathrm{S2}} = 0$, $\Delta_{\mathrm{S1}} = \Delta_{\mathrm{S2}} = V/2$, and $\Delta_{\mathrm{S1}} = 0$, $\Delta_{\mathrm{S2}} = V$. To a good approx-

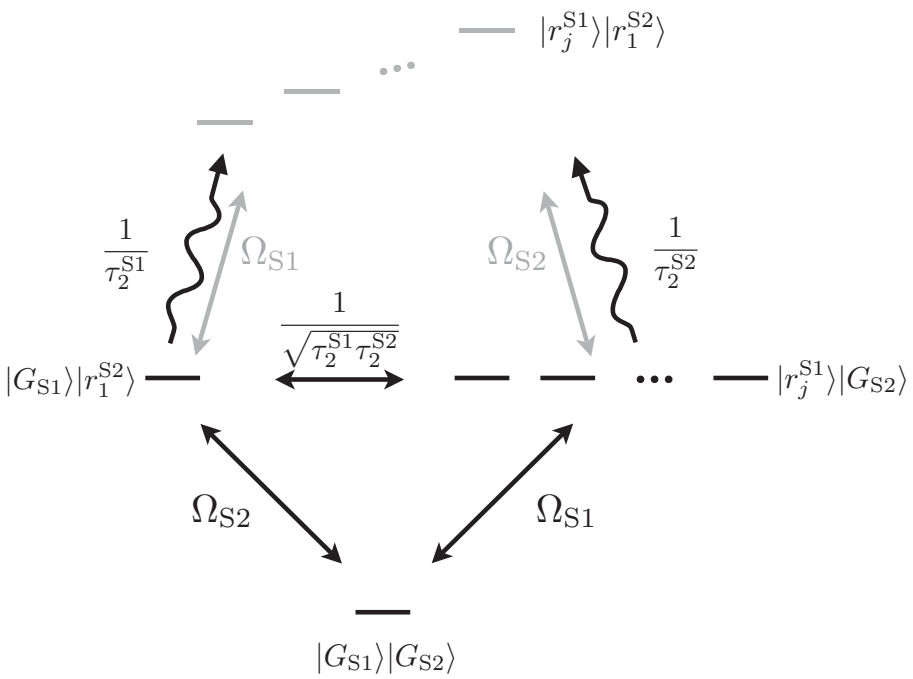

Figure 7.8: Energy level scheme, where the faded couplings and levels represent the full scheme before the Markovian Approximation.

imation, we find in each case the ideal detuning tends to $V_{\max} = \pi\sqrt{N_{S1}}\Omega_{S1}/2$ for increasing N_{S1}, and the decay timescale is

$$\tau_{\mathrm{d}} = \sqrt{\frac{2}{\pi}}\frac{N_{S1}\Omega_{S1}^2}{V_{\max}\Omega_{S2}^2} = \left(\frac{2}{\pi}\right)^{\frac{3}{2}}\frac{\sqrt{N_{S1}}\Omega_{S1}}{\Omega_{S2}^2}. \tag{7.53}$$

As explained, the limiting element of the speed is indeed the single atom. We remove this constraint in the following section.

7.3.2 Many atoms

We now the general case of system 2 having N_{S2}, i.e., the replacements

$$c_{\mathrm{S2}}(t)|G_{\mathrm{S1}}\rangle|r_1^{\mathrm{S1}}\rangle \to \sum_{j=1}^{N_{\mathrm{S2}}} c_j^{\mathrm{S2}}(t)|G_{\mathrm{S1}}\rangle|r_j^{\mathrm{S2}}\rangle, \tag{7.54a}$$

$$\sum_{j=1}^{N_{\mathrm{S1}}} d_j(t)|r_j^{\mathrm{S1}}\rangle|r_1^{\mathrm{S2}}\rangle \to \sum_{j=1}^{N_{\mathrm{S1}}}\sum_{k=1}^{N_{\mathrm{S2}}} d_{j,k}(t)|r_j^{\mathrm{S1}}\rangle|r_k^{\mathrm{S2}}\rangle, \tag{7.54b}$$

in Eq. (7.49). With the Markovian approximation, we have

$$i\dot{c}_g(t) = \Omega_{\mathrm{S1}}\sum_{j=1}^{N_{\mathrm{S1}}} c_j^{\mathrm{S1}}(t) + \Omega_{\mathrm{S2}}\sum_{j=1}^{N_{\mathrm{S2}}} c_j^{\mathrm{S2}}(t) \tag{7.55a}$$

$$\begin{aligned} i\dot{c}_j^{\mathrm{S1}}(t) = \Omega_{\mathrm{S1}}c_g(t) + \left(\Omega_{\mathrm{S2}}^2\sum_{k=1}^{N_{\mathrm{S2}}}\frac{e^{-iV_{jk}t}-1}{V_{jk}} - \Delta_{\mathrm{S1}}\right)c_j^{\mathrm{S1}}(t) \\ + \Omega_{\mathrm{S1}}\Omega_{\mathrm{S2}}\sum_{k=1}^{N_{\mathrm{S2}}}\frac{e^{-iV_{jk}t}-1}{V_{jk}}c_k^{\mathrm{S2}}(t) \end{aligned} \tag{7.55b}$$

$$\begin{aligned} i\dot{c}_k^{\mathrm{S2}}(t) = \Omega_{\mathrm{S2}}c_g(t) + \left(\Omega_{\mathrm{S1}}^2\sum_{j=1}^{N_{\mathrm{S1}}}\frac{e^{-iV_{jk}t}-1}{V_{jk}} - \Delta_{\mathrm{S2}}\right)c_k^{\mathrm{S2}}(t) \\ + \Omega_{\mathrm{S1}}\Omega_{\mathrm{S2}}\sum_{j=1}^{N_{\mathrm{S1}}}\frac{e^{-iV_{jk}t}-1}{V_{jk}}c_j^{\mathrm{S1}}(t), \end{aligned} \tag{7.55c}$$

where $V_{jk} = \tilde{V}_{jk} - \Delta_{\mathrm{S1}} - \Delta_{\mathrm{S2}}$. Now, we presume $\Delta_{\mathrm{S1}} = \Delta_{\mathrm{S1}} = \Delta$, $\Omega_{\mathrm{S1}} = \Omega_{\mathrm{S2}} = \Omega$, $N_{\mathrm{S1}} = N_{\mathrm{S2}} = N$, each atom experiences the same linear detuning, and N is large. We also make the symmetric approximation to obtain the effective

three level system

$$i\dot{c}_g(t) = \sqrt{N}\Omega c_{\mathrm{S1}}(t) + \sqrt{N}\Omega c_{\mathrm{S2}}(t), \tag{7.56a}$$

$$i\dot{c}_{\mathrm{S1}}(t) = \sqrt{N}\Omega c_g(t) - \frac{i}{2\tau_2} c_{\mathrm{S2}}(t) - \left(\frac{i}{2\tau_2} + \Delta\right) c_{\mathrm{S1}}(t), \tag{7.56b}$$

$$i\dot{c}_{\mathrm{S2}}(t) = \sqrt{N}\Omega c_g(t) - \frac{i}{2\tau_2} c_{\mathrm{S1}}(t) - \left(\frac{i}{2\tau_2} + \Delta\right) c_{\mathrm{S2}}(t), \tag{7.56c}$$

where

$$\frac{1}{\tau_2} = \frac{\pi N \Omega^2}{V}. \tag{7.57}$$

Here, the fastest decay timescale is simply τ_2, where this reduction of the decay time scale compared to the single-atom case, Eq. (7.53), again reflects that the limiting speed will be the decay time through the singly-excited manifold.

7.4 Summary, concluding remarks, and outlook

The ancilla assisted dynamics presented in Sec. 7.2 exhibit deterministic absorption of a single photon owed to Rydberg blockade and the ancilla acting to inhomogeneously broaden the excited states of the atomic system. The excitation dynamics are readily understood via a Markovian approximation and linear examples (Sec. 7.2.1). The ground state is coupled to the bright symmetric state with the full collective enhancement, then, the excited state populations are redistributed by the inhomogeneous broadening from the uniform atomic population to a Lorentzian distribution about the atom with zero detuning. Realistically, the detuning will not be linear, affecting the excitation timescales and the dynamics in the excitation manifold. The dynamics in the excitation manifold will no longer be dispersionless, potentially leading to premature deexcitation as population disperses into the bright mode. However, our studies give us insight that for optimal performance we must chose the geometry, interaction, and detuning, such that we maximise the linear character of the detunings around the atom with zero detuning.

The excitation manifold dynamics (Sec. 7.2.3) correspond to a lighthouse-like sweeping of the emitted photon's direction (Sec. 7.2.5). To avoid this, one could wait the revival time of the system for mode matched emission. However, this depends on the number of atoms N, and an analysis will have to be performed on the emitted photons sensitivity to the Poissonian fluctuations of N. An alternative is to freeze the manifold dynamics by deexciting the ancilla as the dynamics are conditioned on the ancilla being excited. Then, with additional ancilla(s), one could fully or partially reverse the temporal manifold dynamics, giving a deterministic mode matched single photon source. In addition, the dynamics can be reversed via Rydberg states of the ancilla where the interaction between the ancilla and system are of identical strength, but opposite sign. This could be performed with Rydberg Stark states in an electric field, where the linear Stark splitting yields states with opposite polarity giving the desired opposite interaction.

The systems considered here lend themselves to system-reservoir dynamical studies for structured baths and (non)Markovian dynamics, and quantum measurements (decoherence). The multi-ensemble examples exhibit highly correlated dynamics that may lead to interesting emission characteristics, while the conditional dynamics could be used to perform quantum gates.

APPENDIX A

CANONICAL TRANSFORMATIONS

In classical mechanics, canonical transformations are transformations of the phase-space variable that preserves the Poisson brackets

$$\{\mathbf{r}, \mathbf{p}\} = 1. \tag{A.1}$$

The quantum mechanical equivalent is the transformation of the noncommuting phase-space variables that preserves the commutator relations

$$[\hat{\mathbf{r}}, \hat{\mathbf{p}}] = i\hbar, \tag{A.2}$$

or equivalently,

$$\left[\hat{a}, \hat{a}^\dagger\right]_\pm = 1, \tag{A.3}$$

where the (anti)commutator, indicated by $(+)-$, is used for (fermions)bosons. Canonical transformations are utilised for evolution, to prove physical equivalence (isometric transformations), and solve theory. As they are defined algebraically, they in general need not be unitary, nor, linear transformations.

Here, we discuss *linear* canonical transformations of creation and annihilation operators. Such transformations are also commonly referred to as Bogoliubov transformations. We only concern ourselves with boson, however, the book for Blaizot and Ripka [79] treats both the bosonic and fermionic cases. The bosonic case is also studied in [147]. Our treatment largely follows [79, 147], while we adapt and expand where it suits our needs.

A.1 Matrix notation

We collect the creation and annihilation operators into the column vector

$$\boldsymbol{\alpha} = \begin{bmatrix} \hat{\mathbf{a}} \\ \hat{\mathbf{a}}^* \end{bmatrix}, \qquad \boldsymbol{\alpha}^\dagger = \boldsymbol{\alpha}^T \boldsymbol{\gamma} = \left[[\hat{\mathbf{a}}^*]^T \, \hat{\mathbf{a}}^T \right], \tag{A.4}$$

where

$$\hat{\mathbf{a}} \; = \left[\hat{a}_1 \cdots \hat{a}_N \right]^T, \qquad \hat{\mathbf{a}}^* = \left[\hat{a}_1^\dagger \cdots \hat{a}_N^\dagger \right]^T, \tag{A.5}$$

and the symplectic matrix $\boldsymbol{\Omega}_{\mathrm{A}}$ and absolute value, $\boldsymbol{\gamma}$, are

$$\boldsymbol{\Omega}_{\mathrm{A}} = \begin{bmatrix} \mathbf{0} & \mathbf{I} \\ -\mathbf{I} & \mathbf{0} \end{bmatrix}, \qquad \boldsymbol{\gamma} = |\boldsymbol{\Omega}_{\mathrm{A}}| = \begin{bmatrix} \mathbf{0} & \mathbf{I} \\ \mathbf{I} & \mathbf{0} \end{bmatrix}. \tag{A.6}$$

We denote the commutator relations by

$$\left[\boldsymbol{\alpha}, \boldsymbol{\alpha}^T\right] = \boldsymbol{\Omega}_{\mathrm{A}} = \begin{bmatrix} \begin{bmatrix} \left[\hat{a}_1, \hat{a}_1\right] & \cdots & \left[\hat{a}_1, \hat{a}_N\right] \\ \vdots & \ddots & \vdots \\ \left[\hat{a}_N, \hat{a}_1\right] & \cdots & \left[\hat{a}_N, \hat{a}_N\right] \end{bmatrix} & \begin{bmatrix} \left[\hat{a}_1, \hat{a}_1^\dagger\right] & \cdots & \left[\hat{a}_1^\dagger, \hat{a}_N\right] \\ \vdots & \ddots & \vdots \\ \left[\hat{a}_N^\dagger, \hat{a}_1\right] & \cdots & \left[\hat{a}_N^\dagger, \hat{a}_N\right] \end{bmatrix} \\ \begin{bmatrix} \left[\hat{a}_1^\dagger, \hat{a}_1\right] & \cdots & \left[\hat{a}_1^\dagger, \hat{a}_N\right] \\ \vdots & \ddots & \vdots \\ \left[\hat{a}_N^\dagger, \hat{a}_1\right] & \cdots & \left[\hat{a}_N^\dagger, \hat{a}_N\right] \end{bmatrix} & \begin{bmatrix} \left[\hat{a}_1^\dagger, \hat{a}_1^\dagger\right] & \cdots & \left[\hat{a}_1^\dagger, \hat{a}_N^\dagger\right] \\ \vdots & \ddots & \vdots \\ \left[\hat{a}_N^\dagger, \hat{a}_1^\dagger\right] & \cdots & \left[\hat{a}_N^\dagger, \hat{a}_N^\dagger\right] \end{bmatrix} \end{bmatrix}. \tag{A.7}$$

The Bogoliubov transformation is given by

$$\boldsymbol{\beta} = \left[\hat{b}_1 \cdots \hat{b}_N \; \hat{b}_1^\dagger \cdots \hat{b}_N^\dagger\right]^T = \mathbf{T}\boldsymbol{\alpha} + \boldsymbol{\delta} = \begin{bmatrix} \mathbf{U} & \mathbf{V} \\ \mathbf{W} & \mathbf{Z} \end{bmatrix} \boldsymbol{\alpha} + \begin{bmatrix} \mathbf{c} \\ \mathbf{d} \end{bmatrix}. \tag{A.8}$$

In general, the new creation operators $\hat{b}_j^\dagger$ are not the hermitian conjugates of their corresponding annihilation operators $\hat{b}_j$. This only occurs when the canonical transformation is unitary. We will return to this in the following section.

The transformation is *canonical* when it preserves the commutation relations

$$\left[\boldsymbol{\beta}, \boldsymbol{\beta}^T\right] = \boldsymbol{\Omega}_{\mathrm{A}}, \tag{A.9}$$

which places the symplectic condition on $\mathbf{T}$

$$\mathbf{T}\boldsymbol{\Omega}_{\mathrm{A}}\mathbf{T}^T = \boldsymbol{\Omega}_{\mathrm{A}}. \tag{A.10}$$

Matrices satisfying this equation form the symplectic group $Sp\left(2n, C\right)$.

We may write the Bogoliubov transformation (A.8) in terms of the operator $\hat{S}$ acting in Fock space

$$\hat{b}_j = \hat{S}\hat{a}_j\hat{S}^{-1}, \qquad \hat{b}_j^\dagger = \hat{S}\hat{a}_j^\dagger\hat{S}^{-1}. \tag{A.11}$$

Using the Campbell-Baker-Hausdorff expansion, the operator $\hat{S}$ can be shown to have the form

$$\hat{S} = \exp\left(\frac{1}{2}\boldsymbol{\alpha}^T\mathbf{K}\boldsymbol{\alpha} + \mathbf{l}^T\boldsymbol{\alpha}\right), \tag{A.12}$$

where K is symmetric, i.e., $\mathbf{K} = \mathbf{K}^T$, and

$$\mathbf{T} = \exp\left(-\boldsymbol{\Omega}_{\mathrm{A}}\mathbf{K}\right), \qquad \boldsymbol{\delta} = -\boldsymbol{\Omega}_{\mathrm{A}}\mathbf{l}. \tag{A.13}$$

The symmetric condition ensures that the symplectic condition (A.10) is satisfied, i.e.,

$$\mathbf{T}^{-1} = -\boldsymbol{\Omega}_{\mathrm{A}}\mathbf{T}^T\boldsymbol{\Omega}_{\mathrm{A}} = \exp\left(\boldsymbol{\Omega}_{\mathrm{A}}\mathbf{K}\right). \tag{A.14}$$

It can also be shown that

$$\begin{aligned}\hat{S} =: \exp\Bigg\{\frac{1}{2}\hat{\mathbf{a}}^T\mathbf{W}\mathbf{U}^{-1}\hat{\mathbf{a}} \; &- \frac{1}{2}\left[\hat{\mathbf{a}}^*\right]^T\mathbf{U}^{-1}\mathbf{V}\hat{\mathbf{a}}^* - \left[\hat{\mathbf{a}}^*\right]^T\left(\mathbf{U}^{-1}+1\right)\hat{\mathbf{a}} \\ &- \hat{\mathbf{a}}^T\mathbf{W}\mathbf{U}^{-1}\mathbf{c} + \mathbf{d}^T\hat{\mathbf{a}} \; - \left[\hat{\mathbf{a}}^*\right]^T\mathbf{U}^{-1}\mathbf{c}\Bigg\} :,\end{aligned} \tag{A.15}$$

where : • : indicates normal ordering.

The vacuum states

$$\hat{a}_j|\mathbf{0}\rangle_a = 0, \qquad \hat{b}_j|\mathbf{0}\rangle_b = 0, \qquad \text{etc.}, \tag{A.16}$$

are related by

$$|\mathbf{0}\rangle_b = \hat{S}|\mathbf{0}\rangle_a = \exp\{-\frac{1}{2}[\hat{\mathbf{a}}^\dagger]^T\mathbf{U}^{-1}\mathbf{V}\hat{\mathbf{a}}^\dagger + [\hat{\mathbf{a}}^\dagger]^T\mathbf{U}^{-1}\mathbf{c}\}|\mathbf{0}\rangle_a, \quad {}_b\langle\mathbf{0}| = {}_a\langle\mathbf{0}|\hat{S}^{-1}. \tag{A.17}$$

Also, note that the number states are related by

$$|\mathbf{n}\rangle_b = \frac{1}{\sqrt{n_1!n_2!\cdots n_N!}}\left[\hat{b}_1^\dagger\right]^{n_1}\left[\hat{b}_2^\dagger\right]^{n_2}\cdots\left[\hat{b}_N^\dagger\right]^{n_N}|\mathbf{0}\rangle_b = \hat{S}|\mathbf{n}\rangle_a \tag{A.18}$$

where $n = n_1 + \cdots + n_N$.

A.2 Unitary canonical transformations

Here, *unitary canonical transform* means $\hat{S}^{-1} = \hat{S}^\dagger$. Not $\mathbf{T}^{-1} = \mathbf{T}^\dagger$. Now the transformed creation and annihilation operators are hermitian conjugate operators

$$\hat{b}_j = \hat{S}\hat{a}_j\hat{S}^\dagger, \qquad \hat{b}_j^\dagger = \hat{S}\hat{a}_j^\dagger\hat{S}^\dagger. \tag{A.19}$$

From Eq. (A.8), we have

$$\mathbf{U} = \mathbf{Z}^*, \qquad \mathbf{V} = \mathbf{W}^*, \qquad \mathbf{d} = \mathbf{c}^*. \tag{A.20}$$

That is

$$\boldsymbol{\beta} = \begin{bmatrix} \mathbf{U} & \mathbf{V} \\ \mathbf{V}^* & \mathbf{U}^* \end{bmatrix}\boldsymbol{\alpha} + \begin{bmatrix} \mathbf{c} \\ \mathbf{c}^* \end{bmatrix}, \tag{A.21}$$

with the relations

$$\mathbf{T}^\dagger = \boldsymbol{\gamma}\mathbf{T}^T\boldsymbol{\gamma}, \qquad \mathbf{T}^{-1} = \boldsymbol{\eta}\mathbf{T}^\dagger\boldsymbol{\eta}, \qquad \boldsymbol{\delta}^* = \boldsymbol{\gamma}\boldsymbol{\delta}, \tag{A.22a}$$

$$\boldsymbol{\eta} = \boldsymbol{\Omega}_{\mathrm{A}}\boldsymbol{\gamma} = -\boldsymbol{\gamma}\boldsymbol{\Omega}_{\mathrm{A}} = \begin{bmatrix} \mathbf{I} & \mathbf{0} \\ \mathbf{0} & -\mathbf{I} \end{bmatrix}. \tag{A.22b}$$

We modify the form of the operator $\hat{S}$ (A.12) to

$$\hat{S} = \exp\left(\frac{i}{2}\boldsymbol{\alpha}^\dagger \mathbf{K}\boldsymbol{\alpha} + i\mathbf{l}^\dagger\boldsymbol{\alpha}\right), \tag{A.23a}$$

$$\mathbf{K}^\dagger = \mathbf{K}, \qquad \mathbf{l}^* = \boldsymbol{\gamma}\mathbf{l}, \qquad \mathbf{K}^T = \boldsymbol{\gamma}\mathbf{K}\boldsymbol{\gamma}, \tag{A.23b}$$

$$\mathbf{T} = \exp\left(-i\boldsymbol{\eta}\mathbf{K}\right), \qquad \boldsymbol{\delta} = -i\boldsymbol{\eta}\mathbf{l}. \tag{A.23c}$$

A.3 Diagonalization of quadratic hamiltonians

Quadratic Hamiltonians can be solved exactly by unitary canonical transformations. The general form of a quadratic bosonic Hamiltonian is

$$\hat{H} = \sum_{ij} A_{ij}\hat{a}_i^\dagger\hat{a}_j + \frac{1}{2}\sum_{ij}\left(B_{ij}\hat{a}_i\hat{a}_j + B_{ij}^*\hat{a}_i^\dagger\hat{a}_j^\dagger\right) + H_0, \tag{A.24a}$$

$$\mathbf{A} = \mathbf{A}^\dagger, \qquad \mathbf{B} = \mathbf{B}^T, \qquad H_0 = \text{const.} \tag{A.24b}$$

This can be re-expressed as

$$\hat{H} = \frac{1}{2}\left(\boldsymbol{\alpha}^\dagger\mathbf{M}\boldsymbol{\alpha} - \mathrm{Tr}\mathbf{A}\right) + H_0, \tag{A.25a}$$

$$\mathbf{M} = \begin{bmatrix} \mathbf{A} & \mathbf{B} \\ \mathbf{B}^* & \mathbf{A}^* \end{bmatrix}. \tag{A.25b}$$

To diagonalize the system, we must transform the system into a collection of noninteraction harmonic oscillators, i.e.,

$$\hat{H} = \sum_j E_j\hat{c}_j^\dagger\hat{c}_j + \text{const.} \tag{A.26}$$

The new creation and annihilation operators, in general, do not create and annihilate particles, but linear combinations of them. These are called quasiparticles, and for the bosonic case, are often called the normal modes of the system. To diagonalize the system, we make the unitary canonical transform $\boldsymbol{\beta} = \mathbf{T}\boldsymbol{\alpha}$,

$$\hat{H} = \frac{1}{2}\left(\boldsymbol{\beta}^\dagger\boldsymbol{\eta}\mathbf{T}\boldsymbol{\eta}\mathbf{M}\mathbf{T}^{-1}\boldsymbol{\beta} - \mathrm{Tr}\mathbf{A}\right) + H_0, \tag{A.27}$$

and we see that $\boldsymbol{\eta}\mathbf{M}$ must be diagonalized to bring the system into diagonal form. I.e.,

$$\mathbf{T}\boldsymbol{\eta}\mathbf{M}\mathbf{T}^{-1} = \mathbf{D}, \tag{A.28}$$

where $\mathbf{D}$ is a diagonal matrix.

We have the eigenvalue problem

$$\boldsymbol{\eta}\mathbf{M}\begin{bmatrix} \mathbf{U}_j \\ -\mathbf{V}_j^* \end{bmatrix} = E_j \begin{bmatrix} \mathbf{U}_j \\ -\mathbf{V}_j^* \end{bmatrix}, \tag{A.29}$$

where $\mathbf{U}_j$ ($\mathbf{V}_j$) is the jth row of the matrix $\mathbf{U}$ ($\mathbf{V}$). Unfortunately, $\boldsymbol{\eta}\mathbf{M}$ is nonhermitian, thus, we cannot use our standard diagonalization methods for hermitian matrices.

A.3.1 Properties of the eigenvectors and values

Now, we take $\mathbf{M}$ to consist of real elements. The significant differences between the real case and the complex case in the following is that the transpose operation becomes the hermitian conjugate, and the treatment of the zero eigenvalue modes changes (see [79] for details).

Since, $\mathbf{M}$ is real and positive semi-definite, the right eigenvectors

$$\mathbf{X}_j = \begin{pmatrix} \mathbf{U}_j \\ -\mathbf{V}_j \end{pmatrix}, \tag{A.30}$$

can be chosen to be real with real eigenvalues. The corresponding left eigenvectors with the same eigenvalues are $\mathbf{X}_j^T\boldsymbol{\eta}$. For every eigenvector $\mathbf{X}_j$ with eigenvalue E_j, there is a corresponding right eigenvector $\mathbf{Y}_j = \boldsymbol{\gamma}\mathbf{X}_j$ with eigenvalue $-E_j$.

Right eigenvectors with $E_j = 0$ are a special case. We focus on the case for only one zero eigenvalue right eigenvector $\mathbf{P}$. Here, the eigenspace is incomplete. For a complete basis, and to obtain a canonical transformation, we need to establish the corresponding generalized eigenvector $\boldsymbol{\mathcal{X}}$, which is given by

$$\boldsymbol{\eta}\mathbf{M}\boldsymbol{\mathcal{X}} = -i\hbar\omega_0\mathbf{P}, \tag{A.31}$$

where ω_0 is some positive constant. We may have the normalization

$$\boldsymbol{\mathcal{X}}^\dagger\mathbf{M}\boldsymbol{\mathcal{X}} = \hbar\omega_0, \qquad \boldsymbol{\mathcal{X}}^\dagger\boldsymbol{\eta}\mathbf{P} = i, \qquad \mathbf{P}^T\boldsymbol{\eta}\mathbf{P} = \boldsymbol{\mathcal{X}}^\dagger\boldsymbol{\eta}\boldsymbol{\mathcal{X}} = 0. \tag{A.32}$$

and write

$$\mathbf{P} = \begin{pmatrix} \mathbf{p} \\ -\mathbf{p} \end{pmatrix}, \qquad \boldsymbol{\mathcal{X}} = -i \begin{pmatrix} \mathbf{x} \\ \mathbf{x} \end{pmatrix}, \qquad \{p_j, x_j\} \in \mathbb{R}, \tag{A.33}$$

which gives

$$2\mathbf{x}^T\mathbf{p} = 1. \tag{A.34}$$

With this generalized eigenvector, we have a complete set, and we can formulate the correct canonical transformation with

$$\mathbf{X}_0 = \frac{1}{\sqrt{2}}\left[\mathbf{P} + i\boldsymbol{\mathcal{X}}\right], \qquad \mathbf{Y}_0 = \frac{1}{\sqrt{2}}\left[i\boldsymbol{\mathcal{X}} - \mathbf{P}\right], \qquad \left\{x_0^j, y_0^j\right\} \in \mathbb{R}. \tag{A.35}$$

The eigenvectors are orthonormal with the metric $\boldsymbol{\eta}$

$$\mathbf{X}_j^T\boldsymbol{\eta}\mathbf{X}_k = -\mathbf{Y}_j^T\boldsymbol{\eta}\mathbf{Y}_k = \mathbf{U}_j^T\mathbf{U}_k - \mathbf{V}_j^T\mathbf{V}_k = \delta_{jk}, \qquad \mathbf{X}_j^T\boldsymbol{\eta}\mathbf{Y}_k = 0, \tag{A.36}$$

and we obtain the closure relation

$$\sum_{j\geq 0}(\mathbf{X}_j\,\mathbf{X}_j^T - \mathbf{Y}_j\,\mathbf{Y}_j^T)\boldsymbol{\eta} = \sum_{j>0}(\mathbf{X}_j\,\mathbf{X}_j^T - \mathbf{Y}_j\,\mathbf{Y}_j^T)\boldsymbol{\eta} + i[\boldsymbol{\mathcal{X}}\mathbf{P}^T - \mathbf{P}\boldsymbol{\mathcal{X}}^\dagger]\boldsymbol{\eta} = \mathbf{I}. \tag{A.37}$$

The new creation and annihilation operators are given by

$$\hat{b}_j = \mathbf{X}_j^T\boldsymbol{\eta}\boldsymbol{\alpha} = -\boldsymbol{\alpha}^\dagger\boldsymbol{\eta}\mathbf{Y}_j\,, \tag{A.38a}$$

$$\hat{b}_j^\dagger = -\mathbf{Y}_j^T\boldsymbol{\eta}\boldsymbol{\alpha} = \boldsymbol{\alpha}^\dagger\boldsymbol{\eta}\mathbf{X}_j\,. \tag{A.38b}$$

The orthonormality (A.36) yields the correct commutation relations

$$\left[\hat{b}_j, \hat{b}_k\right] = \left[\hat{b}_j^\dagger, \hat{b}_k^\dagger\right] = 0, \qquad \left[\hat{b}_j, \hat{b}_k^\dagger\right] = \delta_{jk}. \tag{A.39}$$

A.3.2 Diagonal form

We can obtain diagonal form by multiplying $\mathbf{M}$ by the closure relation (A.37)

$$\mathbf{M} = \boldsymbol{\eta}\boldsymbol{\eta}\mathbf{M}\sum_{j\geq 0}\left(\mathbf{X}_j\mathbf{X}_j^\dagger - \mathbf{Y}_j\mathbf{Y}_j^\dagger\right)\boldsymbol{\eta} \tag{A.40}$$

$$= \boldsymbol{\eta}\left[\sum_{j>0} E_j\left(\mathbf{X}_j\,\mathbf{X}_j^T + \mathbf{Y}_j\,\mathbf{Y}_j^T\right)\boldsymbol{\eta} + \hbar\omega_0\mathbf{P}\mathbf{P}^T\right]\boldsymbol{\eta}. \tag{A.41}$$

Thus, the Hamiltonian (A.25) becomes

$$\begin{aligned}\hat{H} &= \sum_{j>0} E_j \hat{b}_j^\dagger \hat{b}_j + \frac{\hbar\omega_0}{2}\hat{\mathscr{P}}^2 + \frac{1}{2}\left(\sum_{j>0} E_j - \mathrm{Tr}\mathbf{A}\right) + H_0 \\ &= \sum_{j>0} E_j \hat{b}_j^\dagger \hat{b}_j + \frac{\hbar\omega_0}{2}\hat{\mathscr{P}}^2 - \sum_{j>0} E_j \mathbf{Y}_j^T \mathbf{Y}_j - \frac{\hbar\omega_0}{2}\mathbf{P}^T\mathbf{P} + H_0, \end{aligned} \tag{A.42}$$

where the operator $\hat{\mathscr{P}}$ is interpreted as a "momentum" operator given by

$$\hat{\mathscr{P}} = \boldsymbol{\alpha}^\dagger \boldsymbol{\eta} \mathbf{P} = \mathbf{P}^T \boldsymbol{\eta} \boldsymbol{\alpha} = \frac{1}{\sqrt{2}}\left(\hat{b}_0 + \hat{b}_0^\dagger\right), \tag{A.43}$$

while the correspond "position" operator is given by

$$\hat{\mathscr{X}} = \boldsymbol{\alpha}^\dagger \boldsymbol{\eta} \boldsymbol{\mathscr{X}} = \boldsymbol{\mathscr{X}}^\dagger \boldsymbol{\eta} \boldsymbol{\alpha} = \frac{-i}{\sqrt{2}}\left(\hat{b}_0^\dagger - \hat{b}_0\right), \tag{A.44}$$

for which the canonical commutator relation holds

$$\left[\hat{\mathscr{X}}, \hat{\mathscr{P}}\right] = i. \tag{A.45}$$

We see that a canonical transformation cannot bring the Hamiltonian into diagonal form. What can be achieved, however, is a description where all modes are noninteracting. The zero energy normal mode behaves as a free quasiparticle, while the other modes are simple harmonic oscillators. Thus, we may easily write down the ground state of the system

$$|\mathbf{0}\rangle, \qquad \hat{b}_j|\mathbf{0}\rangle = 0 \quad \forall\, j > 0, \qquad \hat{\mathscr{P}}|\mathbf{0}\rangle = 0. \tag{A.46}$$

A "free parameter"

The existence of a zero mode is generally the result of an approximation or an ansatz of a $U(1)$ broken symmetry, Sec. 2.2. It introduces a free parameter in the transformation, which must be fixed by appealing to the physics of the problem considered.

Consider the normalisation conditions for the zeroth mode. We may consistently introduce the factor α

$$\mathbf{P} = \alpha \mathbf{P}' \qquad \boldsymbol{\mathcal{X}} = \frac{1}{\alpha}\boldsymbol{\mathcal{X}}' \qquad \omega_0' = \alpha^2 \omega_0. \tag{A.47}$$

With this, the normalisation conditions (A.32) are invariant

$$\boldsymbol{\mathcal{X}}'^{\dagger}\mathbf{M}\boldsymbol{\mathcal{X}}' = \hbar\omega_0', \qquad \boldsymbol{\mathcal{X}}'^{\dagger}\boldsymbol{\eta}\mathbf{P}' = i, \qquad \mathbf{P}'^{T}\boldsymbol{\eta}\mathbf{P}' = \boldsymbol{\mathcal{X}}'^{\dagger}\boldsymbol{\eta}\boldsymbol{\mathcal{X}}' = 0. \tag{A.48}$$

as well as the Hamiltonian

$$\frac{\hbar\omega_0}{2}\hat{\mathscr{P}}^2 = \frac{\hbar\omega_0'}{2}\hat{\mathscr{P}}'^2. \tag{A.49}$$

As it stands, the theory does not prescribe a fixed value for α.

The transformation (A.47) is a scale transformation, or equivalently, a squeezing transformation. Of course, averages taken with a prescribed initial state are invariant to these unitary canonical transformations. However, the applicability of approximations performed in Chapter 2 are dependent upon the diffusion rate of the zero mode. Thus, the importance of appropriately fixing the parameter is evident.

APPENDIX B

1D THOMAS-FERMI SOLUTIONS

Here, we review the TF solutions used in [56, 66, 148] to solve the Bogoliubov modes in the 1D mean field regime.

B.1 Thomas-Fermi BEC

The TF approximation is to neglect the kinetic energy when the interaction energy is dominant. In the trapped gas case, the approximation will yield good results in the bulk, while failing to describe the edges of the BEC owing to the faster spatial variation. Neglecting the kinetic energy in the 1D GPE (2.24) yields the solution

$$\psi(x) = \begin{cases} \sqrt{\frac{\mu}{g_{1\mathrm{D}}}}\sqrt{1-(x/R_{\mathrm{TF}})^2} & \text{if } x < R_{\mathrm{TF}}, \\ 0 & \text{otherwise}, \end{cases} \tag{B.1}$$

where the TF radius is

$$R_{\mathrm{TF}} = \sqrt{\frac{2\mu}{m\omega_x^2}}. \tag{B.2}$$

The chemical potential is determined by the total number of particles in the BEC

$$\mu = \left[\frac{3N_0 g_{1\mathrm{D}}}{4}\sqrt{\frac{m\omega_x^2}{2}}\right]^{\frac{2}{3}}. \tag{B.3}$$

Integrating the 1D GPE (2.24) gives $N_0\mu = H_0 + E_{\rm int}$, where H_0 is given in Eq. (2.22a) and the interaction energy is given by

$$E_{\rm int} = \frac{g_{\rm 1D}}{2}\int dx\,|\psi(x)|^4\,. \tag{B.4}$$

Noting that $\mu = \partial H_0/\partial N_0$, one obtains the thermodynamic relation

$$\frac{\partial\mu}{\partial N_0} = \frac{1}{N_0}\frac{\partial E_{\rm int}}{\partial N_0}. \tag{B.5}$$

We also have the relations

$$\frac{E_{\rm tot}}{N_0} = \frac{3}{5}\mu, \qquad \frac{E_{\rm int}}{N_0} = \frac{2}{5}\mu, \qquad \frac{E_{\rm pot}}{N_0} = \frac{1}{5}\mu, \tag{B.6}$$

where $E_{\rm tot} = E_{\rm int} + E_{\rm pot}$ is the total energy excluding the kinetic contribution and $E_{\rm pot}$ is the potential energy contribution. Using Eq. (B.5) and Eq. (B.6), one has

$$\frac{\partial\mu}{\partial N_0} = \frac{2}{3}\frac{\mu}{N_0}. \tag{B.7}$$

To be in the TF regime, we require the interaction energy to be much greater than that of the kinetic energy

$$\frac{g_{\rm 1D}n_{\rm 1D}}{2} \gg \frac{\hbar^2}{2mR_{\rm TF}^2}, \tag{B.8}$$

or equivalently,

$$n_{\rm 1D}a_{\rm sc} \gg \frac{1}{2^{\frac{3}{2}}}\left(\frac{l_0}{l_x}\right)^2, \tag{B.9}$$

where $n_{\rm 1D} = \mu/g_{\rm 1D}$ is taken to be the maximum density of the TF profile Eq. (B.1).

B.2 Thomas-Fermi excitations

The Bogoliubov-de Gennes equations (2.32) can be decoupled

$$\mathcal{L}_+\mathcal{L}_- f_j^+(x) = (\hbar\omega_j)^2 f_j^+(x), \tag{B.10a}$$
$$\mathcal{L}_-\mathcal{L}_+ f_j^-(x) = (\hbar\omega_j)^2 f_j^-(x). \tag{B.10b}$$

The kinetic energy term is neglected where it is less significant. That is, the TF solution for the BEC wavefunction Eq. (B.1) is taken along with the approximation

$$\begin{aligned}\mathcal{L}_+ &= \left[-\frac{\hbar^2}{2m}\frac{\partial^2}{\partial x^2} + V(x) - \mu + g_{1\mathrm{D}} n_0(x)\right] + 2g_{1\mathrm{D}} n_0(x) \\ &\simeq 2g_{1\mathrm{D}} n_0(x) = 2[\mu - V(x)].\end{aligned} \tag{B.11}$$

Such an approximation is equivalent to neglecting terms second order in $\hbar\omega_x/\mu$ [148]. Equations (B.10) become

$$2g_{1\mathrm{D}} n_0(x)\mathcal{L}_- f_j^+(x) = (\hbar\omega_j)^2 f_j^+(x), \tag{B.12a}$$
$$2g_{1\mathrm{D}}\mathcal{L}_- n_0(x) f_j^-(x) = (\hbar\omega_j)^2 f_j^-(x), \tag{B.12b}$$

Taking $f_j^\pm(x) = C_j^\pm \psi(x)^{\pm 1}\phi_j^\pm(x)$ and noting that

$$\frac{\partial\psi(x)}{\partial x} = -\frac{\psi(x)}{2g_{1\mathrm{D}} n_0(x)}\frac{\partial V(x)}{\partial x}, \tag{B.13}$$

one obtains

$$-\frac{\hbar^2}{m}\left[g_{1\mathrm{D}} n_0(x)\frac{\partial^2}{\partial x^2} - \frac{\partial V(x)}{\partial x}\frac{\partial}{\partial x}\right]\phi_j^\pm(x) = (\hbar\omega_j)^2\phi_j^\pm(x). \tag{B.14}$$

The derivation of this equation relies on the exact expression for the BEC wavefunction, not the TF approximation of it. The following argument is given in Ref. [148]. In deriving the TF wavefunction, the kinetic energy of the wavefunction is neglected, however, for the excitations with energies comparable to the trap frequency, this would lead to an incorrect result. The wavefunctions of these

excitations vary over the entire BEC, hence, the kinetic energy of the BEC, and excitations are equally important.

Now, explicitly using the harmonic oscillator potential

$$V(x) = \frac{m\omega_x^2}{2}x^2, \tag{B.15}$$

and

$$\hbar\omega_j = \hbar\omega_x\sqrt{j\,(j+1)\,/2}, \tag{B.16}$$

one arrives at

$$\left[\left(R_{\mathrm{TF}}^2 - x^2\right)\frac{\partial^2}{\partial x^2} - 2x\frac{\partial}{\partial x} + j\,(j+1)\right]\phi_j^{\pm}(x) = 0. \tag{B.17}$$

The solutions are the Legendre polynomials $P_j\,(x/R_{\mathrm{TF}})$. As defined in Arfken and Weber [149], they have the orthogonality condition

$$\frac{1}{R_{\mathrm{TF}}}\int_{-R_{\mathrm{TF}}}^{R_{\mathrm{TF}}} P_j\left(\frac{x}{R_{\mathrm{TF}}}\right)P_k\left(\frac{x}{R_{\mathrm{TF}}}\right)dx = \frac{2\delta_{jk}}{2j+1}. \tag{B.18}$$

B.2.1 Normalization

All that remains is the normalisation of

$$f_j^{\pm}(x) = C_j^{\pm}\psi(x)^{\pm 1}P_j\left(\frac{x}{R_{\mathrm{TF}}}\right), \tag{B.19}$$

and a discussion of the zero mode. The solutions are normalised according too

$$\int dx\left[f_j^{+}(x)f_k^{-}(x) + f_k^{+}(x)f_j^{-}(x)\right] = \delta_{jk}, \tag{B.20}$$

yielding

$$C_j^{+} = \frac{1}{C_j^{-}}\frac{2j+1}{4R_{\mathrm{TF}}}. \tag{B.21}$$

Finally, one substitutes into the coupled BdG equations Eqs. (2.32), and using the GPE and Legendre differential equation,

$$C_j^{\pm} = \left(\frac{2g_{1\mathrm{D}}}{\hbar\omega_j}\right)^{\pm\frac{1}{2}} \sqrt{\frac{2j+1}{4R_{\mathrm{TF}}}}. \tag{B.22}$$

Clearly, the zero mode does not satisfy the normalisation (B.22). However, the obtained solutions correspond to the redefinition of the zero mode, Eq. (A.35), but are normalised according to

$$\mathcal{L}_+\Phi_0(x) \simeq 2g_{1\mathrm{D}}n_0(x)\Phi_0(x) = \hbar\omega_0\sqrt{\frac{n_0(x)}{2N_0}}, \tag{B.23}$$

$$2\int_{-R_{\mathrm{TF}}}^{R_{\mathrm{TF}}} dx\, \Phi_0(x)\sqrt{\frac{n_0(x)}{2N_0}} = 1, \tag{B.24}$$

and $\hbar\omega_0 = 4\mu/3$. Thus, the solutions are

$$f_j^{\pm}(x) = \begin{cases} \left(\frac{2g_{1\mathrm{D}}}{\hbar\omega_j}\right)^{\pm\frac{1}{2}} \sqrt{\frac{2j+1}{4R_{\mathrm{TF}}}}\psi(x)^{\pm 1}P_j\left(x/R_{\mathrm{TF}}\right) & j > 0, \\ f_0^+(x) = \sqrt{\frac{n_0(x)}{2N_0}}, \qquad f_0^-(x) = \frac{1}{4R_{\mathrm{TF}}}\left[f_0^+(x)\right]^{-1} & j = 0. \end{cases} \tag{B.25}$$

Note that the other orthogonality conditions

$$\int dx \left[f_j^-(x)f_k^+(x) - f_j^+(x)f_k^-(x)\right] = 0, \tag{B.26}$$

are also satisfied.

APPENDIX C

WILLIAMSON'S THEOREM

Here, we provide an adaption of the proof presented in Ref. [150] of Williamson's theorem [151] which illuminates how to construct the diagonalizing sympletic matrix. Williamson's theorem guarantees that any $2n \times 2n$ covariance matrix (symmetric and positive definite) can be diagonalized via a symplectic transformation,

$$\mathbf{A} = \mathbf{S}^T \mathbf{W} \mathbf{S}, \tag{C.1}$$

where $\mathbf{S}$ is a symplectic transform, $\mathbf{W}$ is in diagonal form with $\mathbf{W} = \bigoplus_{k=1}^{n} d_k \mathbf{I}_2$, and, $\pm d_k$ are the eigenvalues of $i\mathbf{\Omega}\mathbf{A}$.

Since the scalar product $\langle \mathbf{z}, \mathbf{z}' \rangle_{\mathbf{A}} = \langle \mathbf{A}\mathbf{z}, \mathbf{z}' \rangle = (\mathbf{z}')^T \mathbf{A}\mathbf{z}$ and standard sympletic form, $\sigma(\mathbf{z}, \mathbf{z}') = \langle \mathbf{\Omega}\mathbf{z}, \mathbf{z}' \rangle$ with

$$\mathbf{\Omega} = \bigoplus_{k=1}^{n} \begin{bmatrix} 0 & 1 \\ -1 & 0 \end{bmatrix}, \tag{C.2}$$

are nondegenerate, there exist an unique invertible matrix $\mathbf{K}$, for which,

$$\left\langle \mathbf{z}, \mathbf{K}\mathbf{z}' \right\rangle_{\mathbf{A}} = \sigma(\mathbf{z}, \mathbf{z}'). \tag{C.3}$$

Using, $\mathbf{K}^T \mathbf{A} = \mathbf{\Omega} = -\mathbf{\Omega}^T = -\mathbf{A}\mathbf{K}$, the transpose w.r.t. the scalar product $\langle \mathbf{z}, \mathbf{z}' \rangle_{\mathbf{A}}$ is

$$\mathbf{K}^A = \mathbf{A}^{-1} \mathbf{K}^T \mathbf{A} = -\mathbf{K}. \tag{C.4}$$

Thus, $\mathbf{K} = -\mathbf{A}^{-1}\mathbf{\Omega}$ ($\mathbf{K}^{-1} = \mathbf{\Omega}\mathbf{A}$) is an invertible real skew-symmetric matrix with purely imaginary eigenvalues that occur is pairs, $\pm i\lambda_j$ ($\mp i/\lambda_j$) and $\lambda_j > 0$, with the corresponding $\langle .,. \rangle_{\mathbf{A}}$ orthonormal eigenvectors $e'_j \pm i f'_j$, where e'_j and f'_j are real. As $2^{\frac{1}{2}} e'_j$ and $2^{\frac{1}{2}} f'_j$ also form a $\langle .,. \rangle_{\mathbf{A}}$ orthonormal basis, $e_j = (2/\lambda_j)^{\frac{1}{2}} e'_j$ and $f_j = (2/\lambda_j)^{\frac{1}{2}} f'_j$ form a sympletic basis, i.e.,

$$\begin{aligned}
\sigma(e_i, e_j) &= \langle e_i, \mathbf{K} e_j \rangle_{\mathbf{A}} = \lambda_j \langle e_i, f_j \rangle_{\mathbf{A}} = 0, \\
\sigma(f_i, f_j) &= \langle f_i, \mathbf{K} f_j \rangle_{\mathbf{A}} = \lambda_j \langle f_i, e_j \rangle_{\mathbf{A}} = 0, \\
\sigma(e_i, f_j) &= \langle e_i, \mathbf{K} f_j \rangle_{\mathbf{A}} = \lambda_j \langle e_i, e_j \rangle_{\mathbf{A}} = \delta_{ij}, \\
\sigma(f_i, e_j) &= \langle f_i, \mathbf{K} e_j \rangle_{\mathbf{A}} = -\lambda_j \langle f_i, f_j \rangle_{\mathbf{A}} = -\delta_{ij}.
\end{aligned} \tag{C.5}$$

A sympletic transform preserves $\mathbf{P}^T \mathbf{\Omega} \mathbf{P} = \mathbf{\Omega}$, and consequently, $\sigma(.,.)$. Constructing $\mathbf{S}^{-1} = [e_1, f_1, e_2, f_2, \ldots, e_n, f_n]$, then,

$$[\mathbf{S}^{-1}]^T \mathbf{\Omega} \mathbf{S}^{-1} = \mathbf{\Omega} =$$
$$\begin{bmatrix}
\sigma(e_1,e_1) & \sigma(e_1,f_1) & \sigma(e_1,e_2) & \sigma(e_1,f_2) & \ldots & \sigma(e_1,e_n) & \sigma(e_1,f_n) \\
\sigma(f_1,e_1) & \sigma(f_1,f_1) & \sigma(f_1,e_2) & \sigma(f_1,f_2) & \ldots & \sigma(f_1,e_n) & \sigma(f_1,f_n) \\
\sigma(e_2,e_1) & \sigma(e_2,f_1) & \sigma(e_2,e_2) & \sigma(e_2,f_2) & \ldots & \sigma(e_2,e_n) & \sigma(e_2,f_n) \\
\sigma(f_2,e_1) & \sigma(f_2,f_1) & \sigma(f_2,e_2) & \sigma(f_2,f_2) & \ldots & \sigma(f_2,e_n) & \sigma(f_2,f_n) \\
\vdots & \vdots & \vdots & \vdots & \ddots & \vdots & \vdots \\
\sigma(e_n,e_1) & \sigma(e_n,f_1) & \sigma(e_n,e_2) & \sigma(e_n,f_2) & \ldots & \sigma(e_n,e_n) & \sigma(e_n,f_n) \\
\sigma(f_n,e_1) & \sigma(f_n,f_1) & \sigma(f_n,e_2) & \sigma(f_n,f_2) & \ldots & \sigma(f_n,e_n) & \sigma(f_n,f_n)
\end{bmatrix}. \tag{C.6}$$

Thus, we have the desired result

$$[\mathbf{S}^{-1}]^T\mathbf{A}\mathbf{S}^{-1} = \mathrm{diag}([1/\lambda_1, 1/\lambda_1, 1/\lambda_2, 1/\lambda_2, \ldots, 1/\lambda_n, 1/\lambda_n]) = \mathbf{W} =$$

$$\begin{bmatrix} \langle e_1, e_1\rangle_{\mathbf{A}} & \langle e_1, f_1\rangle_{\mathbf{A}} & \langle e_1, e_2\rangle_{\mathbf{A}} & \langle e_1, f_2\rangle_{\mathbf{A}} & \cdots & \langle e_1, e_n\rangle_{\mathbf{A}} & \langle e_1, f_n\rangle_{\mathbf{A}} \\ \langle f_1, e_1\rangle_{\mathbf{A}} & \langle f_1, f_1\rangle_{\mathbf{A}} & \langle f_1, e_2\rangle_{\mathbf{A}} & \langle f_1, f_2\rangle_{\mathbf{A}} & \cdots & \langle f_1, e_n\rangle_{\mathbf{A}} & \langle f_1, f_n\rangle_{\mathbf{A}} \\ \langle e_2, e_1\rangle_{\mathbf{A}} & \langle e_2, f_1\rangle_{\mathbf{A}} & \langle e_2, e_2\rangle_{\mathbf{A}} & \langle e_2, f_2\rangle_{\mathbf{A}} & \cdots & \langle e_2, e_n\rangle_{\mathbf{A}} & \langle e_2, f_n\rangle_{\mathbf{A}} \\ \langle f_2, e_1\rangle_{\mathbf{A}} & \langle f_2, f_1\rangle_{\mathbf{A}} & \langle f_2, e_2\rangle_{\mathbf{A}} & \langle f_2, f_2\rangle_{\mathbf{A}} & \cdots & \langle f_2, e_n\rangle_{\mathbf{A}} & \langle f_2, f_n\rangle_{\mathbf{A}} \\ \vdots & \vdots & \vdots & \vdots & \ddots & \vdots & \vdots \\ \langle e_n, e_1\rangle_{\mathbf{A}} & \langle e_n, f_1\rangle_{\mathbf{A}} & \langle e_n, e_2\rangle_{\mathbf{A}} & \langle e_n, f_2\rangle_{\mathbf{A}} & \cdots & \langle e_n, e_n\rangle_{\mathbf{A}} & \langle e_n, f_n\rangle_{\mathbf{A}} \\ \langle f_n, e_1\rangle_{\mathbf{A}} & \langle f_n, f_1\rangle_{\mathbf{A}} & \langle f_n, e_2\rangle_{\mathbf{A}} & \langle f_n, f_2\rangle_{\mathbf{A}} & \cdots & \langle f_n, e_n\rangle_{\mathbf{A}} & \langle f_n, f_n\rangle_{\mathbf{A}} \end{bmatrix}, \tag{C.7}$$

and $\mathbf{S} = \mathbf{W}^{-1}[\mathbf{S}^{-1}]^T\mathbf{A}$.

Bibliography

[1] A. C. J. Wade, J. F. Sherson, and K. Mølmer, *Squeezing and Entanglement of Density Oscillations in a Bose-Einstein Condensate*, Phys. Rev. Lett. **115**, 060401 (2015)

[2] A. C. J. Wade, J. F. Sherson, and K. Mølmer, *Manipulation of collective quantum states in Bose-Einstein condensates by continuous imaging*, In preparation. (2015)

[3] A. C. J. Wade, D. D. Bhaktavatsala Rao, and K. Mølmer, *Efficient storage and retrieval of single photons from an ensemble of Rydberg interacting atoms*, In preparation. (2015)

[4] C. K. Andersen and A. C. J. Wade, *Bohr vs. Einstein: Fortolkning af kvantemekanikken*, Kvant **24**, 27 (2013)

[5] A. Einstein, *Quantentheorie des einatomigen idealen Gases*, Sitzungsber. Kgl. Preuss. Akad. Wiss. **3**, 18 (1925)

[6] S. N. Bose, *Plancks Gesetz und Lichtquantenhypothese*, Zeitschrift für Physik **26**, 178 (1924)

[7] M. H. Anderson, J. R. Ensher, M. R. Matthews, C. E. Wieman, and E. A. Cornell, *Observation of Bose-Einstein Condensation in a Dilute Atomic Vapor*, Science **269**, 198 (1995)

[8] W. Ketterle, D. Durfee, and D. Stamper-Kurn, *Making, probing and understanding Bose-Einstein condensates*, arXiv preprint cond-mat/9904034(1999)

[9] I. Bloch, J. Dalibard, and W. Zwerger, *Many-body physics with ultracold gases*, Rev. Mod. Phys. **80**, 885 (2008)

[10] C. Chin, R. Grimm, P. Julienne, and E. Tiesinga, *Feshbach resonances in ultracold gases*, Rev. Mod. Phys. **82**, 1225 (2010)

[11] L.-A. Wu, H. J. Kimble, J. L. Hall, and H. Wu, *Generation of Squeezed States by Parametric Down Conversion*, Phys. Rev. Lett. **57**, 2520 (1986)

[12] A. Furusawa, J. L. Sørensen, S. L. Braunstein, C. A. Fuchs, H. J. Kimble, and E. S. Polzik, *Unconditional Quantum Teleportation*, Science **282**, 706 (1998)

[13] J. Estève, C. Gross, A. Weller, S. Giovanazzi, and M. Oberthaler, *Squeezing and entanglement in a Bose-Einstein condensate*, Nature **455**, 1216 (2008)

[14] T. Berrada, S. van Frank, R. Bücker, T. Schumm, J.-F. Schaff, and J. Schmiedmayer, *Integrated Mach-Zehnder interferometer for Bose-Einstein condensates*, Nat. Commun. **4** (2013)

[15] M. Riedel, P. Böhi, Y. Li, T. Hänsch, A. Sinatra, and P. Treutlein, *Atom-chip-based generation of entanglement for quantum metrology*, Nature **464**, 1170 (2010)

[16] C. Gross, H. Strobel, E. Nicklas, T. Zibold, N. Bar-Gill, G. Kurizki, and M. Oberthaler, *Atomic homodyne detection of continuous-variable entangled twin-atom states*, Nature **480**, 219 (2011)

[17] C. Hamley, C. Gerving, T. Hoang, E. Bookjans, and M. Chapman, *Spin-nematic squeezed vacuum in a quantum gas*, Nature Phys. **8**, 305 (2012)

[18] B. Lücke, M. Scherer, J. Kruse, L. Pezzé, F. Deuretzbacher, P. Hyllus, O. Topic, J. Peise, W. Ertmer, J. Arlt, L. Santos, A. Smerzi, and C. Klempt,

Twin Matter Waves for Interferometry Beyond the Classical Limit, Science **334**, 773 (2011)

[19] C. Gross, T. Zibold, E. Nicklas, J. Estève, and M. Oberthaler, *Nonlinear atom interferometer surpasses classical precision limit*, Nature **464**, 1165 (2010)

[20] W. Muessel, H. Strobel, D. Linnemann, D. B. Hume, and M. K. Oberthaler, *Scalable Spin Squeezing for Quantum-Enhanced Magnetometry with Bose-Einstein Condensates*, Phys. Rev. Lett. **113**, 103004 (2014)

[21] J. M. Vogels, K. Xu, and W. Ketterle, *Generation of Macroscopic Pair-Correlated Atomic Beams by Four-Wave Mixing in Bose-Einstein Condensates*, Phys. Rev. Lett. **89**, 020401 (2002)

[22] A. Perrin, H. Chang, V. Krachmalnicoff, M. Schellekens, D. Boiron, A. Aspect, and C. I. Westbrook, *Observation of Atom Pairs in Spontaneous Four-Wave Mixing of Two Colliding Bose-Einstein Condensates*, Phys. Rev. Lett. **99**, 150405 (2007)

[23] M. Keller, M. Kotyrba, F. Leupold, M. Singh, M. Ebner, and A. Zeilinger, *Bose-Einstein condensate of metastable helium for quantum correlation experiments*, Phys. Rev. A **90**, 063607 (2014)

[24] K. V. Kheruntsyan, J.-C. Jaskula, P. Deuar, M. Bonneau, G. B. Partridge, J. Ruaudel, R. Lopes, D. Boiron, and C. I. Westbrook, *Violation of the Cauchy-Schwarz Inequality with Matter Waves*, Phys. Rev. Lett. **108**, 260401 (2012)

[25] R. J. Lewis-Swan and K. V. Kheruntsyan, *Proposal for demonstrating the Hong-Ou-Mandel effect with matter waves*, Nat. Commun. **5**, 3752 (2014)

[26] R. Lopes, A. Imanaliev, A. Aspect, M. Cheneau, D. Boiron, and C. I. Westbrook, *Atomic Hong-Ou-Mandel experiment*, Nature **520**, 66 (2015)

[27] T. D. Ladd, F. Jelezko, R. Laflamme, Y. Nakamura, C. Monroe, and J. L. O'Brien, *Quantum computers*, Nature **464**, 45 (2010)

[28] M. Lewenstein, A. Sanpera, V. Ahufinger, B. Damski, A. Sen, and U. Sen, *Ultracold atomic gases in optical lattices: mimicking condensed matter physics and beyond*, Adv. Phys. **56**, 243 (2007)

[29] I. Bloch, J. Dalibard, and S. Nascimbène, *Quantum simulations with ultracold quantum gases*, Nat. Phys. **8**, 267 (2012)

[30] H. Müntinga, H. Ahlers, M. Krutzik, A. Wenzlawski, S. Arnold, D. Becker, K. Bongs, H. Dittus, H. Duncker, N. Gaaloul, C. Gherasim, E. Giese, C. Grzeschik, T. W. Hänsch, O. Hellmig, W. Herr, S. Herrmann, E. Kajari, S. Kleinert, C. Lämmerzahl, W. Lewoczko-Adamczyk, J. Malcolm, N. Meyer, R. Nolte, A. Peters, M. Popp, J. Reichel, A. Roura, J. Rudolph, M. Schiemangk, M. Schneider, S. T. Seidel, K. Sengstock, V. Tamma, T. Valenzuela, A. Vogel, R. Walser, T. Wendrich, P. Windpassinger, W. Zeller, T. van Zoest, W. Ertmer, W. P. Schleich, and E. M. Rasel, *Interferometry with Bose-Einstein Condensates in Microgravity*, Phys. Rev. Lett. **110**, 093602 (2013)

[31] C. Burrage, E. J. Copeland, and E. Hinds, *Probing dark energy with atom interferometry*, J. Cosmol. Astropart. Phys. **2015**, 042 (2015)

[32] A. Kuzmich, L. Mandel, and N. P. Bigelow, *Generation of Spin Squeezing via Continuous Quantum Nondemolition Measurement*, Phys. Rev. Lett. **85**, 1594 (2000)

[33] G. Vasilakis, H. Shen, K. Jensen, M. Balabas, D. Salart, B. Chen, and E. S. Polzik, *Generation of a squeezed state of an oscillator by stroboscopic back-action-evading measurement*, Nature Phys. **11**, 389Ð392 (2015)

[34] B. Julsgaard, A. Kozhekin, and E. S. Polzik, *Experimental long-lived entanglement of two macroscopic objects*, Nature **413**, 400 (2001)

[35] J. Sherson, H. Krauter, R. Olsson, B. Julsgaard, K. Hammerer, I. Cirac, and E. Polzik, *Quantum teleportation between light and matter*, Nature **443**, 557 (2006)

[36] B. Julsgaard, J. Sherson, J. I. Cirac, J. Fiurasek, and E. Polzik, *Experimental demonstration of quantum memory for light*, Nature **432**, 482 (2004)

[37] M. R. Andrews, M.-O. Mewes, N. J. van Druten, D. S. Durfee, D. M. Kurn, and W. Ketterle, *Direct, Nondestructive Observation of a Bose Condensate*, Science **273**, 84 (1996)

[38] M. R. Andrews, D. M. Kurn, H.-J. Miesner, D. S. Durfee, C. G. Townsend, S. Inouye, and W. Ketterle, *Propagation of Sound in a Bose-Einstein Condensate*, Phys. Rev. Lett. **79**, 553 (1997)

[39] C. C. Bradley, C. A. Sackett, and R. G. Hulet, *Bose-Einstein Condensation of Lithium: Observation of Limited Condensate Number*, Phys. Rev. Lett. **78**, 985 (1997)

[40] D. M. Stamper-Kurn, A. P. Chikkatur, A. Görlitz, S. Inouye, S. Gupta, D. E. Pritchard, and W. Ketterle, *Excitation of Phonons in a Bose-Einstein Condensate by Light Scattering*, Phys. Rev. Lett. **83**, 2876 (1999)

[41] M. Saba, T. A. Pasquini, C. Sanner, Y. Shin, W. Ketterle, and D. E. Pritchard, *Light Scattering to Determine the Relative Phase of Two Bose-Einstein Condensates*, Science **307**, 1945 (2005)

[42] C. Sanner, E. J. Su, A. Keshet, W. Huang, J. Gillen, R. Gommers, and W. Ketterle, *Speckle Imaging of Spin Fluctuations in a Strongly Interacting Fermi Gas*, Phys. Rev. Lett. **106**, 010402 (2011)

[43] F. Kaminski, N. S. Kampel, M. P. H. Steenstrup, A. Griesmaier, E. S. Polzik, and J. H. Müller, *In-situ dual-port polarization contrast imaging of Faraday rotation in a high optical depth ultracold 87Rb atomic ensemble*, Eur. Phys. J. D **66**, 227 (2012)

[44] M. Gajdacz, P. L. Pedersen, T. Mørch, A. J. Hilliard, J. Arlt, and J. F. Sherson, *Non-destructive Faraday imaging of dynamically controlled ultracold atoms*, Rev. Sci. Instrum. **84**, 083105 (2013)

[45] I. B. Mekhov and H. Ritsch, *Quantum optics with ultracold quantum gases: towards the full quantum regime of the light-matter interaction*, J. Phys. B **45**, 102001 (2012)

[46] P. Hauke, R. J. Sewell, M. W. Mitchell, and M. Lewenstein, *Quantum control of spin correlations in ultracold lattice gases*, Phys. Rev. A **87**, 021601 (2013)

[47] M. Hush, S. Szigeti, A. Carvalho, and J. Hope, *Controlling spontaneous-emission noise in measurement-based feedback cooling of a Bose-Einstein condensate*, New J. Phys. **15**, 113060 (2013)

[48] M. D. Lee and J. Ruostekoski, *Classical stochastic measurement trajectories: Bosonic atomic gases in an optical cavity and quantum measurement backaction*, Phys. Rev. A **90**, 023628 (2014)

[49] H. M. Wiseman and G. J. Milburn, *Quantum measurement and control*, 1st ed. (Cambridge University Press, 2009)

[50] D. A. R. Dalvit, J. Dziarmaga, and R. Onofrio, *Continuous quantum measurement of a Bose-Einstein condensate: A stochastic Gross-Pitaevskii equation*, Phys. Rev. A **65**, 053604 (2002)

[51] S. S. Szigeti, M. R. Hush, A. R. R. Carvalho, and J. J. Hope, *Continuous measurement feedback control of a Bose-Einstein condensate using phase-contrast imaging*, Phys. Rev. A **80**, 013614 (2009)

[52] M. Hiller, M. Rehn, F. Petruccione, A. Buchleitner, and T. Konrad, *Unsharp continuous measurement of a Bose-Einstein condensate: Full quantum state estimation and the transition to classicality*, Phys. Rev. A **86**, 033624 (2012)

[53] C. J. Pethick and H. Smith, *Bose-Einstein Condensation in Dilute Gases*, 1st ed. (Cambridge University Press, 2001)

[54] N. N. Bogoliubov, *On the theory of superfluidity*, Izv. Akad. Nauk USSR **11**, 77 (1947)

[55] N. N. Bogoliubov, *On the theory of superfluidity*, J. Phys. **11**, 23 (1947)

[56] D. S. Petrov, G. V. Shlyapnikov, and J. T. M. Walraven, *Regimes of Quantum Degeneracy in Trapped 1D Gases*, Phys. Rev. Lett. **85**, 3745 (2000)

[57] D. Petrov, D. M. Gangardt, and G. V. Shlyapnikov, in *J. Phys. IV*, Vol. 116 (2004) pp. 5–44

[58] M. Olshanii, *Atomic Scattering in the Presence of an External Confinement and a Gas of Impenetrable Bosons*, Phys. Rev. Lett. **81**, 938 (1998)

[59] F. Dalfovo, S. Giorgini, L. P. Pitaevskii, and S. Stringari, *Theory of Bose-Einstein condensation in trapped gases*, Rev. Mod. Phys. **71**, 463 (1999)

[60] E. H. Lieb, R. Seiringer, and J. Yngvason, *Justification of c-Number Substitutions in Bosonic Hamiltonians*, Phys. Rev. Lett. **94**, 80401 (2005)

[61] E. H. Lieb, R. Seiringer, and J. Yngvason, *Bose-Einstein Condensation and Spontaneous Symmetry Breaking*, Rep. Math. Phys. **59**, 389 (2007)

[62] V. I. Yukalov, *Basics of Bose-Einstein condensation*, Phys. Part. Nucl. **42**, 460 (2011)

[63] M. R. Andrews, C. G. Townsend, H.-J. Miesner, D. S. Durfee, D. M. Kurn, and W. Ketterle, *Observation of Interference Between Two Bose Condensates*, Science **275**, 637 (1997)

[64] J. Javanainen and S. M. Yoo, *Quantum Phase of a Bose-Einstein Condensate with an Arbitrary Number of Atoms*, Phys. Rev. Lett. **76**, 161 (1996)

[65] K. Mølmer, *Optical coherence: A convenient fiction*, Phys. Rev. A **55**, 3195 (1997)

[66] K. Mølmer, *Phase collapse and excitations in Bose-Einstein condensates*, Phys. Rev. A **58**, 566 (1998)

[67] J. Goldstone, A. Salam, and S. Weinberg, *Broken Symmetries*, Phys. Rev. **127**, 965 (1962)

[68] M. Lewenstein and L. You, *Quantum Phase Diffusion of a Bose-Einstein Condensate*, Phys. Rev. Lett. **77**, 3489 (1996)

[69] A. Negretti, C. Henkel, and K. Mølmer, *Quantum fluctuations in the image of a Bose gas*, Phys. Rev. A **78**, 023630 (2008)

[70] R. Kanamoto, H. Saito, and M. Ueda, *Critical fluctuations in a soliton formation of attractive Bose-Einstein condensates*, Phys. Rev. A **73**, 033611 (2006)

[71] C. Lobo and Y. Castin, *Nonclassical scissors mode of a vortex lattice in a Bose-Einstein condensate*, Phys. Rev. A **72**, 043606 (2005)

[72] M. Ueda and T. Nakajima, *Nambu-Goldstone mode in a rotating dilute Bose-Einstein condensate*, Phys. Rev. A **73**, 043603 (2006)

[73] T. Simula, *Zero-energy states in rotating trapped Bose-Einstein condensates*, J. Phys. Condens. Matter **25**, 285602 (2013)

[74] S. Uchino, M. Kobayashi, M. Nitta, and M. Ueda, *Quasi-Nambu-Goldstone Modes in Bose-Einstein Condensates*, Phys. Rev. Lett. **105**, 230406 (2010)

[75] A. L. Fetter, *Nonuniform states of an imperfect Bose gas*, Ann. Phys. **70**, 67 (1972), ISSN 0003-4916

[76] A. L. Fetter and J. D. Walecka, *Quantum Theory of Many-Particle Systems*, 1st ed. (Dover Publications, New York, 2003)

[77] N. M. Hugenholtz and D. Pines, *Ground-State Energy and Excitation Spectrum of a System of Interacting Bosons*, Phys. Rev. **116**, 489 (1959)

[78] P. C. Hohenberg and P. C. Martin, *Microscopic Theory of Superfluid Helium*, Ann. Phys. **34**, 291 (1965)

[79] J. P. Blaizot and G. Ripka, *Quantum Theory of Finite Systems* (The MIT Press, Cambridge, Massachusetts, 1986)

[80] M. Girardeau and R. Arnowitt, *Theory of Many-Boson Systems: Pair Theory*, Phys. Rev. **113**, 755 (1959)

[81] C. W. Gardiner, *Particle-number-conserving Bogoliubov method which demonstrates the validity of the time-dependent Gross-Pitaevskii equation for a highly condensed Bose gas*, Phys. Rev. A **56**, 1414 (1997)

[82] Y. Castin and R. Dum, *Low-temperature Bose-Einstein condensates in time-dependent traps: Beyond the $U(1)$ symmetry-breaking approach*, Phys. Rev. A **57**, 3008 (1998)

[83] K. Jacobs and D. A. Steck, *A straightforward introduction to continuous quantum measurement*, Contemp. Phys. **47**, 279 (2006)

[84] K. Hammerer, A. S. Sørensen, and E. S. Polzik, *Quantum interface between light and atomic ensembles*, Rev. Mod. Phys. **82**, 1041 (2010)

[85] D. V. Vasilyev, K. Hammerer, N. Korolev, and A. S. Sørensen, *Quantum noise for Faraday light-matter interfaces*, Journal of Physics B: Atomic **45**, 4007 (2012)

[86] K. Eckert, L. Zawitkowski, A. Sanpera, M. Lewenstein, and E. S. Polzik, *Quantum Polarization Spectroscopy of Ultracold Spinor Gases*, Phys. Rev. Lett. **98**, 100404 (2007)

[87] K. Eckert, O. Romero-Isart, M. Rodriguez, M. Lewenstein, E. Polzik, and A. Sanpera, *Quantum non-demolition detection of strongly correlated systems*, Nature Phys. **4**, 50 (2008)

[88] G. M. Bruun, B. M. Andersen, E. Demler, and A. S. Sørensen, *Probing Spatial Spin Correlations of Ultracold Gases by Quantum Noise Spectroscopy*, Phys. Rev. Lett. **102**, 030401 (2009)

[89] T. Roscilde, M. Rodríguez, K. Eckert, O. Romero-Isart, M. Lewenstein, E. Polzik, and A. Sanpera, *Quantum polarization spectroscopy of correlations in attractive fermionic gases*, New Journal of Physics **11**, 5041 (2009)

[90] I. de Vega, J. I. Cirac, and D. Porras, *Detection of spin correlations in optical lattices by light scattering*, Phys. Rev. A **77**, 051804 (2008)

[91] G. De Chiara, O. Romero-Isart, and A. Sanpera, *Probing magnetic order in ultracold lattice gases*, Phys. Rev. A **83**, 021604(R) (2011)

[92] O. Romero-Isart, M. Rizzi, C. A. Muschik, E. S. Polzik, M. Lewenstein, and A. Sanpera, *Quantum Memory Assisted Probing of Dynamical Spin Correlations*, Phys. Rev. Lett. **108**, 065302 (2012)

[93] B. Rogers, M. Paternostro, J. F. Sherson, and G. De Chiara, *Characterization of Bose-Hubbard models with quantum nondemolition measurements*, Phys. Rev. A **90**, 043618 (2014)

[94] L. B. Madsen and K. Mølmer, *Spin squeezing and precision probing with light and samples of atoms in the Gaussian description*, Phys. Rev. A **70**, 052324 (2004)

[95] *Quantum Information with Continuous Variables of Atoms and Light*, edited by N. J. Cerf, G. Leuchs, and E. S. Polzik (Imperial College Press, London, 2007)

[96] X.-B. Wang, T. Hiroshima, A. Tomita, and M. Hayashi, *Quantum information with Gaussian states*, Phys. Rep. **448**, 1 (2007)

[97] J. Eisert, S. Scheel, and M. B. Plenio, *Distilling Gaussian States with Gaussian Operations is Impossible*, Phys. Rev. Lett. **89**, 137903 (2002)

[98] V. B. Braginskiĭ, Y. I. Vorontsov, and K. S. Thorne, *Quantum nondemolition measurements*, Science **209**, 547 (1980)

[99] J. K. Stockton, J. M. Geremia, A. C. Doherty, and H. Mabuchi, *Robust quantum parameter estimation: Coherent magnetometry with feedback*, Phys. Rev. A **69**, 032109 (2004)

[100] H. Kwakernaak and R. Sivan, *Linear Optimal Control Systems*, 1st ed. (Wiley Interscience, New York, 1972)

[101] J. Dalibard, Y. Castin, and K. Mølmer, *Wave-function approach to dissipative processes in quantum optics*, Phys. Rev. Lett. **68**, 580 (1992)

[102] A. J. Laub, *A Schur method for solving algebraic Riccati equations*, Automatic Control, IEEE Transactions on **24**, 913 (1979)

[103] S. S. Szigeti, M. R. Hush, A. R. R. Carvalho, and J. J. Hope, *Feedback control of an interacting Bose-Einstein condensate using phase-contrast imaging*, Phys. Rev. A **82**, 043632 (2010)

[104] L.-M. Duan, J. I. Cirac, P. Zoller, and E. S. Polzik, *Quantum Communication between Atomic Ensembles Using Coherent Light*, Phys. Rev. Lett. **85**, 5643 (2000)

[105] V. B. Braginskiĭ, Y. I. Vorontsov, and F. Y. Khalili, *Optimal quantum measurements in detectors of gravitation radiation*, JETP Lett. **27**, 276 (1978)

[106] K. S. Thorne, R. W. P. Drever, C. M. Caves, M. Zimmermann, and V. D. Sandberg, *Quantum Nondemolition Measurements of Harmonic Oscillators*, Phys. Rev. Lett. **40**, 667 (1978)

[107] R. Ruskov, K. Schwab, and A. N. Korotkov, *Squeezing of a nanomechanical resonator by quantum nondemolition measurement and feedback*, Phys. Rev. B **71**, 235407 (2005)

[108] J. Suh, A. J. Weinstein, C. Lei, E. Wollman, S. Steinke, P. Meystre, A. Clerk, and K. Schwab, *Mechanically detecting and avoiding the quantum fluctuations of a microwave field*, Science **344**, 1262 (2014)

[109] G. Vasilakis, V. Shah, and M. Romalis, *Stroboscopic backaction evasion in a dense alkali-metal vapor*, Phys. rev. lett. **106**, 143601 (2011)

[110] P. Marian and T. A. Marian, *Hellinger distance as a measure of Gaussian discord*, J. Phys. A: Math. Theor. **48**, 115301 (2015)

[111] C. Weedbrook, S. Pirandola, R. García-Patrón, N. J. Cerf, T. C. Ralph, J. H. Shapiro, and S. Lloyd, *Gaussian quantum information*, Rev. Mod. Phys. **84**, 621 (2012)

[112] E. Titchmarsh, *Some integrals involving Hermite polynomials*, J. London Math. Soc. **23**, 15 (1948)

[113] I. Busbridge, *Some integrals involving Hermite polynomials*, J. London Math. Soc. **23**, 135 (1948)

[114] S. A. Goorden, J. Bertolotti, and A. P. Mosk, *Superpixel-based spatial amplitude and phase modulation using a digital micromirror device*, Opt. Express **22**, 17999 (2014)

[115] D. McGloin, G. Spalding, H. Melville, W. Sibbett, and K. Dholakia, *Applications of spatial light modulators in atom optics*, Opt. Express **11**, 158 (2003)

[116] C. Ryu, P. W. Blackburn, A. A. Blinova, and M. G. Boshier, *Experimental Realization of Josephson Junctions for an Atom SQUID*, Phys. Rev. Lett. **111**, 205301 (2013)

[117] M. K. Pedersen, J. J. W. Sørensen, M. C. Tichy, and J. F. Sherson, *Many-body state engineering using measurements and fixed unitary dynamics*, New J. Phys. **16**, 113038 (2014)

[118] G. Mazzucchi, W. Kozlowski, S. F. Caballero-Benitez, T. J. Elliott, and I. B. Mekhov, *Quantum Measurement-induced Dynamics of Many-Body Ultracold Bosonic and Fermionic Systems in Optical Lattices*, arXiv preprint arXiv:1503.08710(2015)

[119] R. Labouvie, B. Santra, S. Heun, S. Wimberger, and H. Ott, *Negative Differential Conductivity in an Interacting Quantum Gas*, Phys. Rev. Lett. **115**, 050601 (2015)

[120] R. Bücker, J. Grond, S. Manz, T. Berrada, T. Betz, C. Koller, U. Hohenester, T. Schumm, A. Perrin, and J. Schmiedmayer, *Twin-atom beams*, Nature Physics **7**, 608 (2011)

[121] J.-C. Jaskula, G. B. Partridge, M. Bonneau, R. Lopes, J. Ruaudel, D. Boiron, and C. I. Westbrook, *Acoustic Analog to the Dynamical Casimir Effect in a Bose-Einstein Condensate*, Phys. Rev. Lett. **109**, 220401 (2012)

[122] S. Finazzi and I. Carusotto, *Entangled phonons in atomic Bose-Einstein condensates*, Phys. Rev. A **90**, 033607 (2014)

[123] J. Reidl, G. Bene, R. Graham, and P. Szépfalusy, *Kohn mode for trapped Bose gases within the dielectric formalism*, Phys. Rev. A **63**, 043605 (2001)

[124] C. Menotti and S. Stringari, *Collective oscillations of a one-dimensional trapped Bose-Einstein gas*, Phys. Rev. A **66**, 043610 (2002)

[125] L. P. Pitaevskii and A. Rosch, *Breathing modes and hidden symmetry of trapped atoms in two dimensions*, Phys. Rev. A **55**, R853 (1997)

[126] F. Werner and Y. Castin, *Unitary gas in an isotropic harmonic trap: Symmetry properties and applications*, Phys. Rev. A **74**, 053604 (2006)

[127] K. Hammerer, K. Mølmer, E. S. Polzik, and J. I. Cirac, *Light-matter quantum interface*, Phys. Rev. A **70**, 044304 (2004)

[128] A. Widera, S. Trotzky, P. Cheinet, S. Fölling, F. Gerbier, I. Bloch, V. Gritsev, M. D. Lukin, and E. Demler, *Quantum Spin Dynamics of Mode-Squeezed Luttinger Liquids in Two-Component Atomic Gases*, Phys. Rev. Lett. **100**, 140401 (2008)

[129] T. Langen, R. Geiger, M. Kuhnert, B. Rauer, and J. Schmiedmayer, *Local emergence of thermal correlations in an isolated quantum many-body system*, Nat. Phys. **9**, 640 (2013)

[130] E. Haller, M. Gustavsson, M. J. Mark, J. G. Danzl, R. Hart, G. Pupillo, and H.-C. Nägerl, *Realization of an Excited, Strongly Correlated Quantum Gas Phase*, Science **325**, 1224 (2009)

[131] M. Saffman, T. G. Walker, and K. Mølmer, *Quantum information with Rydberg atoms*, Rev. Mod. Phys. **82**, 2313 (2010)

[132] T. E. Lee, H. Häffner, and M. C. Cross, *Collective Quantum Jumps of Rydberg Atoms*, Phys. Rev. Lett. **108**, 023602 (2012)

[133] A. K. Mohapatra, M. G. Bason, B. Butscher, K. J. Weatherill, and C. S. Adams, *A giant electro-optic effect using polarizable dark states*, Nature Phys. **4**, 890 (2008)

[134] M. Saffman and T. G. Walker, *Creating single-atom and single-photon sources from entangled atomic ensembles*, Phys Rev A **66**, 065403 (2002)

[135] I. I. Beterov, M. Saffman, E. A. Yakshina, V. P. Zhukov, D. B. Tretyakov, V. M. Entin, I. I. Ryabtsev, C. W. Mansell, C. MacCormick, S. Bergamini, and M. P. Fedoruk, *Quantum gates in mesoscopic atomic ensembles based on adiabatic passage and Rydberg blockade*, Physical Review A **88**, 10303 (2013)

[136] C. Weitenberg, M. Endres, J. F. Sherson, M. Cheneau, P. Schauss, T. Fukuhara, I. Bloch, and S. Kuhr, *Single-spin addressing in an atomic Mott insulator*, Nature **471**, 319 (2011)

[137] J. Honer, R. Loew, H. Weimer, T. Pfau, and H. P. Buechler, *Artificial Atoms Can Do More Than Atoms: Deterministic Single Photon Subtraction from Arbitrary Light Fields*, Phys Rev Lett **107**, 093601 (2011)

[138] T. Peyronel, O. Firstenberg, Q.-Y. Liang, S. Hofferberth, A. V. Gorshkov, T. Pohl, M. D. Lukin, and V. Vuletić, *Quantum nonlinear optics with single photons enabled by strongly interacting atoms*, Nature **488**, 57 (2012)

[139] C. S. Hofmann, G. Günter, H. Schempp, M. R. de Saint-Vincent, M. Gärttner, J. Evers, S. Whitlock, and M. Weidemüller, *Sub-Poissonian Statistics of Rydberg-Interacting Dark-State Polaritons*, Phys. Rev. Lett. **110**, 203601 (2013)

[140] D. Petrosyan and K. Mølmer, *Stimulated adiabatic passage in a dissipative ensemble of atoms with strong Rydberg-state interactions*, Physical Review A **87**, 33416 (2013)

[141] B. Olmos, W. Li, S. Hofferberth, and I. Lesanovsky, *Amplifying single impurities immersed in a gas of ultracold atoms*, Phys. Rev. A **84**, 41607 (2011)

[142] G. Günter, M. R. de Saint-Vincent, H. Schempp, C. S. Hofmann, S. Whitlock, and M. Weidemüller, *Interaction Enhanced Imaging of Individual Rydberg Atoms in Dense Gases*, Phys. Rev. Lett. **108**, 13002 (2012)

[143] F. Bariani, Y. Dudin, T. Kennedy, and A. Kuzmich, *Dephasing of Multiparticle Rydberg Excitations for Fast Entanglement Generation*, Phys. Rev. Lett. **108**, 030501 (2012)

[144] Y. Miroshnychenko, U. V. Poulsen, and K. Mølmer, *Directional emission of single photons from small atomic samples*, Phys. Rev. A **87**, 23821 (2013)

[145] Y. Miroshnychenko and K. Mølmer, *Off-resonant transitions in the collective dynamics of multi-level atomic ensembles*, J. Phys. B **46**, 224009 (2013)

[146] N. Malossi, M. Valado, S. Scotto, P. Huillery, P. Pillet, D. Ciampini, E. Arimondo, and O. Morsch, *Full counting statistics and phase diagram of a dissipative Rydberg gas*, Phys. Rev. Lett. **113**, 023006 (2014)

[147] H. Matsumoto and S. Sakamoto, *Quantum Phase Coordinate as a Zero-Mode in Bose-Einstein Condensed States*, Prog. Theor. Phys. **107**, 679 (2002)

[148] P. Öhberg, E. L. Surkov, I. Tittonen, S. Stenholm, M. Wilkens, and G. V. Shlyapnikov, *Low-energy elementary excitations of a trapped Bose-condensed gas*, Phys. Rev. A **56**, R3346 (1997)

[149] G. B. Arfken and H. J. Weber, *Mathematical Methods For Physicists International Student Edition* (Academic press, 2005)

[150] M. A. de Gosson, *Symplectic Methods in Harmonic Analysis and in Mathematical Physics*, 1st ed. (Springer, 2011)

[151] J. Williamson, *On the algebraic problem concerning the normal forms of linear dynamical systems*, Am. J. Math., 141(1936)